Abstract

The use of products and technologies based upon nanotechnology and nanosciences become more and more frequent in both the domestic and industrial environment. The increased use of engineered nanoparticles also increase human exposure levels, and as the exposure level increase so does risk of adverse effects. For relevant toxicological experimentation the controlled generation of nanoparticles must be explored and characterized. In order to achieve this two means of nanoparticle generation is explored, by Palas CFG 1000 spark discharge generator and hight temperature evaporation condensation, and the resulting nanoparticles are quantitatively characterized.

The nanoparticles are generated from gold bulk material and suspended into aerosol phase. The characterization is done by TEM, T-DMA, SMPS and APM. Deposition was calculated using size dependent deposition data from a novel cell exposure system (ALI) and the human respiratory tract. Dosages were calculated for mass and particle surface area.

The spark discharge system generates an aerosol more abundant in particles while the particles generated by evaporation condensation are fewer but with more mass. The mass fractal dimension is comparable for the two generation methods used but a significant difference in the effective density between the methods are observed. By TEM the primary particles are determined to be larger for the evaporation condensation system. Deposition and dose calculations indicate that relevant doses can be produced from within 1 to 2 hours of deposition for the two generation methods. The doses calculated for the human respiratory system are roughly a factor 1000 less than for the ALI system, due to the great surface area of the human lung.

The adverse effects of nanoparticles – how can we learn of their toxicity?

We are all day all the time surrounded by a so called aerosol, air with suspended particles in it. The size of these particles can vary greatly from dust which can be fractions of a millimeter to soot which can be fractions of a micrometer. It has for a long time been known that exposure to a high concentration of aerosol particles can have negative effects on human health, sometimes exposure leads even to an early end. The very smallest fraction of aerosol particles is of special interest from a toxicological point of view, the particles that are teens to hundreds of nanometers. This is because these particles deposit deep within our respiratory system, most in the region called the alveolus region.

As technology advances so does the use of new novel materials and techniques. Some of these are constructed of engineered nanoparticles. Particles specifically designed to have new and exciting properties that can be totally different than any bulk material. As their use increase so does the risk of being exposed to high levels of the particles. For example a worker at an industry producing paint or cosmetics are exposed to high levels of titaniumdioxide, a nanoparticle 10 of nanometers in size. Another example is exposure to carbon naotubes, a new material used as a composite to enhance the properties of new materials.

In order to gain knowledge of nanoparticle toxicity so called dose response relationships are established for the various nanoparticles. This is a method where one studies the response, in for example cell cultures or other organisms, in relation to a certain dose and exposure time. There is an ongoing debate within nanoparticle toxicology what means of describing dose, shall it be in mass or volume for example. The debate is founded in the fact that particles of similar or the same material can have different effects even at the same dose. This leads to ideas that perhaps particle shape or surface area is a better way of measuring the dose of nanoparticles. In many recent publications the particle surface area has actually proven to be more useful and produce more coherent dose response relationships.

Question is then how can we study the particles and their effects in an accurate manner? So we don’t leave it to history to decide what was dangerous and what was not. A continuation of the work done within my thesis will be the use of a new air liquid interface chamber for cell exposure studies, so called ALI system. This system closely mimics the deposition pattern of nanoparticles in the human lung and closely replicates physiological conditions in the lung. The aerosol particles are deposited using an electrical field and deposit directly on cell cultures. The cell cultures are later studied using various techniques to determine the particles effects.

The knowledge of what we deposit is every bit as important as the fact that we are able to deposit it in the first place and the use of highly characterized model particles would be very useful. For the course of my thesis gold was generated as such a model aerosol and it was characterized very well in order to know as much as possible of the aerosol particles. Various techniques was used in order to characterize the gold aerosol and techniques included measurement of size, mass and particle number. Electron microscopy was also carried out for the aerosol particles.

With the data from the characterization and knowledge of how the particle deposition is dependent on particle properties a very detailed image can be produced of how many particles deposit in a system, such as the ALI system or the human lung. Knowing how many particles deposit is also to know which particle surface area are deposited, since various analytic methods exist that can accurately calculate the particle surface area. It is also to know what mass dose or what volume dose is deposited in the system.

Having a state of the art deposition system, such as the ALI system, and having knowledge of its deposition pattern is to know what deposits in it. In addition having a clear image of what the particles are like when they deposit gives us the opportunity to produce very relevant toxicological experiments. The methodology used during the generation and characterization process is not limited to gold particles, there are many materials that can be generated by the methods employed for the course of the thesis. Also the methodology of the characterization can be used for virtually any sub-micron aerosol particles.

Contents

1 Acknowledgements

I love to learn! This said I can honestly say that I have indeed learned much as my time as a master thesis worker at the EAT.

I am very grateful towards all of the department of EAT for accepting me as a master theis worker, but there is two persons who I would like to give special thanks to. I would like to thank Jenny Rissler and Joakim Pagels for their guidance, for their good spirits and their commitment to my master thesis! Know that I am truly grateful for all your support!

I would also like to give special thanks to Maria Messing and Bengt Mueller at the department of Solid State Physics. Thank you for answering my endless questions and making the experimentation in June possible. Thank you Maria for the many interesting discussions during our long days of experimentation!

I would like to thank my family and my friends for their ears and support during this endeavor. I am especially grateful towards my grandfather Erich Svensson for making me curious of the world and all things in it.

Also special thanks to Linus Anderson for wanting to be my opponent.

You all have my warmest gratitude and thanks!

2 Abbreviations and symbols

ρ_{eff}	Effective density
H	Viscosity
λ	Mean free path
a	Primary particle radius
ω	Angular velocity
ALI	Air-liquid deposition system described by Savi et al (2008)
APM	Aerosol particle mass analyzer
AS	Amorphous silica
C_C	Cunningham slip correction factor
CPC	Condensation particle counter
CTAB	Cetyltrimethyl ammonium bromide
Df	Fractal dimension
DMA	Differential mobility analyzer
Dme	Electrical mobility diameter
e	Electron charge
E	Electrical field strength
FCAW	Flux core arc welding
GMAW	Gas metal arc welding
HT	High temperature evaporation/condensation furnace
Hz	Frequency
IA	Idealized aggregate theory
ICRP	International commission for radiological protection
Il-8 gene	Gene associated with inflammatory response
In vitro	Outside the organism
In vivo	In the organism

Kn	Knudsen number
LC50	Lethal concentration, 50 % mortality
mRNA	Messenger RNA
n	Number of electron charges
Np	Number of primary particles
OPC	Optical particle counter
PMN	Polymorphonuclear cells
r_1	Inner cylinder radius
r_2	Outer cylinder radius
r_c	Average radius
s	Specific mass
SD	Spark discharge generator
SMAW	Shielded metal electrode electric arc welding
SMPS	Scanning mobility particle sizer
TEM	Transmission electron microscope/microscopy
TSP	Total suspended particles
TWA	Total weight average
V	Voltage
Vte	Terminal settling velocity
Z	Electrical mobility

3 Introduction

It happens all the time. We inhale, filling our lungs with air and we live yet another moment. We don't think about it, it would no doubt be a harsh existence if we should have to, the action in itself or how important it is to us. As it for most of us is automatic, perhaps it is not strange we take breathing and air for granted. Every day, all the time, a grown man draws about 12 breaths per minute. This equals in average 6 l per minute for a grown man, it goes without saying that this is an average and extremes for both higher and lower values do occur (NE, 2010).

Every breath we take we also inhale a vast number of particles, many of which are deposited in the respiratory system. The particles are of various sizes, the particles of most interest for this thesis is in the nanometer range so called nanoparticles. Where and to which degree deposition takes place depends on the size and inertia of the particles (Bailey et al., 1994). The mix of gas and particles are called an aerosol (NE, 2010). Mankind, and all other organisms for that matter, has always been exposed to aerosols, and particles in that aerosol have always been deposited in the respiratory tract. Since a build-up of various particles in the respiratory tract can be harmful in itself all organisms have evolved defenses against such build-ups, these defenses include clearance of deposited particles and also metabolism of various particles (Hinds, W. C., 1999).

However respiratory defense mechanisms have their limits. As mankind progress and the world becomes ever more urbanized and industrialized it has been shown that the air quality in many cases has been affected. In many cases the air quality has been so deteriorated that adverse effects on human health has been observed, as for example in Pakistan where air quality has been shown be of very poor quality and many health problems are believed to be induced as a result (Colbeck et al., 2009).

The concentration of nanoparticles, aerosols or other, one might encounter in a workplace can be many magnitudes greater than that of the average urban aerosol or environment. Exposure to soot, metals, and metal oxides are an everyday occurrence for many people. Exposure in taverns where smoking is allowed has been shown to greatly increase exposure to various particles (Ott et al., 1996). Workplaces where welding and other metal works take place has also been shown to greatly increase the exposure to aerosol nanoparticles particles (Stephenson et al., 2003). Also a new breed of material is rising, the engineered nanoparticles and nano-materials. New materials and particles with properties that cannot be predicted by bulk material information give rise to new environmental and health issues.

However it is not enough to stop at the conclusion that exposure to aerosol nanoparticles with a mass concentration of particles can under certain circumstances have adverse effects. In order to gain knowledge of what can be toxic we must employ a toxicological approach to the problem. Today the study of aerosol and nanomaterial toxicology occupies quite many people and new studies are published all the time. There are however problems when it comes to aerosol and nanoparticle toxicity. One problem is the possible differences between in vitro and in vivo exposure to aerosols during toxicological studies. Other problems are difficulties in depositing relevant amounts of aerosol particles. Yet another problem is the dosimetry of

aerosol nanoparticle particle exposure, mass dose or particle number seems inadequate as dose when it comes the toxicity of low toxicity particles as shown for example by (Waters et al., 2009).

It is the aim of the recently started FAS project (”Exposures and Health Effects of Manufactured Nanoparticles in Production and Nanotechnology Applications” dnr 2009-1291), which will be described in greater detail in the following chapter, to investigate the toxicity of aerosols and engineered nanoparticles and address the problems previously presented. The project will use a new deposition device which mimics the deposition pattern in the human lung and also the physiological conditions, by air liquid interface (ALI), to create a highly relevant deposition environment (Savi et al., 2008). The project will also investigate a newly described means of quantifying aerosol particle dose, one where the particle surface area of the particles is used to create dose response relationships (Waters et al., 2009).

This thesis is one of the first steps in the FAS project. Two means of generating aerosol nanoparticles will be presented, one commercially available spark discharge generator Palas CFG 1000 (SD) and one high temperature evaporation/condensation furnace (HT). The two generation methods will produce aerosols with different particle properties such as size, mass etc. The generation of aerosol nanoparticles with different properties can produce very interesting and relevant experiments. For example particles with similar mass but different structure can be deposited and the toxicity can then be studied for various particle properties. Also a comparison between the two methods can increase knowledge of particle formation processes and allow for a more precise particle production. The generated particles can then for the course of the FAS project and beyond be used as model nanoparticles when it comes to toxicological studies on nanoparticles. Dose calculations and deposition will be modeled for the aerosols using data for the new deposition chamber and the ICRP respiratory deposition model. An aerosol particle mass analyzer (APM) will be used and used for particles below 40nm in size possibly for the first time.

The primary goal is to see if the generation methods are suitable for toxicological studies in the FAS project and to quantify the mass dose and particle surface area dose the aerosols can yield. The aerosol created will be comprised of gold particles in the size range of 1 – 100 nm. The thesis will also present a literature review of nanoparticle toxicology, the respiratory system and the ICRP model, nanoparticle dosimetry and aerosol measurement apparatus.

3.1 The FAS project

The overall purpose of the newly started FAS project (FAS projektansökan, 2009) is described as “The objective is to characterize exposures and health relevant properties of manufactured nanoparticles and to identify their toxic effects in human in vitro and in vivo studies”, this is the overall purpose of the newly started FAS project (FAS projektansökan, 2009).

The method of the FAS project will be to work through and complete four phases.

1. Characterization of collected aerosols and generated particles.

2. Generation of workplace relevant aerosols in laboratory.
3. In vitro toxicological studies on aerosol exposed cell cultures.
4. In vivo exposure studies to determine toxicological response using human test subjects.

In the first step different workplaces will be identified where every day handling of nanomaterial takes place. When the workplaces have been identified three will be selected where particle collection and characterization will take place. Already the FAS project has identified some workplaces of which one is the solid state physics department at the University of Lund. In the workplaces the individual exposure for each worker will be assessed and in addition an aerosol mass spectrometer will be used in one selected workplace. The characterization of the workplace aerosols include scanning mobility spectrometer (SMPS) scanning, transmission electron microscopy (TEM) imagery, determination, mass dose of particles and surface area dose of particles.

The second step of the FAS project is the in vitro phase of the project. Here the workplace aerosols and the aerosols generated in a laboratory environment will be deposited upon human lung epithelial cells. The deposition will be performed using a special air-liquid deposition chamber described by Savi et al (2008) (ALI), through funding by Vinnova and "Crafordstiftelsen".

After deposition on the human lung epithelial cells toxicological analysis will begin, the analysis will deduce changes in genomic expressions i.e. up or down regulation of certain proteins. Dose response relationships will then be created for mass dose, surface area dose etc. for the genomic changes observed. These findings will be the basis for the third phase of in vivo human exposure studies.

The third and final phase of the FAS project is that of controlled human exposure. A total of 18 workers from three different workplaces will be exposed for three hours to a relevant aerosol particle level. The relevance of the exposure level is linked to the workplace. The workers will during the course of the test be exposed to both generated aerosol and clean air. Medical examinations will take place both before and after exposure. In addition to genomic analysis based upon the second phase findings blood analysis, urine, breath, spirometry, nasal lavage and acustic rhinometry will be examined. The analysis aims at determining levels of oxidative stress and inflammation.

The FAS project is a multidisciplinary project within from the METALUND cooperation (www.metalund.lu.se). METALUND is collaboration and joint research effort consisting of the Division of occupational and environmental medicine (OEM), the Faculty of ergonomics and aerosol technology (EAT), Solid state physics at Lunds university, institute of public health at Copenhagen university and the cardiology department of the Karolinska institute (www.metalund.lu.se,2010). The FAS project will also be linked to the nanometer structure consortium at Lunds University (nmC). The consortium is a multidisciplinary center promoting research within the area of nanotechnology within all from life science to material technology (www.nano.lth.se, 2010).

It is the intention of the FAS project to link its research with other METALUND projects, as other current research efforts include controlled human exposure to aerosols and toxicological studies of nanomaterials.

3.2 Objectives of this thesis

The thesis will be comprised of a theoretical part and an experimental part. The theoretical part is a literature overview of aerosol toxicology, the respiratory system, the ICRP model, current aerosol particle dosimetric theory and the necessary theoretical basis in order to understand the thesis and the results it will generate. The experimental part of the thesis was carried out at the department of Solid State Physics at Lunds University and the aim of the experimentation was to characterize generated aerosols. The was generated by the SD system and the HT system.

The characterization will consist of the following elements:

- Particle size distributions for both the SD and the HT system for different relevant settings.
- Determination of so called effective density, based upon electrical mobility and particle mass, and mass fractal dimension which gives quantitative data on the agglomeration state of the particles. From this in turn the mass size distribution will be calculated.
- Determination of particle surface area dose for both the ALI deposition chamber and human lung for the characterized particle size distributions.
- Determination of particle mass dose for both the ALI deposition chamber and the human lung for the characterized particle size distributions.

3.3 Overview of the thesis

The first part of this thesis will be focused on theory and a literature study. Aerosols will be introduced from a wide perspective and narrowed down to the more relevant aerosols for this thesis. Also the respiratory system will be overviewed in light of aerosols and particle deposition, aerosol and particle toxicology will also be reviewed and a new way of establishing dose response relations will be presented from new literature. Important and recurring concepts and parameters will be presented and described that will be important for the full comprehension of this thesis and lastly the apparatus making this thesis possible will be described.

4 The various aerosols

This chapter introduces the concept of an aerosol and also gives examples of different kinds of aerosols. The chapter also aims at giving perspective on aerosol particle exposure and what different environments are like in this respect, this to be able to put the results of this thesis in perspective to real world conditions.

4.1 Aerosols

The air around us is by physical definition a fluid, one that can host various particles both solid and liquid. When particles are suspended in the fluid water the mix of particles suspended in the water is called hydrosol, when particles become suspended in air the mix is called aerosol (Hinds, W. C., 1999). Naturally we don't call a glass of water a hydrosol but merely water, as we do with air even though particle free air is an imaginary thing. Stating the obvious we now know that we all the time breathe and that every breath holds vast amounts of particles of different origins. The various particles vary greatly in size all from hundreds of micrometers for dust to hundreds of nanometers of the finest of particles. The particles of interest for this thesis is those in the nanometer range.

4.2 The natural aerosol

The air as it would be without anthropogenic activity constitutes the concept of the natural aerosol, anthropogenic activity is another word for manmade activity and in that sense not naturally occurring. The natural aerosol depends on direct emissions and gas to particle formation. By mass the largest of these emissions to the natural aerosol comes from vegetation, the ocean and desserts. The emissions to the natural aerosol are mainly composed of soil dust sea salt and various organic components. These emissions are then confined to the first kilometers of the troposphere, all in all most of the particulate mass of the atmosphere are found in the troposphere. Moving up in the troposphere, past a few kilometers, particle levels in the aerosol drops dramatically and levels take on a background character undisturbed by natural or anthropogenic emissions. What is clean air is subject to debate but around 700 / cm^3 can be said to constitute a natural background aerosol, similar to that of altitudes higher than 2 kilometers or to vary arid areas (Hinds, W. C., 1999).

4.3 The anthropogenic aerosol

Already at the everyday level of urban exposure health effects have been observed and pollution is suspected of being the cause of many adverse health effects (Matson, 2004). The anthropogenic aerosol can most often be found in the lowest kilometer of the troposphere in close proximity to human activities. What particle mass and number concentrations would be in urban areas are subject to great variability. The mass and number concentration distribution, see figure 1 – 2, is typical for most urban outdoor aerosols containing smog (Hinds, W. C., 1999). Although most of the particles are present in the nuclei mode their numbers represent virtually no mass at all compared to the much fewer in numbers accumulation mode and course particle mode. The nuclei mode and accumulation mode both constitute the fine fraction of the aerosol. Particles in the nuclei mode come mainly from combustion processes or gas to particle formation. They rapidly undergo coagulation or react with particles from the accumulation mode and grow to become part of the accumulation mode. The nuclei particles are often acidic in nature and also consist of sulphate, ammonium and various hydrocarbons. Accumulation mode particles are composed of coagulated nuclei particles and photo chemically generated smog particles. The course particle mode consists mainly of crustal matter such as silicon, iron or soil dust. The matter in the course particle mode has its primary origins in agriculture, surface mining activities, dust from street canyons or the ocean (Hinds, W. C., 1999).

Studies presented in a literature compilation the Swedish *Socialstyrelsen* presents data suggesting indoor total suspended particles (TSP) ranges from 18 – 70 µg / m^3 in average and that particles with an aerodynamic diameter of < 1 µm ranges from 3000 – 10,000 particles / cm^3 in average. These values were presented as for a Swedish indoors living environment (Socialstyrelsen, 2006). As for an outdoor environment mass concentrations of particles can vary from a few micrograms per cubic meter up to tens of grams per cubic meter depending on circumstances (NE, 2010). When it comes to number concentrations of particles counts can vary from 2000 to 17,000 / cm^3, reported from various locations in Sweden and Denmark (Matson, 2004).

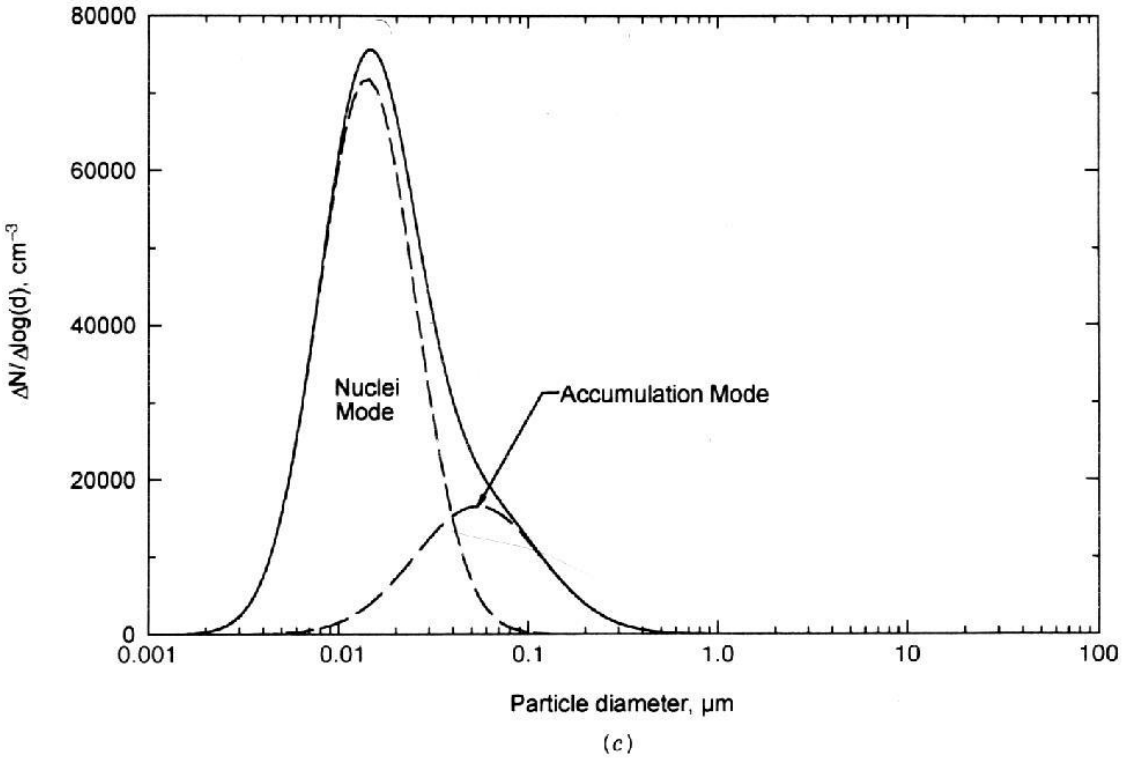

Figure 1 Number concentration profile for a typical urban aerosol. Most particles are present in the nuclei mode and virtually no course mode can be observed (Hinds, W. C., 1999).

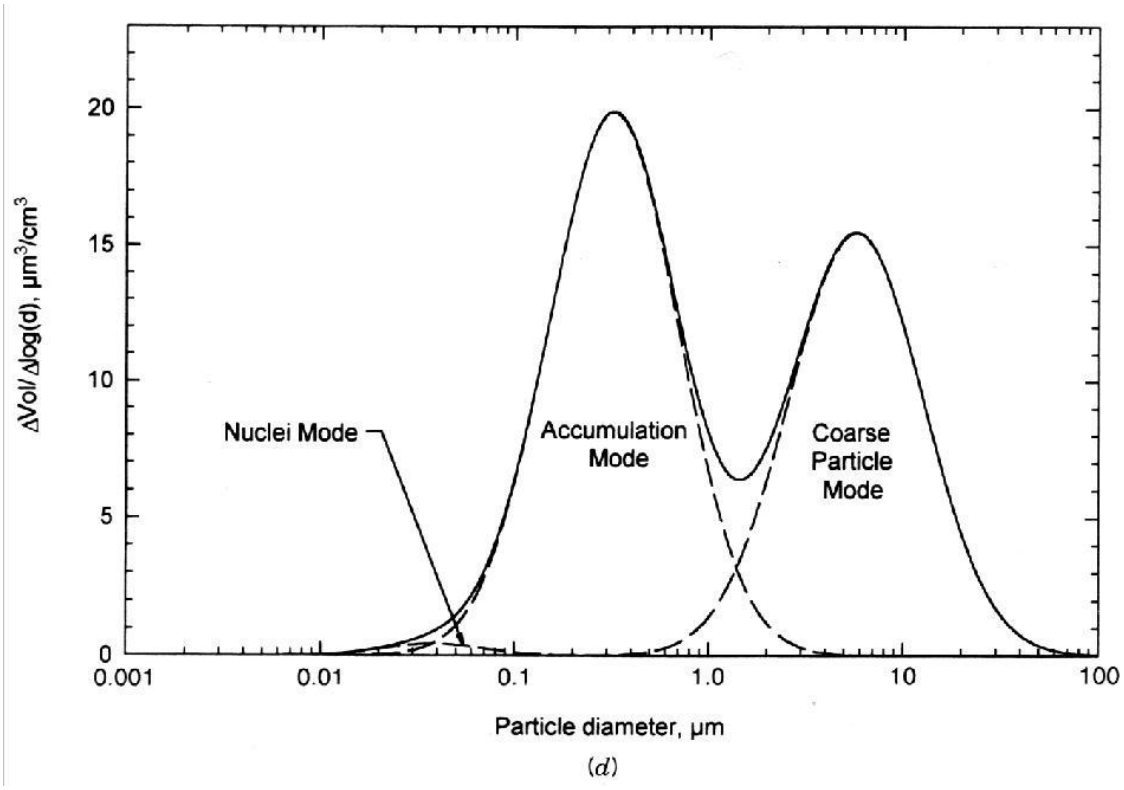

Figure 2 Volume / mass profile for a typical urban aerosol with smog. Most of the mass is partitioned between the accumulation mode and course particle mode, with virtually no mass in the nuclei mode (Hinds, W. C., 1999).

4.4 The industrial aerosol

There are many types of industries and therefore many types of industrial aerosols. The aerosols described here will primarily be the ones created due to welding processes. Research into aerosols created during welding processes is much under development and there is no real consensus on the character on the aerosol. Studies conducted will be presented in order to give a somewhat representative idea of what the welding aerosol is like.

In a study by Stephenson et al (2003) an experimental environment was created to simulate a workshop where welding takes place. Shielded metal electrode electric arc welding (SMAW) of carbon steel was used in order to generate the aerosol in the workshop. Measurements of the generated aerosol was done by a Scanning mobility particle seizer (SMPS), 14 – 600 nm and an optical particle counter (OPC) was used to get size number concentrations for particles 0,3 – 10 µm. Measurements from 8,5 m away from the welding operations was conducted, see figure 3. It is clear that the particles generated by means of welding has a peak at approximately 100 – 150 nm and have a peak number concentration of approximately 500,000 / cm^3. Mass concentration measurements were also carried out during the experiments. Total weight averages (TWA) for both 160 min and 8 hr periods for both respirable and total aerosol mass concentrations were compiled for different zones in the workshop. TWA for 160 min of respirable aerosol in the designated welder breathing zone and 8,5 meters away was 1,38 mg / m^3 and 1,13 mg / m^3 respectively, and TWA for 8 hr of respirable aerosol in the designated welder breathing zone and 8,5 meters away was 0,460 mg / m^3 and 0,377 mg / m^3 respectively. For respirable aerosol the 50 % cut point was set to 3,5 µm. This means that a particle of 3,5 µm in size has a 50 % chance of being respired. Particles

smaller has a higher chance of being respired and larger has a smaller chance (Stephenson et al., 2003).

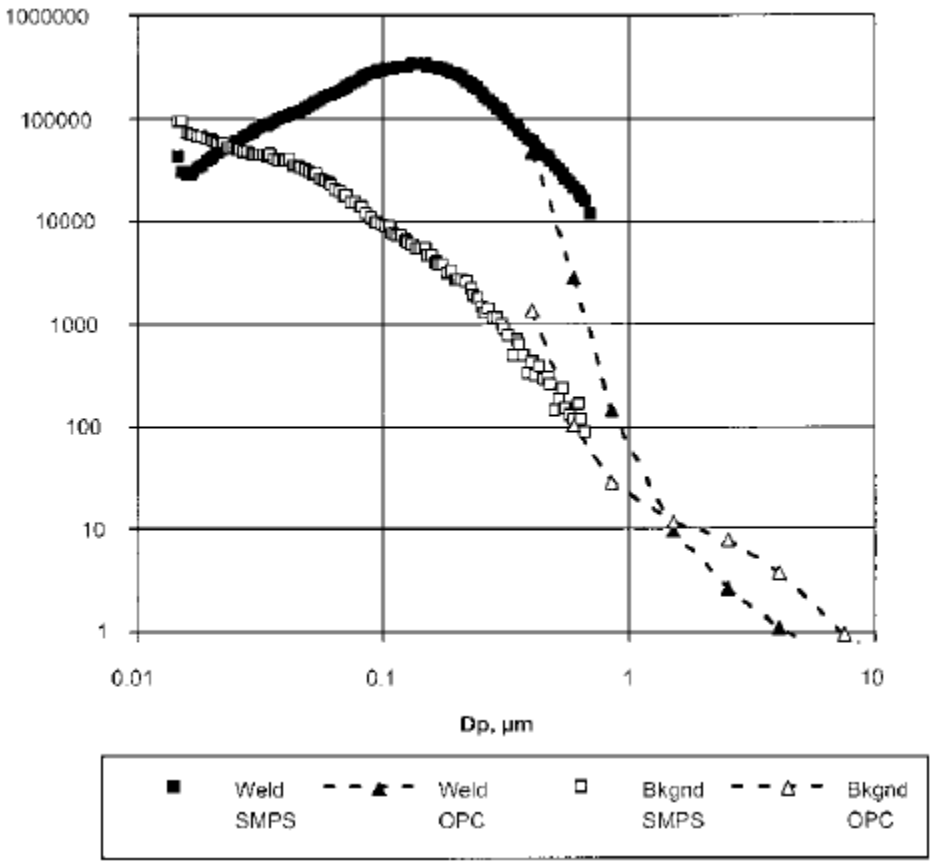

Figure 3 Particle number concentration per cm3 for welding aerosol, aerosol was generated in an experimental environment by Stephenson et al (2003) and measurements conducted with SMPS, 15 – 600 nm, and OPC for particles 0,3 – 10 micrometers. These measurements was carried out 8,5 m horizontally and 1 m above the welding point. Squares indicate measurements with SMPS and triangles measurements with the aid of the OPC.

A study by Isaxson et al (2009) determined the character of the aerosol in a working environment where welding is an integral part of everyday work. The study was conducted in three Swedish workshops and both number and mass concentrations was continuously monitored to determine what exposure was like on a temporal basis. The type of welding of interest in the study was gas metal arc welding (GMAW). The study shows that during breaks particle numbers and mass concentrations are at 100,000 / cm^3 respectively 300 – 400 µg / m^3. A dramatic increase takes place in both particle number concentration and mass concentrations when work intensifies, number concentrations rise to a maximum of 700,000 /

cm^3 and mass to 2500 µg / $m^{3,}$ see figure 4. As work intensity decrease so does both particle number and mass concentrations (Isaxson et al., 2009).

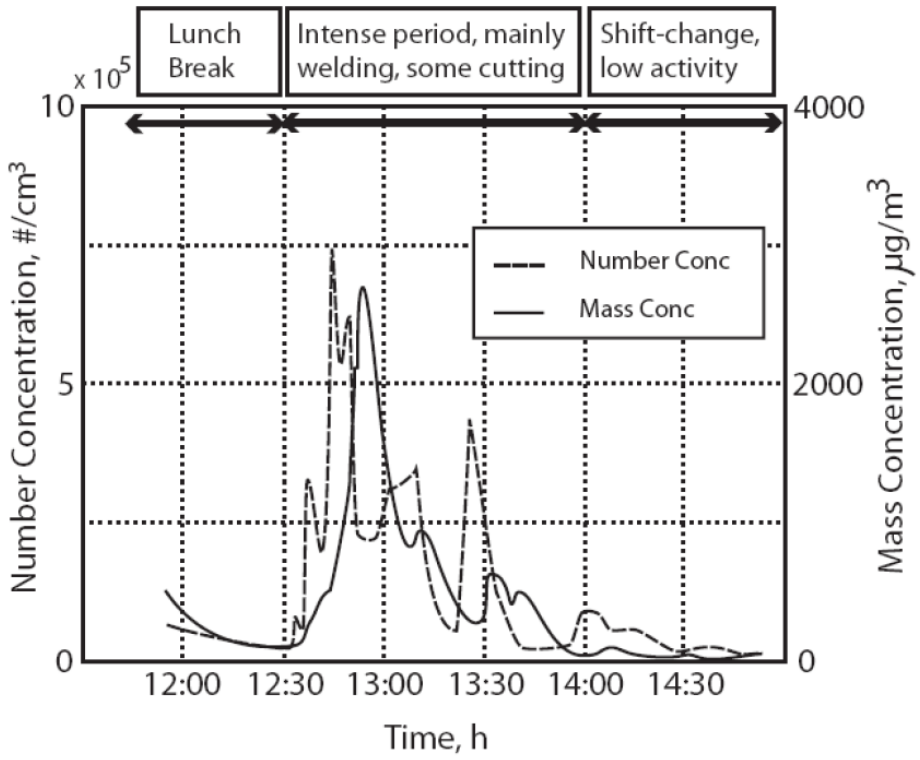

Figure 4 Number concentration and mass concentrations for one of three Swedish workshops during the course of a normal workday. Work consisted mainly of welding activities. Number concentrations are a total value derived by SMPS from 15 – 1000 nm. Mass concentrations are PM10 derived using Tapered element oscillating microbalance (TEOM) (Isaxson et al., 2009).

In addition to mass and number concentration analysis of welding aerosols transmission electron microscopy (TEM) has been carried out by Zimmer et al (2001) in combination with material analysis. Analysis was carried out on both flux core arc welding aerosol (FCAW) and gas metal arc welding (GMAW) aerosol. TEM images of GMAW aerosols show that particles mainly was composed of chain like agglomerates consisting of iron, manganese and silica. FCAW TEM images show that particles consists of a mix between spherical and chainlike structures, particles was composed of similar elements as GMAW particles with the addition of various alkali metals (Zimmer et al., 2003).

4.4.1 Engineered nanoparticles

Virtually any small particle or colloid can be called a nanoparticle. Engineered nanoparticles are ultrafine particles produced for specific purposes, such as creating new materials with superior properties. The particles, a gold aerosol that will be generated for the course of this thesis can be described as engineered nanoparticles. The department of Solid State Physics have long used the gold particles to grow nanowires upon and they can produce particles suiting their needs to accomplish this. The data generated for the course of this thesis can be used to increase the knowledge of how generation parameters affect the particles structure and size, allowing for an even more exact particle production in the future.

Some examples of engineered nanoparticles will be briefly described in this chapter.

4.4.1.1 Titanium dioxide

Titanium dioxide is a naturally occurring mineral and is in industry today refined and produced using a variety of methods. For many applications titanium dioxide is present as an ultrafine dust in the nanometer range, see figure 5 for TEM of titanium dioxide particles.

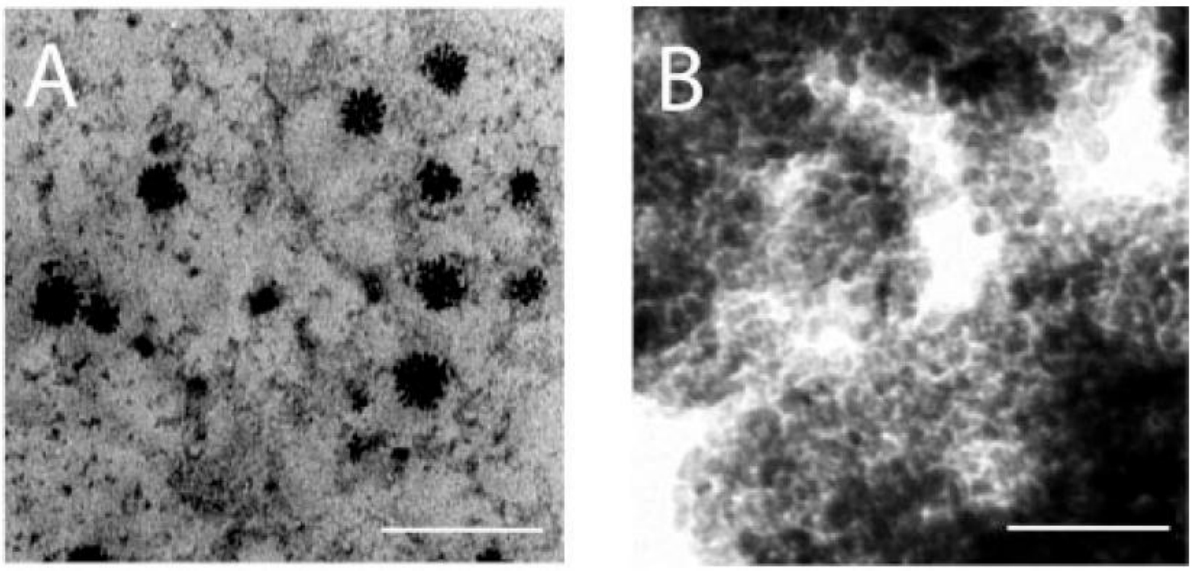

Figure 5 Ultrafine titanium dioxide particles. A) TEM imgae of titanium dioxide particles, B) sonicated titanium dioxide particles. ,

Titanium dioxide has many uses in today's industry. Various self-cleaning surfaces, photo catalyst in sterilization and the paint industry are some examples of industrial usage (Lovern et al., 2006). Today titanium dioxide is suspected of various adverse health and environmental effects.

4.4.1.2 Fullerene C60 and carbon nanotubes

Fullerene C60, also known as Buckminister fullerene, and carbon nanotubes are both part of the fullerene family (NE, 2010). Carbon nanotubes are in larger production in the industry, due to problems with C60 production and refinement. Both exist in the industry as ultrafine nanoparticles, both within the nanometer range. Both C60 and carbon nanotubes have properties highly sought after in the industry and become more frequently used all the time. See figure 6 for TEM imagery of carbon nanotubes.

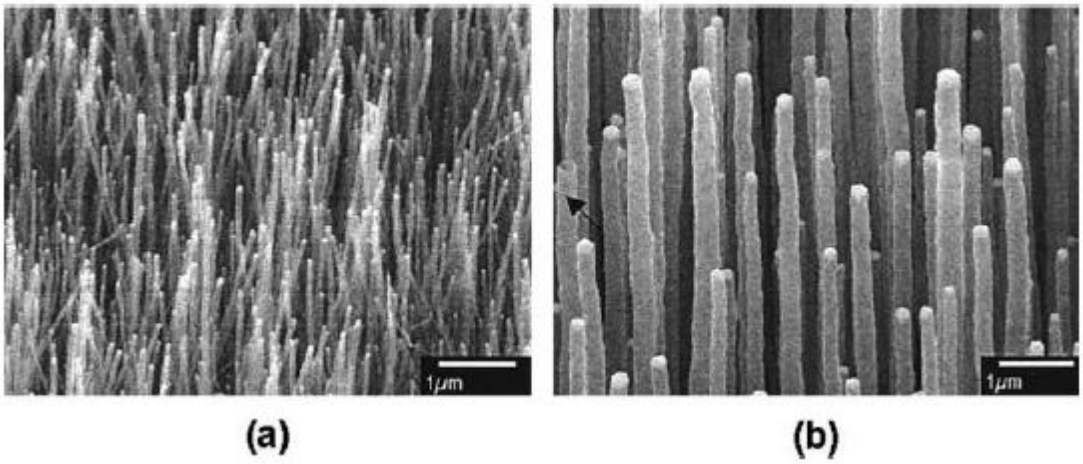

Figure 6 TEM imagery of carbon nanotubes (Thostenson et al., 2001).

In figure 7 C60 fullerenes can be seen by TEM.

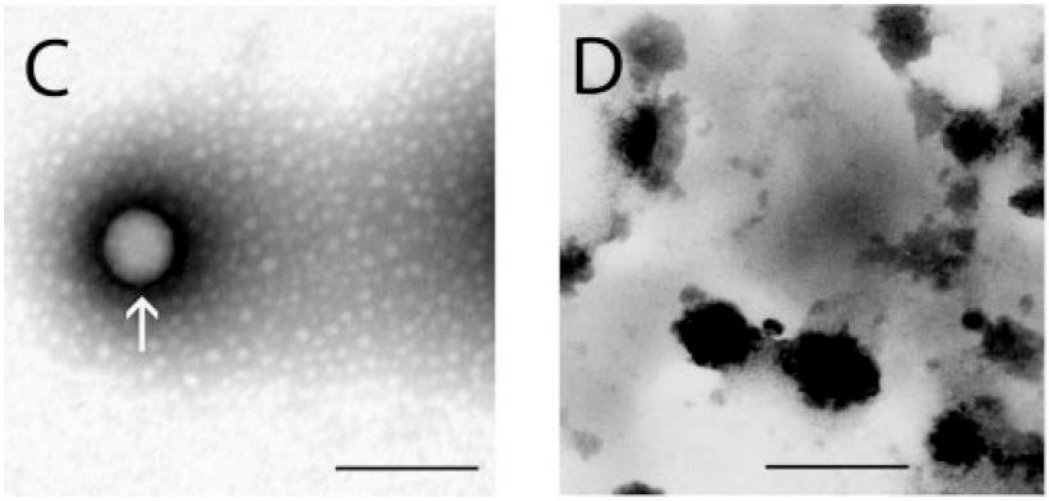

Figure 7 TEM images of C60 buckminister fullerens (Lovern et al., 2006).

Because their use continuously increase in the industry questions have been raised with regards the particles potential toxicity.

4.4.1.3 Gold nanoparticles

Historically there is reason to believe that colloidal gold was a miraculous tonic, in popular culture this is often seen in the occurrence of red potions as means of regaining health. In recent years the use of gold nano particles has increased in both research and for use in the industry, as the use of gold nanoparticles increase so does exposure to it in various forms.

Gold nanoparticles are in both research and in the industry used as means of growing nanotubes of various materials, research on growth of nanotubes currently takes place at the department of Solid State Physics at the Lunds University (Messing et al., 2009).

Gold nanoparticles are also used in research as biosensors and means of highly specific drug delivery systems (Daniel et al., 2004).

5 The respiratory system

Most of us only think of the lungs when thinking about the respiratory system, however when scarping the surface a more complex reality is present. The human respiratory tract is divided into three sections which are the head airways, lung airways and the alveolar region (Hinds, W. C., 1999). The head airways consist of the nose, mouth, pharynx and larynx. The pharynx is a space in the back of the throat where both food and air can pass and the larynx is a protective organ housing the vocal cords (NE, 2010). The lung airways consist of the trachea stretching down to the carina which divides to the main bronchus. The bronchus divides several generations and stop at the so called terminal bronchioles with a diameter of about 1mm, the bronchus has the appearance of an upside down tree. The final section, the alveolar, is the location where the gas exchange takes place. This part of the lung also divides for many generations and end up as the alveolar sacs. There are about 300 million alveolar sacs in the human lung and their combined area is roughly equal to half a tens court. Each sac has an approximate diameter of 500 µm (NE, 2010). An overview of the lower parts of the human lung can be seen in figure 8.

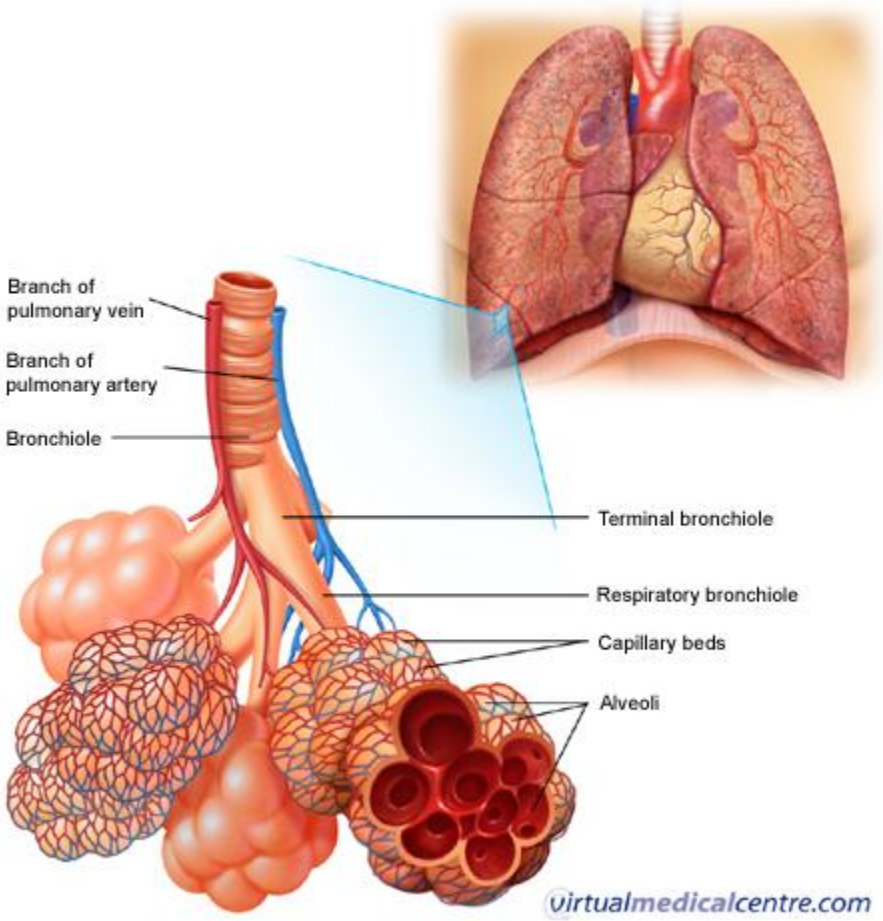

Figure 8 An overview of the lower parts of the human respiratory system (Virtualmedicalcentre.com, 2010).

5.1 Aerosol deposition in the respiratory tract

There are three primary deposition modes for particles entering the respiratory system. They are impaction, gravitational settling and diffusion.

Impaction is the primary mechanism of deposition for larger and courser particles. By mass impaction is the leading deposition mechanism, although it possibly is the one most restricted by sites. The main sites where impaction takes place are the carina, the place where the trachea divides to the two principal bronchi. The bronchi are the two main airways to each of the lung sacs. Impaction takes place at less degree at the other bifurcations further down the lung. It is because the air changes direction quite steeply at these dividing points that impaction is the dominant deposition mechanism (Hinds, W. C., 1999).

Gravitational settling is the primary deposition mechanism in the distal airways, approaching the alveolar region of the lung. It is in the more horizontally oriented airways where flow rate and air way diameter decreased that the mechanism functions best (Hinds, W. C., 1999).

Diffusion is of most importance for the smallest particles in the outer most parts of the lungs, in the alveolar regions. Diffusion is also known as Brownian motion and can be described as the random motion of particles suspended in a fluid. As the particles move randomly and come into contact with a surface, in this case that of the alveolar sacs, they adhere there and do not bounce back. This creates a concentration gradient at the surface and there is a net transport of particles towards the alveolar surface (Hinds, W. C., 1999).

True for all deposition mechanisms is that if the particles are hygroscopic in character they will grow and the possibility of deposition will increase (Hinds, W. C., 1999).

5.1.1 Particle size and deposition mechanism

The predominant deposition mechanisms vary in the respiratory system depending on particle size. Impaction is predominant in the head airways, settling is predominant in the lung airways and also somewhat in the alveolar region and diffusion is predominant in the alveolar region of the lung. The deposition mechanisms will be considered in detail between diffusion and settling in regards to particle size, see table 1.

The importance of diffusion versus settling shifts in the region around 0,3 µm. Above this size settling fast becomes the dominant means of deposition and below diffusion just as fast becomes the dominant deposition mechanism.

Table 1 Diffusion and settling numbers for standard - density particles. Concentration of particles beyond gradient assumed to 1 / cm^3 and time set to 100 s. The relative importance of both settling and diffusion can clearly be seen (Hinds, W. C., 1999).

Diameter (µm)	Diffusion (Number / m^2)	Settling (Number / m^2)
0,001	$2{,}6 \times 10^4$	0,68
0,01	$2{,}6 \times 10^3$	6,9
0,1	$3{,}0 \times 10^2$	88
1	59	3500
10	17	$3{,}1 \times 10^5$

100	5,5	$2{,}5 \times 10^{7}$

5.2 ICRP – deposition model

The International commission of radiological protection, commonly known as the ICRP, is an independent organization working with aerosol safety recommendations. The ICRP develop and use mathematical models to predict total and regional deposition in the respiratory tract, a combined image of total and regional deposition for a specific breathing pattern can be seen in figure 9. Taken into account in the model are variable breathing patterns for males females both children and adults, simulation for essentially all sizes of aerosol particles (Hinds, W. C., 1999). The model calculates deposition for impaction, settling and diffusion for five regions in the respiratory system. These regions are nose and mouth, throat and larynx, bronchi, bronchioles and the alveolar region (Hinds, W. C., 1999).

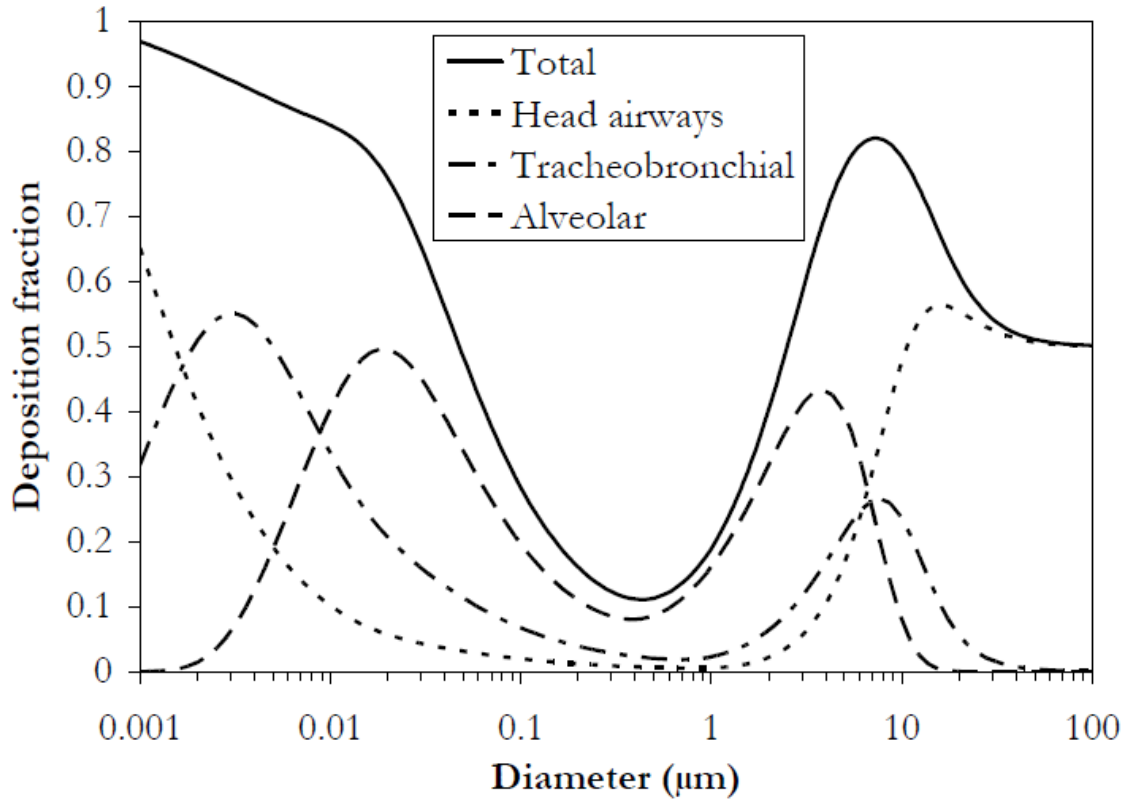

Figure 9 Predicted deposition both in total and in different regions of the lung by the ICRP model for a sitting adult, tidal volume 0,75 l/min and breath frequency 12 / min (Bailey, 1994).

6 Toxicology

Depending on particle properties it will deposit in different places in the respiratory tract. Also depending on particle properties the particle will exert different effects on the area where deposited. Nanoparticles pose a special case when it comes to effects and possible toxicology due to their unique physical characteristics which can be dramatically different than what one would predict from the bulk material. One of these features is a very high surface to volume ratio.

Toxicology is the scientific discipline where the effects of various toxins and the properties of the toxins are studied. Often dose–response relationships are established for different so called endpoints to investigate a toxins effect. The dose–response relationship is often presented as a graph presenting different toxin doses correlated to the toxins measured effect or endpoint. The endpoint or effect exerted by the toxin must be one that can be readily quantified. A common endpoint in for example ecotoxicology is so called LC50 values meaning the concentration of toxin that induces 50 % mortality in the test organisms (Walker, C. H., 2002).

A common response to nanoparticles exposure is an inflammatory response. An inflammatory response is basically a protective response by the body to protect itself from either living or dead matter the body recognizes as foreign. The response can be quantified in various ways although a common one is the measurement of white blood cells, which is a little less final than for example LC50 counts. The response can be triggered by allergens, bacteria, inhaled aerosols or dead tissue and there is a variety of in detail different inflammatory responses (NE, 2010).

Leading to an inflammatory response there is also for different particles various toxicological modes. Particles can for instance act as cytotoxins, a toxin that acts adversely towards cells. A toxin can damage or inhibit cells in many ways of which one is being a genotoxin. A genotoxin is a toxin which damages the genetic material of the organism (Lewinski, N. et al, 2008). The difference between the two types of toxicity is that a cytotoxin acts adverse towards cells in a general way and that a genotoxin damages the organisms genetic material.

6.1 Gold toxicity

The results concerning the toxicity of gold nanoparticles vary in the literature. Some articles propose that gold nanoparticles are not cytotoxic others that the particles exhibit notable toxicity. There is also literature indicating that cell morphology and cell density can be significantly affected when exposed to gold nanoparticles, indicating possible cytotoxicity. There are indications in the literature that the surface coating of the gold particles can play a key role in their toxicity (Lewinski et al., 2008). When gold nanoparticles are created in liquid suspension, also sometimes referred to as colloidal gold, in order to prevent the particles from rapidly aggregating they are conditioned with surface active compounds. These compounds can be for example citrate, thiols and other sulfur ligands (Daniel et al., 2004). Gold nanoparticles can be coated with organic shells when gold(III) compounds are in the presence of thiols, see figure 10.

The particles generated for the course of this evaluation and in the FAS project will not be created in a liquid suspension and coated upon generation with functional compounds. However there is good reason to believe that upon deposition in a physiological medium the gold particles generated by SD or HT will interact with proximate chemical compounds, like the aqueous gold colloids when functionalization takes place.

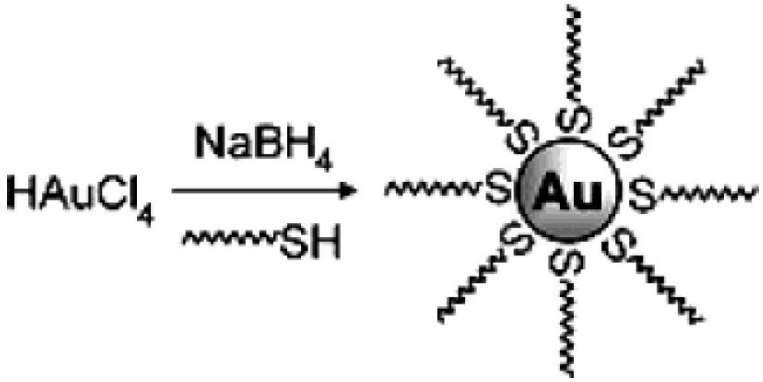

Figure 10 Reduction of Gold(III) compound in presence of thiols form stabilized gold colloids covered in organic shells (Daniel et al., 2004).

A case where gold was found to exert adverse effects on cells where that in Pernodet et al (2006), the study determined how cell morphology and function was affected during long time exposures to gold nanoparticles. They chose morphology over a standard cytotoxicity assay because functional changes may be even more dangerous in the long run than direct decrease in cell viability. The gold nanoparticles were 13 nm in diameter and were covered by citrate during cellular exposure. The cells chosen for the experiment was human dermal fibroblast cells (Pernodet et al., 2006). These cells are very important in the formation of the structures supporting animal cells and important in the healing process (NE, 2010). Concentrations of gold nanoparticles varied between 0 and 0.8 mg / l and exposure from 2 to 6 days. In the presence of gold nanoparticles a modification of the actin structure of the cells became apparent, also the cell proliferation became significantly inhibited for the higher nanoparticle concentrations. Analysis showed that the gold particles had clustered in the lysosomes of the cells and that the citrate coating of the particles had completely dissolved. No penetration into the cellular nucleus could by analysis be detected.

The other side of the coin, where gold nanoparticles are found not to be toxic, are illustrated in experiments conducted in Connor et al (2005). Connor et al showed that gold nanoparticles, for their experimental setup, was not cytotoxic to K562 human leukemia cells but that precursors to the aqueous colloids could be cytotoxic. K562 cells are human leukemia cells immortalized and standardized and are one of the best known cell lines for mimicking erythroid differentiation. An erythroid cell is a developmental precursor to a red blood cell (NE, 2010). Cultures of the K562 cells was exposed to gold spheres of sizes from 4 to 18 nm and coated with various compounds. Citrate and biotin coated gold nanoparticles showed no toxicity to the cells although at comparable concentrations the gold nanoparticle precursor gold-salt showed significant toxicity. Also cetyltrimethylammonium bromide (CTAB) coated gold particles showed cytotoxicity, however the experiment showed that the toxicity probably was due to unbound CTAB associated with the gold particles rather than the CTAB coated

particles themselves. The cells was exposed for the course of three days. The experiment also showed gold nanoparticles coated with citrate clustered in the K562 cells in what was speculated to be endocytic vesicles, the cells was exposed for one hour and the results concerning the clustering of the particles are in agreement with the findings in Pernodet et al (2006) (Connor et al., 2005).

6.2 Dosimetry

As previously discussed the dose of toxic compound in the dose response relationship must be readily quantifiable. A common way of quantifying dosage for aqueous toxins or compounds are as mass per unit volume or in molarity, although mass per unit volume is the one most common. Examples in the literature include toxicological studies of colloidal gold of nanometer size where the usage of mass per unit volume is common. Pernodet et al (2006) and Connor et al (2005) have both conducted toxicological studies using this way of quantifying dosage.

In toxicological studies with regards to aerosols the most common ways of quantifying dosage are mass per unit volume or number concentrations. Often the two are presented in combination with the mean geometric diameter or with an SMPS size number distribution. A highly relevant example is that of Gaschen et al (2010).

6.2.1 The updated measure of dose

In recent years it has become apparent that the "classical" dose quantification strategies are inadequate in creating a coherent dose response relationship for nanoparticles of various sizes and materials. The toxicology of gold nanoparticles for example is highly diverse as the example with Pernodet et al (2006) and Connor et al (2005) illustrate. The question being raised among the lack of coherency among toxicological results is if the dose is being measured and quantified in the wrong way. One important study continuing current ideas in the field and evolving contextual science was that of Tran et al (2000).

The study Tran et al (2000) reevaluated the volumetric hypothesis. The volumetric hypothesis predicts the impairment of lung clearance mechanisms when a certain volumetric load is reached, or expressed for a specific particle type as mass. During the experiment rats was exposed to various loads of titaniumdioxide and bariumsulphate and the total burden per exposure level was determined for the rats. The exposure was measured expressed as total mass burden, total particle number burden and total particle surface area burden to the rats. For both mass and particle number the two particle types gave no coherent results, but when expressed as total lung burden of particle surface area a trend could be seen, see figure 11. The results indicated that an inflammatory response could be seen in the rats at total surface area burdens of approximately 300 cm^2 for both particle types, a surrogate for inflammatory response was in the study the recruitment of so called polymorphonuclear cells (PMN).

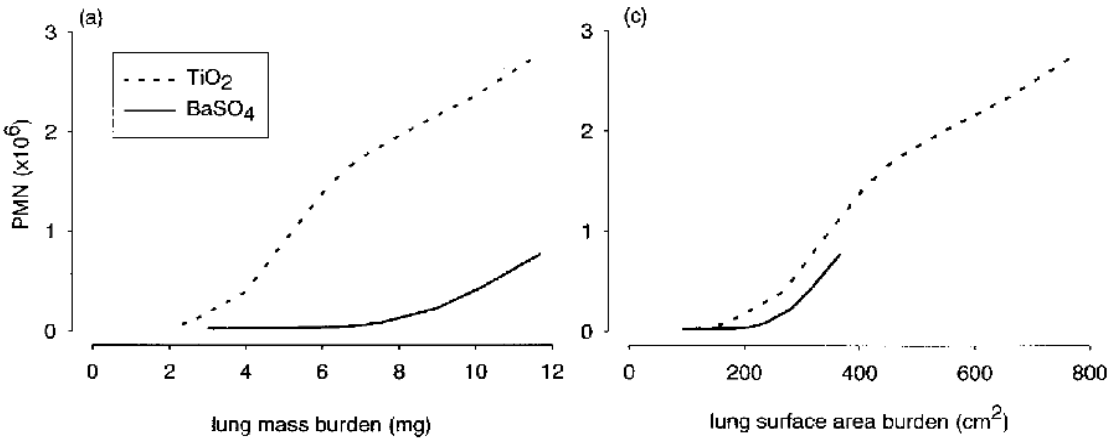

Figure 11 Experimental result from Tran et al (2000) illustrating how total mass burden for titaniumdioxide and bariumsulphate compare to total particle surface area exposure for the two particle types. On the vertical axis is the number of polymorphonuclear cells (PMN).

In Tran et al (2000) it is concluded that particle surface area may be a better measure when it comes to toxicity dosage because it both incorporates particle number and particle size (Tran et al., 2000).

The work in Tran et al (2000) was continued in Donaldson et al (2008). The study normalized the rat lung exposure data from Tran et al (2000) to the surface area of the proximal alveolar region (PAR) or the alveolar surface area including some surface area of the terminal bronchioles, the outer most part of the bronchioles towards the alveolar sacs. The result was a dose of particle surface area per exposed surface area of the PAR, unit area per unit area per se. The study found a threshold value of 1 cm^2 / cm^2 for the exposed rats, se figure 12. At exposure levels higher than 1 cm^2 / cm^2 the number of PMN cells start to increase indicating an inflammatory response in the rat lung.

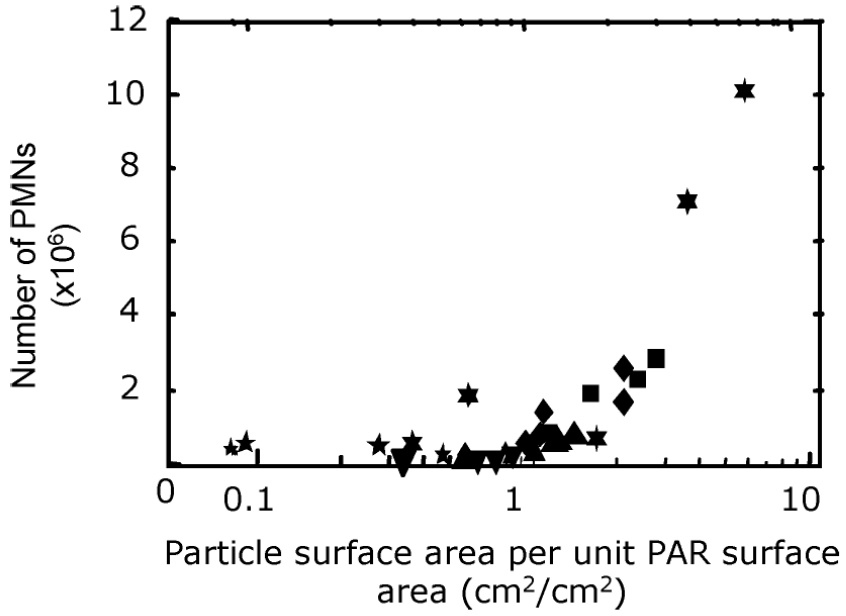

Figure 12 Data from Tran et al (2000) normalized against the PAR surface area of the rat lung. On the vertical axis is the number of PMN cells illustrating increased recruitment and an onset of inflammatory response can be seen when reaching levels of above 1 cm2 / cm2. Plot from Donaldson et al (2008).

In Donaldson et al (2008) in vitro data from human alveolar epithelial A549 cells and their mRNA expression of the Il-8 gene was reprocessed, the original data was produced by Monteiller et al. (2007). This expression served as surrogate for inflammatory response. The il-8 gene codes for an interleukin protein, a type of protein known to be produced when immunization and infection takes place in an organism (NE, 2010). The cells was exposed to the same particles as in the Tran et al (2000) study, however the Donaldson et al (2008) study does not specify for the reused dataset which exposure time was used for the K549 cells and the particles. In the original work by Montellier et al. (2007) exposure time is varied from 6 – 24 hours and the reworked Donaldson et al (2008) data seems coherent with exposure of 6h. The results was then expressed as Il-8 expression against the total particle surface area exposure per cellular exposure area, see figure 13.

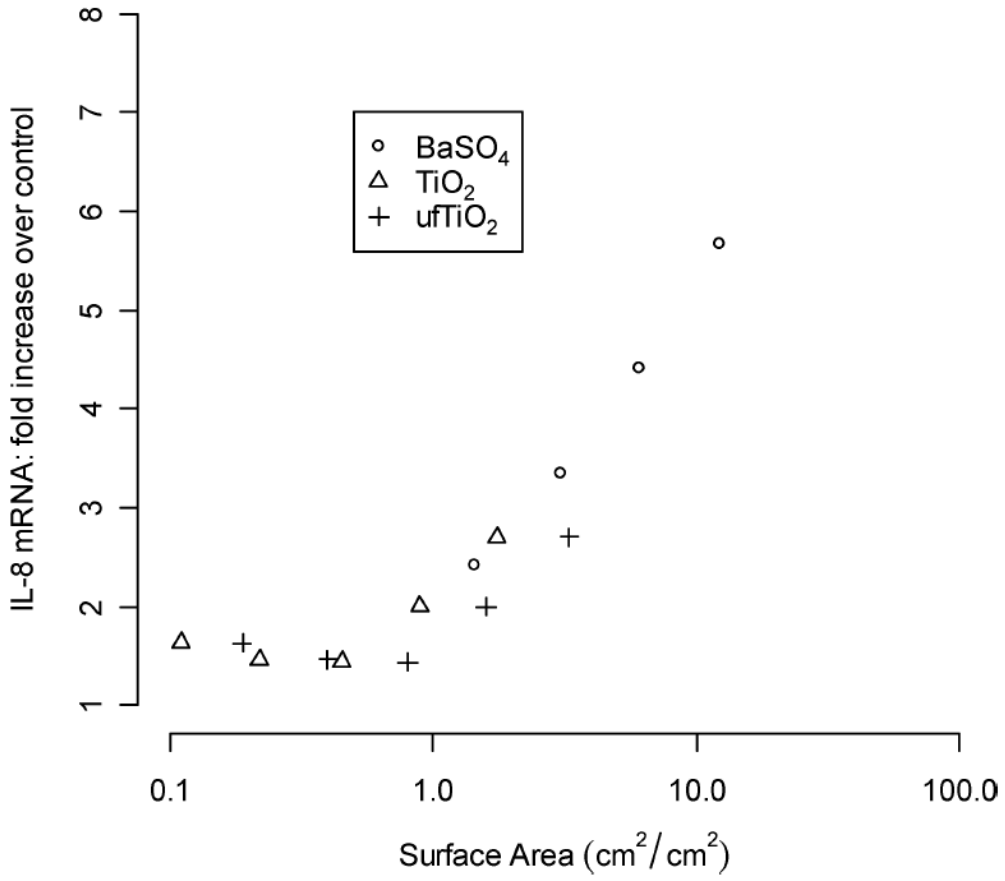

Figure 13 Expression of Il-8 mRNA against particle surface area, particles are bariumsulphate and titaniumdioxide. Data are from in vitro experiments and normalized by Donaldson et al (2008) to exposure surface area.

Conclusions from the study is that using an exposure surface normalized dosage of particle surface area in vitro experiments very well can predict in vivo reactions to particles, it should be kept in mind however that the comparison is between murine, rodent, and human cells.

To further illustrate the viability of particle surface area as dose measurement Waters et al (2009) conducted a study to evaluate genome expression and cell viability when exposed to various particle characteristics. The particles where amorphous silica (AS) particles provided by Polysciences Inc and W.R Grace Co, PS and Ludox particles respectively in figure 14-15. The particles was unopsonized in order to exclude any other compounds toxic effect in conjunction with the AS particles. Opsonization is a process in an organism where xenoobjects are marked by proteins or antibodies to facilitate phagocytosis, phagocytosis is the process where immune cells ingest and break down foreign objects (NE, 2010). The cells exposed to the AS particles was murine RAW 264.7 macrophages. For the viability test of the macrophages they were exposed to various doses of the AS particles for 24 hours, dose response relationships can be seen in figure 14 for both mass and particle number concentration.

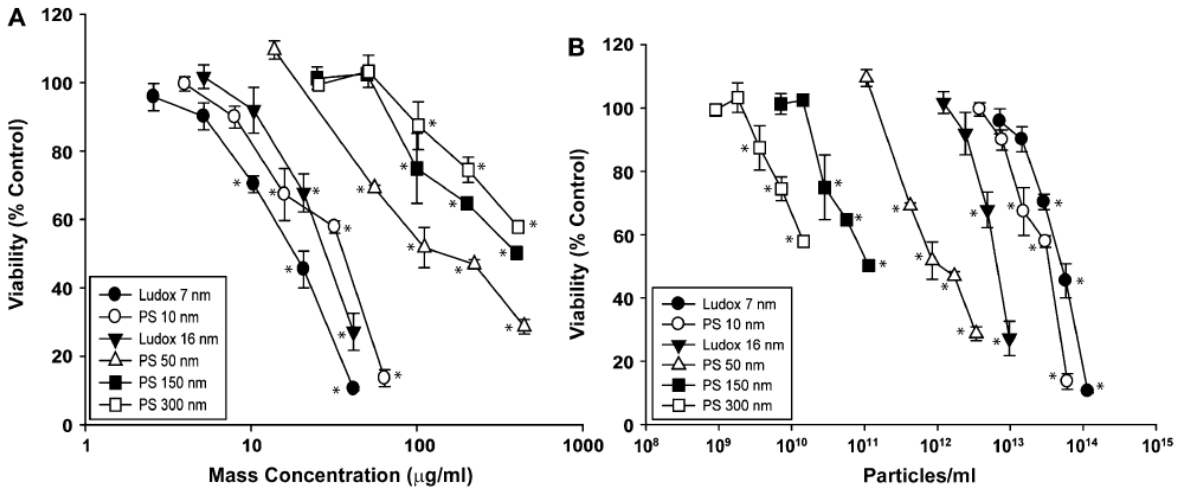

Figure 14 Murine RAW 264.7 macrophage viability after 24h exposure to AS particles of various mass and number concentrations. PS refers to particles provided by Polysciences Inc and Ludox from W.R Grace Co Waters et al (2009).

As can be seen in figure 14 there is no coherent relationship for either of the graphs. However when the dose is expressed as total administered particle surface area to the cell cultures a coherent relationship becomes clear, see figure 15.

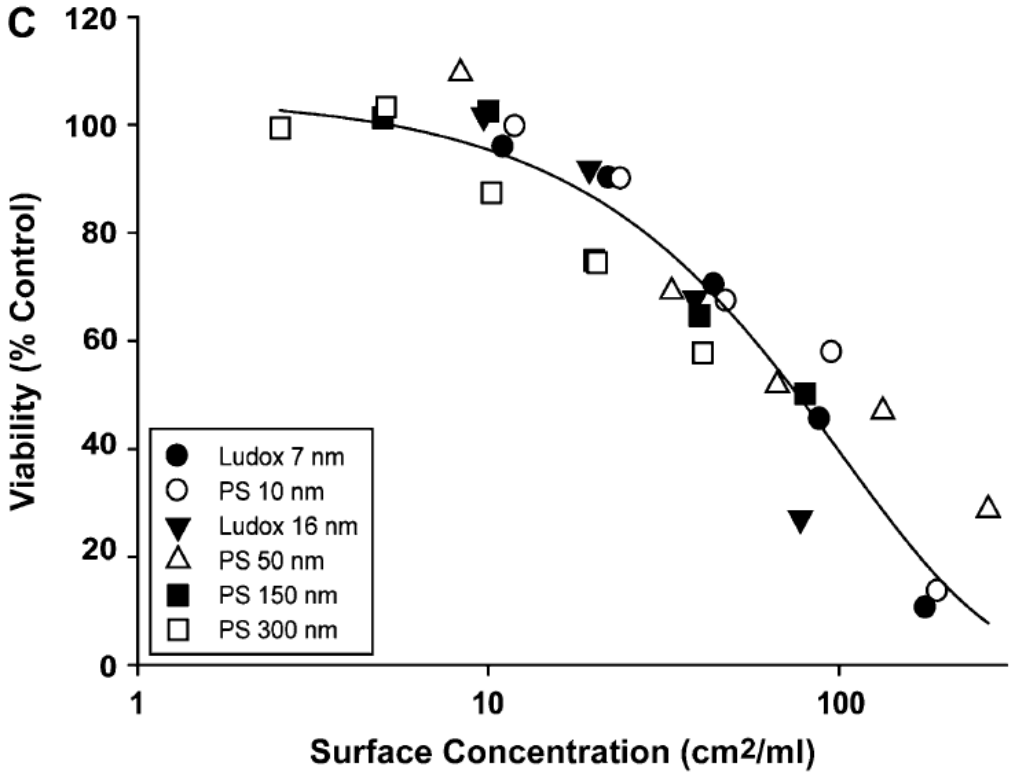

Figure 15 Murine RAW 264.7 macrophage viability after 24h exposure to AS particles of various diameters, dose is here in contrast to that of figure 14 expressed as total administered particle surface area. The plot illustrates how particle surface area gives a coherent toxicological dose response relationship. PS refers to particles provided by Polysciences Inc and Ludox from W.R Grace Co Waters et al (2009).

The dose is not normalized as the doses in the study by Donaldson et al (2008), however Waters et al recognizes 10 cm^2 as a concentration where many cytokines seems to increase in the genomic analysis and converts this to a concentration of 2,5 cm^2 / cm^2 of cell monolayer which is comparable to what the Donaldson et al (2008) study concluded.

6.2.2 Available and extrapolated surface area dosages

Most studies examine toxicology in a liquid interface. Interaction between the respiratory system and aerosol particles occur in a air liquid interface, this is addressed by the scientific community by the development of new technology such as the Savi et al (2008) deposition chamber. The exposure in the liquid medium is almost exclusively expressed as concentration of active toxicant. It would be interesting to translate these concentrations into surface area dosage and see if there is some coherency between the Waters et al. (2008) dose response relationship and the extrapolated concentrations.

The particles Waters et al. (2008) used was amorphous silica (AS) particles and not considered highly toxic, the particles in the other studies will necessarily not be AS particles but composed of other elements. The possibility for particles to express different toxicity even at the same surface area concentration cannot be excluded since they are different in composition after all. Neither can sensitivity of test cells be excluded from having effects on the comparison.

A comparison such as the one being discussed is difficult for several reasons. Firstly the studies being compared utilize different particles, it is a fact that different elements exerts different properties and hence the possibility for varying inherent toxicology cannot be excluded. Not only are the particles different the exposure time is also different for the various particles, plus that any number of other factors could play a part. Although being aware of these factors the information may still be useful for comparison as an overview.

6.2.2.1 Donaldson et al. 2008 – Low soluble and low toxicity particles

In this study Donaldson et al. (2008) compare *in vivo* and *in vitro* dose responses for low soluble low toxic particles. The particles include bariumsulphate, titaniumdioxide both fine and ultrafine fractions. The study shows that a particle surface area dose of approximately 1 cm^2 / cm^2 yields comparable toxicological results in living rats and on A549 cultured cells, for rats the dose reads as particle surface area per respiratory surface area and for the cultured cells as particle surface area per mono cell layer. The response for the study was inflammatory onset for rats and cultured cells.

6.2.2.2 Waters et al. 2009

This study investigates the toxicological effect of amorphous silica particles of different concentrations and of different sizes. Waters et al found that a coherent dose response relationship across sizes and concentrations could be found when dose was expressed as surface area. A concentration of 10 cm^2/ml of particle surface area per unit volume or 2,5 cm^2/cm^2 particle surface area per mono cell layer resulted in an increase in cytokines and gave an inflammatory response Waters et al. (2008).

6.2.2.3 Connor et al. 2005

This study investigates the cellular toxicity of 18nm gold colloids covered in biotin or citrate. Human k562 cells were exposed continuously for three days after which cell survival was measured. No cellular cytotoxicity was found for any of the concentrations varying from 0 – 250 µM of gold, the concentration is given as atoms of gold not of colloids and translates to surface area concentration as 0 – 2,65 cm^2 / cm^2 particle surface area per mono cell layer.

6.2.2.4 Pernodet et al. 2006

Pernodet et al. conducted toxicological experiments on human dermal fibroblast with citrate covered gold colloids. The objective was not to determine only the direct cytotoxic effects of gold particle exposure but to determine how cellular structure and function was affected. The cells was exposed for up to 6 days of gold concentrations ranging from 0 to 0,8 mg / ml. Assuming a mono cell layer and culture plates of 2 cm^2 in size and 1 ml working volume as specified in the article Pernodet et al (2006) the particle surface area exposure becomes 0 to 95,57 cm^2 / cm^2. As presented earlier the study showed adverse cellular effects with increasing exposure concentration and exposure time Pernodet et al. (2006).

6.2.2.5 Summary of dosages and effects

For fast overview the summarized dosages, particle types, exposure time and effects can be seen in table 3.

Particles in the nanometer range sediment i solution extremely slow and sometimes seemingly not at all. It may be the case that the particle surface area dose extrapolated in this chapter are highly overestimated as the particles are suspended in a liquid in many of the studies.

Table 3 Summarized surface area dosages for various studies conducting dose response toxicological research.

Study	Particle type	Particle surface area dose	Exposure time	Effect
Donaldson et al. (2008).	Bariumsulphate Titaniumdioxide	In vivo: 1 cm^2 / cm^2 In vitro: 1 cm^2 / cm^2	6 hours *in vitro* and the *in vivo* dose is total lung burden i.e. exposure until required dose is met	In both in vivo and in vitro inflammatory onset above dose could be observed.
Waters et al. (2009).	Amorphous silica (AS)	2,5 cm^2 / cm^2	24 hours	Increase in cytokine concentrations, could indicate inflammatory response.
Connor et al. (2005).	Au 18nm colloids, biotin or citrate coating	0 – 2,65 cm^2 / cm^2	Three days	No acute cytotoxicity was observed for K562 cells.
Pernodet et al. (2006).	Au 13nm colloids, citrate	0 – 95,6 cm^2 / cm^2	Up to 6 days	Adverse effects on cellular

	coating.			function and morphology

7 The particles

Aerosol particles come in all sizes, shapes and agglomeration states. In this chapter important concepts that are recurring in aerosol science and this thesis will be explained.

7.1 Particle agglomeration

Within aerosol science the concept of agglomerates and agglomeration are a commonly occurring. Agglomeration is a process where particles coagulate and together form a larger complex structure. The resulting complex structures is known as aerosol agglomerates and the particles constituting it primary particles (Hinds, W. C., 1999). Examples of aerosol agglomerates can be seen in figure 16. The particles found under *a)* in figure 16 cannot be classified as agglomerates but spherical particles.

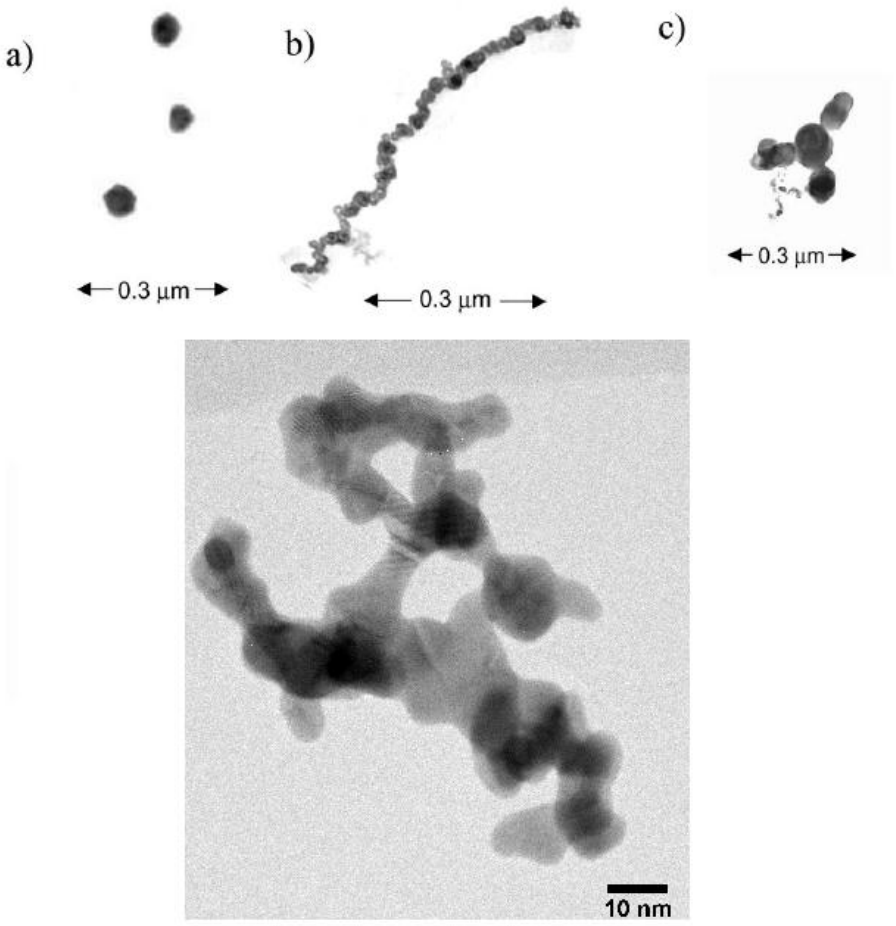

Figure 16 Various aerosol particles, all are agglomerates but the spherical colloid particles to the top left. Particles at the top of the image are from a characterization of welding fumes (Zimmer et al., 2002), particle at the bottom are generated by HT oven system 1575 °C at the Solid State physics department Lunds University.

7.2 Electrical mobility diameter *Dme*

The measure of electrical mobility diameter or as it normally is abbreviated *dme* is one of the most commonly used ways of measuring aerosols. It is measured in a differential mobility analyzer (DMA) and will be briefly described in the apparatus chapter. *dme* is determined through the terminal velocity the particle experiences when exposed to the electrical field and the *dme* is analytically expressed as:

$$Z = \frac{V_{TE}}{E} = \frac{neC_c}{3\pi\eta d_{me}}$$

Z is the electrical mobility and the *dme* is acquired from this value. V_{TE} is the settling velocity for the particles, E is the electrical field strength, n and e refers to number of negative charges, C_c is the cunningham slip correction factor, η is the viscosity of the carrier fluid and *dme* is the electrical mobility of the particles.

The simplest way of describing *dme* is to say: it is the diameter of the sphere moving in the same way through an applied electrical field as the particle being measured upon (Hinds, W. C., 1999) . In other words if the particle moving through the DMA where a sphere the *dme* is the diameter it would have. Often the particles being measured upon are all but perfectly spherical and therefore *dme* should not be used as the true particle diameter, at least without knowing the inherent error in the usage as such.

7.3 Effective density

The effective density is the density of a single particle expressed as:

$$\rho_e = \frac{m}{\pi \frac{d_{me}}{6}} \ [g/cm^3]$$

The effective density, ρ_e, is based upon particle mass, m, and the *dme* and is not the same thing as the particles bulk density, see figure 17 for a principle overview. The *dme* is assumed to be the diameter of a sphere around the agglomerate particle, the sphere that would move in the same way as the agglomerate through an electrical field, the particle mass is then used to calculate the effective density out of these parameters. The bulk density is the particle mass divided by the true agglomerate volume. When the effective density is lower than the bulk density of the particle material it indicates that the particle is to some degree agglomerated.

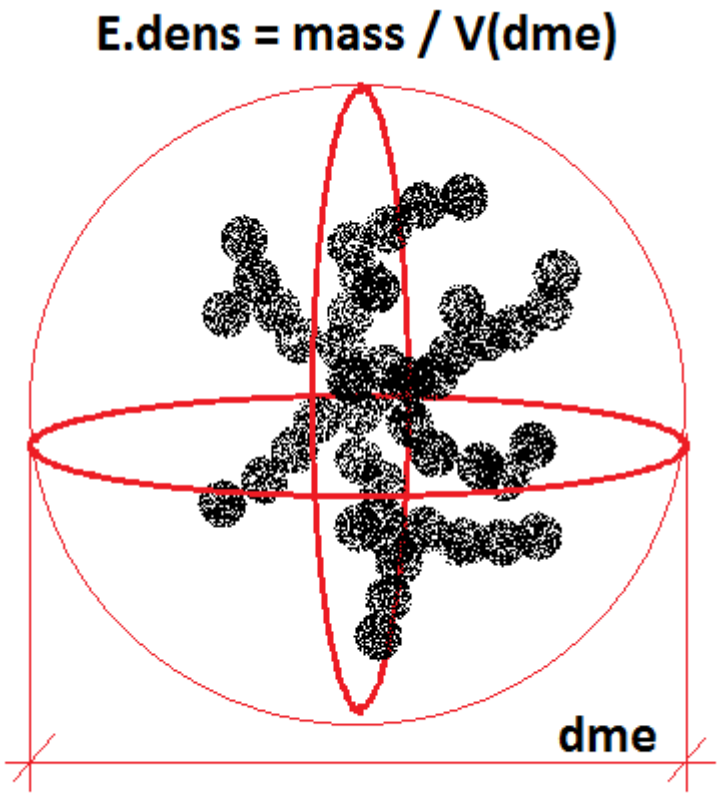

Figure 17 A schematic image of effective density and the parameters which it is based upon. The *dme* of the particle act as the diameter for a sphere around the agglomerate particle the sphere that would move in the same way as the agglomerate through an electrical field. The mass of the particle is calculated using SMPS-APM data and the particle mass and sphere volume yield the effective density.

7.4 Cunningham slip correction factor

As particles within aerosols are very small some physical laws become inaccurate as the surrounding gas become increasingly less continuous and more discrete in nature. Stokes law, a solution to otherwise insoluble differential equations describing fluid motion, also needs correction when scale reaches the nanometer range. When particle size and the mean free path of the gas become increasingly similar in size the particles settle faster than what Stokes law would predict, it is the Cunningham slip correction factor that corrects this and is described by the following relationship (Hinds, W. C., 1999):

$$C_c = 1 + \frac{\lambda}{d_{me}}\left(2{,}34 + 1{,}05e^{\left(-0{,}39\frac{d_{me}}{\lambda}\right)}\right)$$

The Cunningham correction factor, C_c, is based on the diameter, *dme*, and the mean free path λ.

7.5 Mean free path

The mean free path of a gas is the average distance a molecule will travel in the gas until it collides with another molecule. The concept is important when compensating for the increasingly discrete nature of a gas as in the sub-micron region and below. The mean free path is calculated according to the following relationship:

$$\lambda = \frac{1}{\sqrt{2} n \pi d_{me}^2}$$

The mean free path, λ, is derived from the particle density of the surrounding fluid, *n*, and the diamter of the particles *dme*.

7.6 The idealized aggregate theory

Agglomerate volume,i.e the volume occupied by the primary particles, is an important characteristic specially when it comes to calculating agglomerate surface area, which is one of the objectives for this thesis. The volume calculated using the *dme* is not accurate unless the particles are spherical. A better way of obtaining an agglomerates volume is by using the idealized aggregate theory (IA), described by Lall et al 2008. It is an analytical method and relates the number of primary particles and their radius to the *dme* of the agglomerates:

$$v = N_P \frac{4\pi a^3}{3} = \frac{4\pi^2 \lambda a}{c^*} \frac{d_{me}}{C(d_{me})}$$

The agglomerate volume, *v*, is calculated from number of primary particles, N_p, primary particle size, *a*, the mean free path, λ, agglomerate size, *dme*, cunninghamn slip correction factor, C_c and c^* which is the dimensionless drag force.

It was shown that the IA was a good way of calculating agglomerate volume in Lall et al (2008) using various agglomerate particles (Lall et al.,2008). The model is however not boundless and 4 criteria should be filled for it yield good volume calculations.

1. Aggregates are composed of primary particles of the same known diameter.
2. The primary particles are much smaller than the mean free path of the surrounding gas. This corresponds to a Knudsen number of $Kn = \frac{\lambda}{a} \gg 1$ where λ is the mean free path of the gas and a is the primary particle radius.
3. All, or nearly all, surfaces of the agglomerates are exposed to collisions with molecules from the surrounding gas. Acceptable approximation for agglomerates with a fractal dimension less than about 2.
4. Two singly charged particles, one sphere and one agglomerate, have the same electrical mobility diameter if their migration velocities are equal, brownian diffusive speed is neglected.

7.7 Fractal dimension/Mass fractal dimension

The use of fractal dimension in aerosol science differs from the fundamental use within mathematics and physics. The definition and use of the fundamental fractal dimension will not be described in detail in thesis. Within aerosol science an adaptation of the fundamental fractal dimension is used and is called the mass fractal dimension (dfm).

To determine an aerosols *dfm* is to determine its degree and state of agglomeration. The concept has its origins in geometrical structures self-similar properties.

Within aerosol science it is used as a means of quantifying a particles state of agglomeration and thereby its complexion. Within aerosol science the *dfm* of agglomerates is determined by analyzing the particles mass and *dme*, and the basic relationship is described by a power law:

$$m \propto d_{me}^{mD_f-3}$$

Using effective density, previously defined, the relationship can be described as.

$$\rho_e \propto d_{me}^{mD_f-3}$$

The state of agglomeration and complexity is hence determined as how the mass, or effective density, of the agglomerates develops as the *dme* of the particle increases.

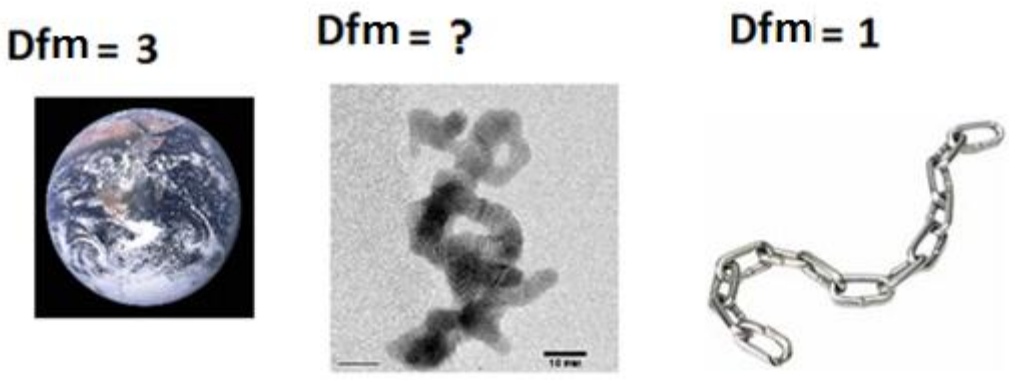

Figure 18 Various geometrical structures and their would be mass fractal dimension, dfm. The dfm of a structure is a measure of its complexity and are within aerosol science used to determine the state of agglomeration of a particle. An aerosol particle completely spherical would have a dfm of 3 whilst a straight chain of primary particles would have a dfm of 1, an agglomerate in between 1 and 3 can be interpreted as a collection of chains going towards a df of 3 as the chains become more and denser.

If the *dfm* would be 3 the effective density would be constant for all *dme* and hence the particle would in fact be a sphere. Whilst in the other extreme case if the fractal dimension was 1 the effective density would dramatically decrease as *dme* increase. The structural interpretation of a *dfm* of 1 would be something like a straight line of agglomerated particles, see figure 18. A *dfm* between one and three would indicate some kind of agglomerate structure (Virtanen et al., 2004).

8 Experimental techniques

This chapter will describe the measurement apparatus used for the experimentation in this thesis.

8.1 SMPS

An SMPS system is a common occurrence within aerosol science. The SMPS system is short for scanning mobility particle spectrometer and is a combination of a bipolar charger, a differential mobility analyzer (DMA) and a condensation particle counter (CPC) (Wang et al., 1990). The SMPS system can characterize the mobility size distribution of particles. A typical

SMPS system, TSI 3934, at the EAT laboratory at the University in Lund can be seen in figure 19.

Figure 19 Typical appearance of a SMPS system. To the left the DMA and the white box to the bottom left the CPC. Picture taken at the EAT laboratory at Lunds University.

A differential mobility analyzer (DMA) is an aerosol particle selection device. The DMA can select particles according to their so called electrical mobility or *Z* and let the selected fraction pass the device whilst other electrical mobility fractions remain in the DMA (Knutson et al., 1975). The *Z* is in turn related to the particles size, *dme*, and structure and is described in further detail in chapter 6. Before entering the DMA the particles passed through a so called bipolar charger. This is to give the particles a well-known charge distribution and eliminate electrostatic interactions due to highly charged particles. After passing the bipolar charger into the DMA the particles are assumed to be charged according to the well-known Fuchs charge distribution. From the Fuchs charge distribution it is possible to gain information on how large a particle fraction is charged with a certain elementary charge (Liu et al., 1974). See figure 20 for a principal overview of the DMA system. The polydisperse aerosol enters the DMA and is carried by a so called sheath flow of air. As the particles are exposed to an electrical field induced by an applied DMA voltage monodisperse aerosol fractions can be selected.

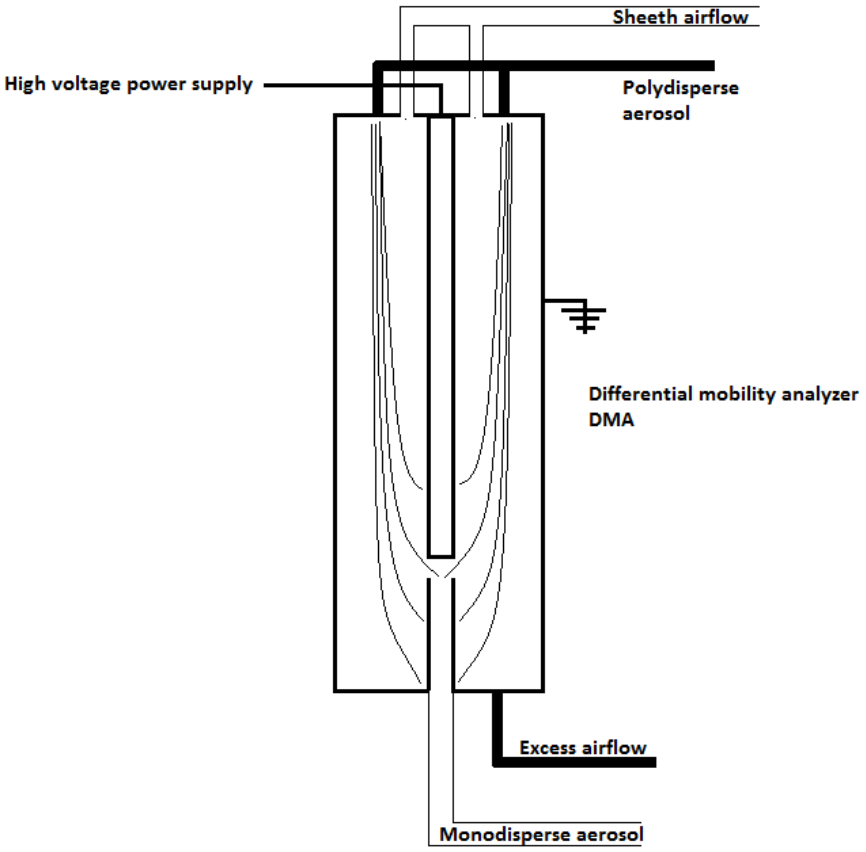

Figure 20 A principal image of the differential mobility analyzer. A sheath flow and a polydisperse aerosol flow is introduced into a cylinder with a cylinder in its center. The outer cylinder is ground and the outer is connected to a high voltage power supply, these cylinders generate an electrical field. The particles entering the cylinders are charged, since they passed a bipolar charger, and respond to the electrical field as they move with the sheath flow. Particles will move differently depending on size and structure and various electrical field strengths will select different fractions based on these properties. The flow exiting the DMA is called a mono disperse flow and is comprised only of one size fraction.

The CPC is an optical particle counter device. The aerosol entering the CPC is saturated with butanol after which a sudden drop in aerosol temperature causes the butanol to condense on the aerosol particles. As the particles grow due to the condensation process it becomes possible to count them as they scatter light (Agarwal et al., 1979).

8.2 APM

The Aerosol particle mass analyzer (APM) is, just like the SMPS system, a device used to characterize aerosol particles. The property of which the characterization is based upon is the specific mass, mass to charge ratio, of the aerosol particles (Ehara et al., 1995). Just as the DMA the APM system allows for online measurements. Often the APM is coupled with a DMA and CPC creating a so called DMA - APM measurement system (McMurry et al., 2002). Outputs from this system is mass distributions for a specific *dme*, effective density and fractal dimension (McMurry et al., 2002)(Scheckman et al., 2009).

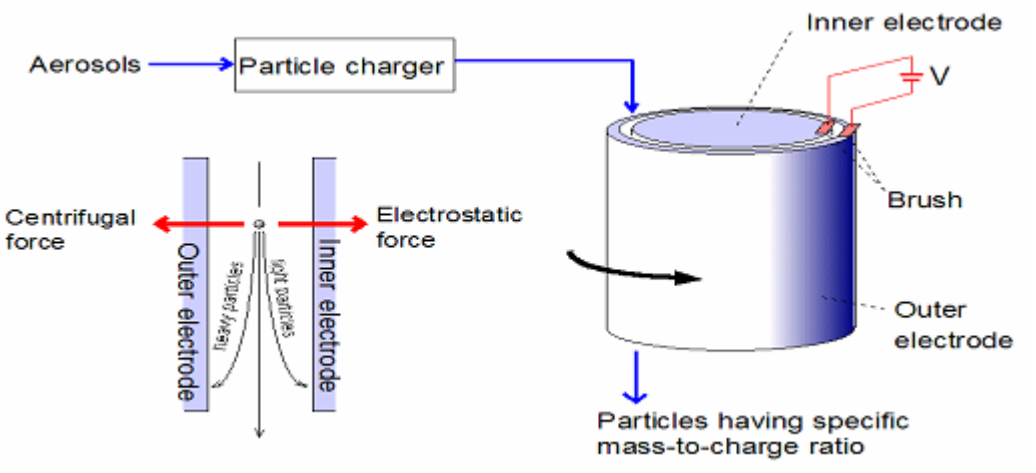

Figure 21 An overview of the APM principle and design. Charged particles enter between two rotating cylinders between which an electrical field is applied. The particles are then exposed to both a centrifugal and electrostatic force. Particles of a specific mass exit the device and the applied voltage calculates into the particles specific mass (Kanomax, APM operation manual).

The principle of the APM is to measure how the particles behave when exposed to an electric field, similar to the DMA. The flow of aerosol is introduced into a slit between two rotating cylinders. The aerosol then also begins to rotate at the same angular velocity as the cylinders. An electrical field is applied between the inner and outer cylinder so that the aerosol in the slit is exposed to it through the entire length of the device. The aerosol particles are now exposed to two forces the first being centrifugal and the second being electrical, see figure 21.

The particles passed a charger before entering the APM system so they are responsive to the electric field. The basic principle is that when these forces are equal the particles will pass between the electrodes and exit the APM, this means that a particular voltage for the electrical field equals a certain particle mass (Ehara et al., 1995). Balance between the centrifugal and electrical field is expressed as:

$$s = \frac{m}{q} = \frac{V}{r_c^2 \omega^2 ln \frac{r_2}{r_1}}$$

The specific mass, *s*, is a ratio between particle mass and its charge. The specific mass is calculated using voltage, *V*, angular velocity, ω, the inner and outer APM cylinder radius, r_1 and r_2 and a combination of the both r_c.

8.3 TEM

Transmission electron microscopy (TEM) is a means of observing and photographing even the smallest of aerosol particles. The principle for a TEM microscope is the same as for an optical microscopy except that instead of photons electrons are used. The TEM contains an electron source that constantly emit a stream of electrons, these are focused by magnetic lenses. The focused electrons hit the sample, which is prepared on a special surface, and what

is seen on a TEM image is the particle standing out due to interaction with the electron stream (Hinds, W. C., 1999).

9 Aerosol generation and deposition

This chapter will describe various means of generating aerosol particles, primarily the ones used in this thesis. Also the deposition chamber will be presented that will be used later in the FAS project.

9.1 Chemical generation

There are many ways to create gold nanoparticles. Many of these take place in what most of us consider being classical chemical environment, in liquid suspension in a lab. The particles hence form a hydrosol and not an aerosol. Conventional methods include reduction of so called gold(III) derivates, gold (III) is one of the gold oxidation states. The gold colloids generated by these methods are then coated with a stabilization agent in order to prevent unwanted aggregation, the stabilization agent can be organic compounds as for example citrate (Daniel et al., 2004).

9.2 Spark discharge generators

The gold particles used in this evaluation are generated by a spark discharge generator, Palas GFG 1000 (SD), and are upon creation directly suspended in a carrier flow gas being high purity nitrogen. The method is one of various methods of creating metal aerosol particles, other methods are for example evaporation in a high temperature oven. The aerosol is generated by the release of a current between the electrodes creating a spark. The spark generates a very high temperature on the electrodes which evaporate electrode material, the evaporated material then form aerosol particles as condensation takes place (Messing et al., 2009). See figure 22 for a schematic overview of the chamber where spark generation takes place in the SD system.

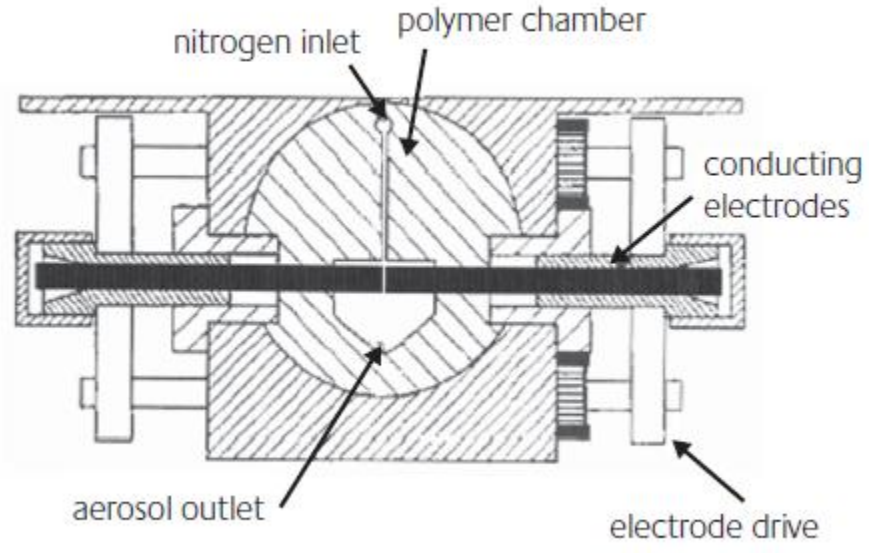

Figure 22 Schematic overview of the Palas CFG 1000 spark discharge generator. A carrier gas flow of nitrogen gas is flowed between the electrodes as the electrodes generate a continuous flow of aerosol particles by spark discharge.

The Palas generator can vary the spark frequency between 0 Hz and 300 Hz. As spark frequency increase so does particle number and peak *dme* as can be seen in figure 23 (Messing et al., 2009).

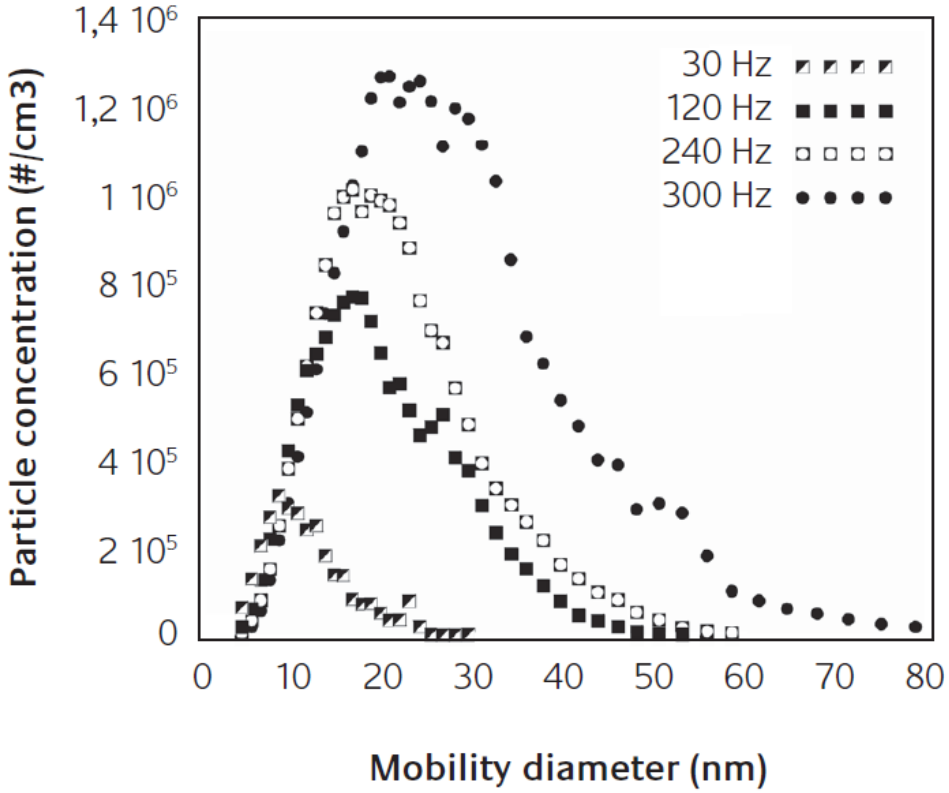

Figure 23 Size number distributions generated by Palas spark discharge generator GFG 1000 for a carrier gas flow rate of 5,9 l/min. High purity nitrogen carrier flow gas and gold electrodes was used, and spark frequency varied between minimum and maximum values of 30 and 300 respectively (Messing et al., 2009).

Gold particles generated by the spark discharge generator (SD) have been investigated with transmission electron microscopy (TEM) and agglomerate and sintered spherical particles can be seen in figure 24. The particles can after generation be sintered at various temperatures to produce spherical gold particles.

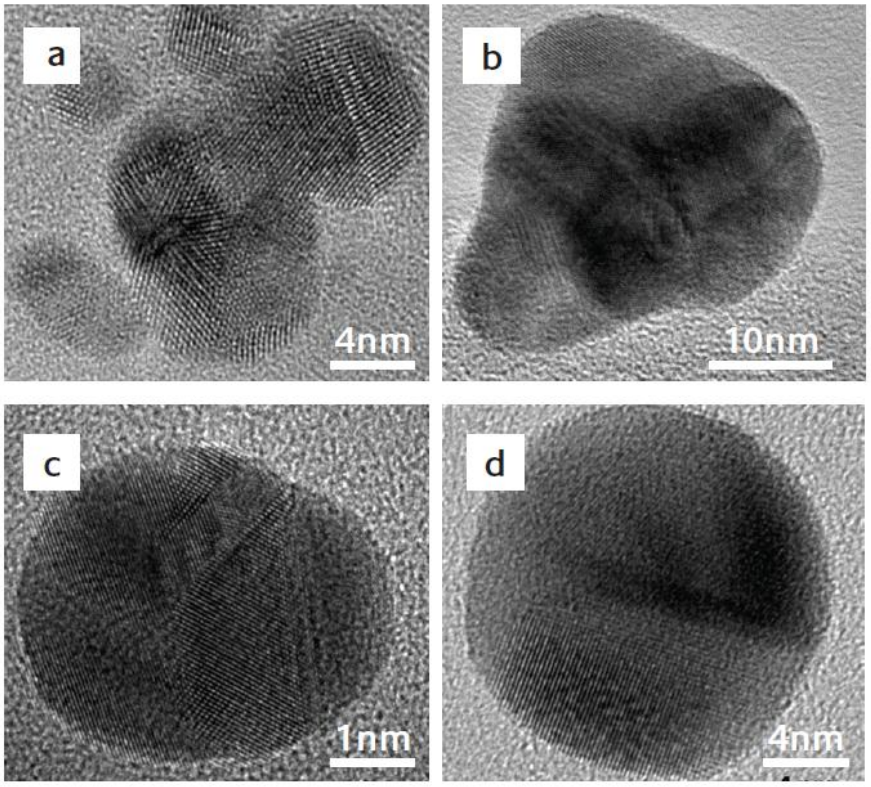

TEM micrographs of (a) agglomerate gold particles and gold particles reshaped at (b) 300°C (c) 600°C (d) 1200°C in a special compaction tube furnace

Figure 24 Gold particles generated by spark discharge generator, Palas. In slot a an unsintered agglomerate can be seen and in the other, b - d, particles reshaped at 300 – 1200 °C. The agglomerate and particles was photographed using TEM (Messing et al., 2009).

9.3 The high temperature evaporation condensation system - HT

The high temperature evaporation condensation system (HT) is a condensation type particle generator, and was one method used for generation of gold nanoparticles in this thesis. The generation takes place by heating a bulk material and creating a saturated gas. After generation of the gas the gas nucleates into primary particles, the next step in the particle generation is that the formed primary particles aggregate into agglomerates (Scheibel et al., 1983).

To generate particles a bulk material is placed inside an electrically heated ceramic tube, a flow rate of nitrogen gas is set to between 2 and 4 l/min and flow through the tube to carry the generated particles. The maximum furnace temperature is 1950 °C, as generation temperature increase so does mass output of gold. Graphite is the base constituent for the ceramic tube. The structural principle of the HT can be seen in figure 25 (Scheibel et al., 1983).

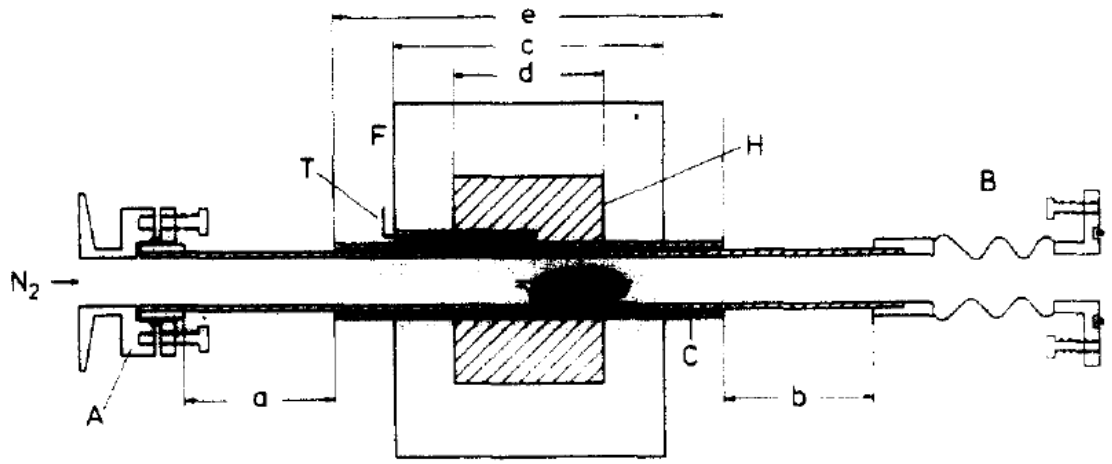

Figure 25 The structural principle of the high temperature condensation generator (HT). A bulk material, in the case of this thesis gold, is placed inside an aluminum oxide ceramic tube which is electrically heated up to 1750 °C. The bulk material is condensate and form primary particles and agglomerates in the nitrogen carrier gas flow which can be varied from 2 – 4 l/min (Scheibel et al., 1983).

The HT is a stable method for generating various aerosols from a bulk material with yields greater than 10^7 particles / cm^3 and narrow size distributions within the scope of 2 and 100 nm in Dme. The two variable system settings are 1) the carrier gas flow rate and 2) the condensation temperature. Experimentation with a variable carrier gas flow rate and a constant temperature has shown that the standard deviation of the size distribution is affected, a high flow rate broadens the distribution around the mean diameter of the distribution. A higher condensation temperature was shown to increase the amount of saturated gas and thereby allowing the particles to grow larger in the particle formation process. A higher condensation temperature was also shown to increase the mean median diameter of the generated aerosol and to somewhat decrease the particle number output, see figure 26 (Scheibel et al., 1983).

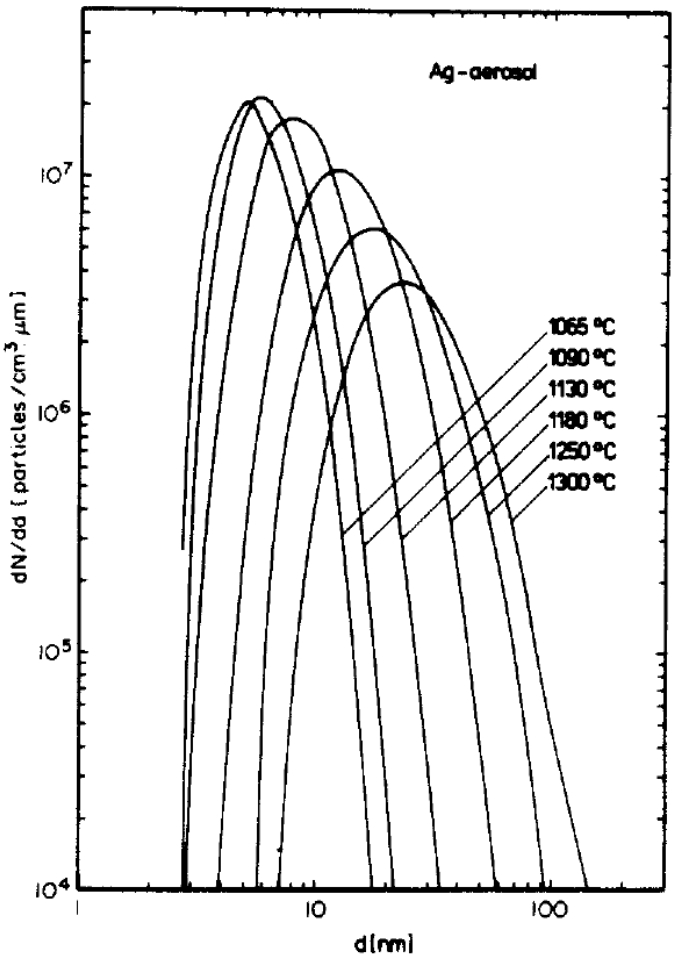

Figure 26 A silver aerosol generated by high temperature condensation generator for single nitrogen carrier gas flow rate and several temperatures to determine effects of various condensation temperatures (Scheibel et al., 1983).

9.4 Deposition chamber

The deposition chamber has many advantages compared to traditional means of particle exposure. The Chamber closely mimics the physiological conditions of the human lung. The chamber allows for deposition of the aerosol directly from the air phase onto the cells, this means that the particles is not coated with surface active chemicals like particles generated in liquid suspension often are. Also there is only a thin film of liquid on the cells when the particles are deposited, this means that the particles are not suspended in a solution but rather settle directly on the cells avoiding problems of confluence (Savi et al., 2008).

The first step of the deposition procedure in the chamber is to generate a known charge equilibrium within the aerosol particles. This is done by letting the aerosol pass through a bipolar charger which radiates the aerosol particles, the radiation causes particles to become charged according to a known size to charge distribution called the Fuchs charge distribution. The charge procedure is done in the same way as when an SMPS system creates charge equilibrium before passing the particles into the DMA. The aerosol is then conditioned to physiological conditions i.e. 75% N_2, 20% O_2 and 5% CO_2. After the physiological conditioning the aerosol is heated to 36 °C and humidified to 85 – 95% relative humidity, all

to produce as natural circumstances as possible (Savi et al.,2008). For an overview of the system see figure 27.

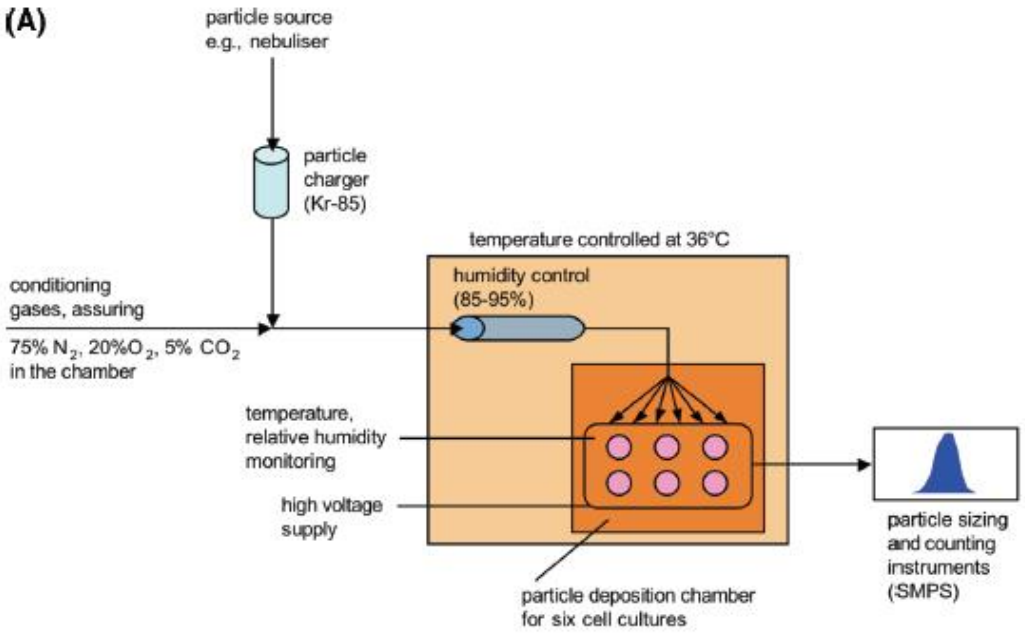

Figure 27 The deposition chamber system developed and tested by Savi et al 2008. The aerosol which one wants to deposit is first charged to a known size charge distribution known as the Fuchs charge distribution using an KR 85 particle bipolar charger. The aerosol is then conditioned to physiological conditions. First the atmospheric composition is adjusted to 75% nitrogen gas, 20% oxygen and 5% carbon dioxide. Lastly before deposition the humidity is adjusted. The deposition of the particles takes place in six filter insets each of 24mm in diameter and an aerosol flow of 50ml / min (Savi et al., 2008).

After the charging and conditioning procedure the aerosol is deposited upon the cell cultures. There are six filter insets in the chamber each of 24mm in diameter and the aerosol flow over each of the insets is regulated to 50ml/min. The aerosol is deposited upon the filters using an alternating electrical field, the field can be set from 0 – 4 KV/cm (Savi et al.,2008). The principle of the deposition and the filter insets can be seen in figure 28. The chamber used in the FAS project will have 24 filter inserts for cell deposition.

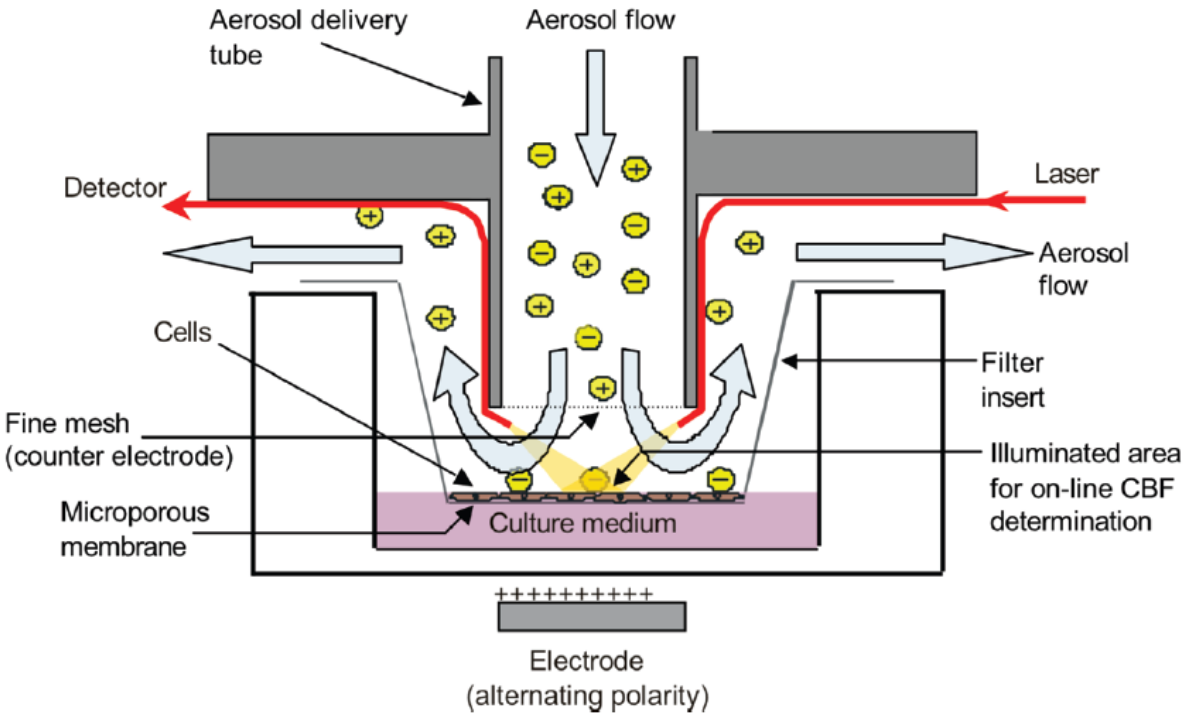

Figur 28 The principle of particle deposition in the deposition chamber developed by Savi et al 2008. The particles is introduced into one of the six filter insets where cell cultures can be placed, each has a diameter of 24mm and an aerosol flow of 50ml/min. The charged particles are deposited upon the cell culture using an electrical field with an alternating polarity, in order that both positive and negative particles may be deposited upon the cell culture and to make sure no charge separation of ions in the cell culture takes place (Savi et al.,2008).

The particles are deposited using an alternating electrical field to prevent accumulation of particles with only one polarity and to ensure that any interference with ionic compounds in the cell culture is minimized. The deposition of charged particles results in an electrical current of about 0,3 fA and Savi et al (2008) concludes that it most likely not will result in any cellular damage. As an comparison damage by for example electroporation occurs at about 100A (Savi et al.,2008).

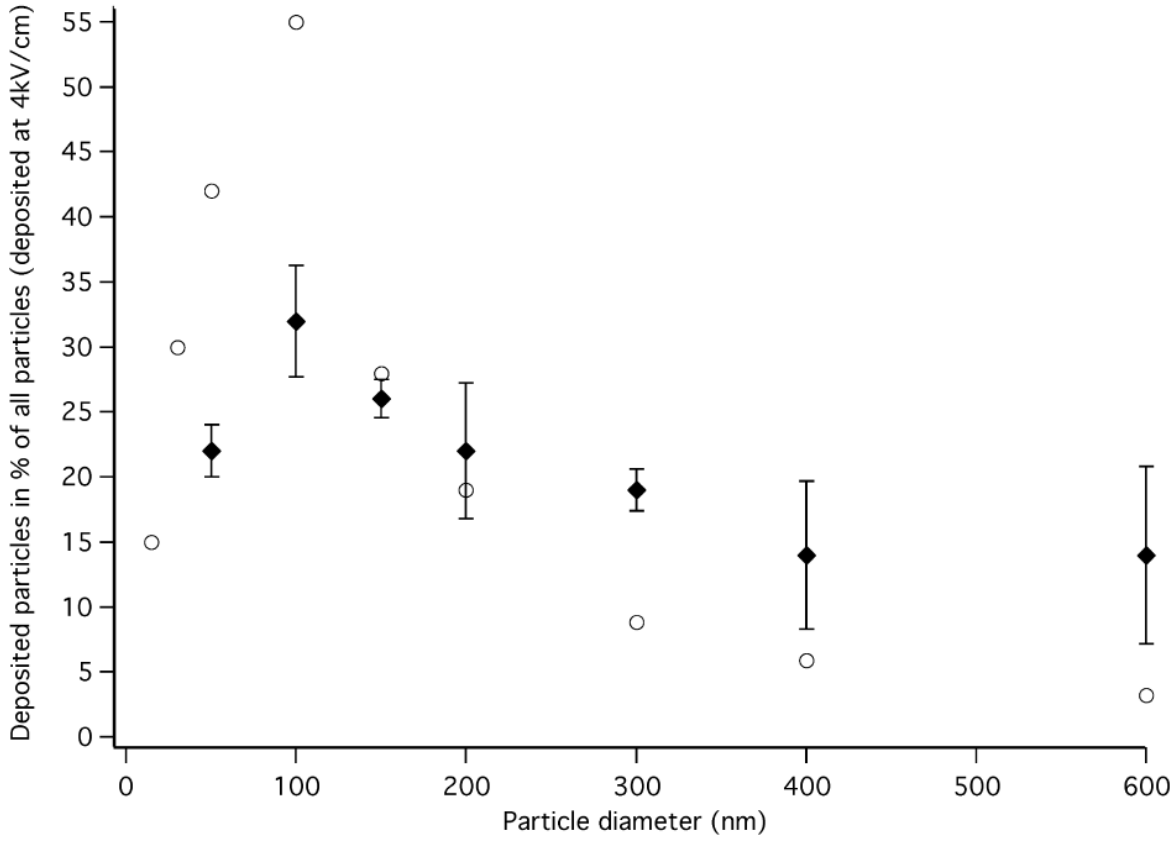

Figure 29 The deposition efficiency for the ALI system, both as modeled (circles) and as experimentally deduced by Savi et al (squares). The efficiencies are valid for an electric field strength of 4 kV/cm in the deposition filter inset. This thesis uses the modeled values to calculate dosages etc.

The deposition efficiency of the deposition chamber was both modeled and experimentally quantified by Savi et al (2008) and a figure of the deposition can be seen in figure 29. The deposition modeled was slightly higher than what Savi et al (2008) experimentally deduced, the deposition efficiency in figure 29 is for an electrical field strength of 4kV/cm. For this thesis and the calculations and adaptation of the modeled deposition was used.

10 Experimentation and modeling

The experiment took place at the department of Solid State Physics at Lunds University. The first experimental session took place in May 2010 and resulted in several particle size distributions generated by the SD system. The size distributions were generated for a spark frequency of 300 Hz.

The second round of experiments took place in June 2010, also at the department of Solid State physics at Lunds University. This time particle size distributions were recreated from the experimentation in May and a high temperature evaporation condensation furnace (HT) was used to create gold aerosol particles of another character. The size distributions was generated for two temperatures for the HT and two different carrier gas flow rates for the

spark discharge system (SD). During the second round of experimentation the APM was also used in order to establish effective density and mass fractal dimension.

In this chapter the system setup, experimental settings and parameters and overview of the methodology will be presented. The methodology will include data processing and relevant modeling.

10.1 May – SD

The experimentation in May was carried out using the SD system of the Solid State Physics department of Lunds Univerisity. The objective of the experiment was to establish a wide range of particle size distributions in order to find distributions with high particle yield and high mean median diameter for the experimentation in June. The mass size distributions were calculated when experimentation in June had taken place and effective density functions had been established for the SD. Also the mass dose and particle surface area dose was calculated for the particle size distributions generated in May using some of the data from the DMA-APM measurements performed in June.

10.1.1 System setup

The system used for experimentation in May was a setup at the Solid State physics department at the University of Lund. The components was integrated into a very dynamic system of tubing, quarter inch steel tubing Svagelok, and any path between the different components could be set, see figure 30 for the system principle. The APM was at this point not introduced into the system. The flow through the system was constant at 1,7 l / min, flow was driven by an overpressure.

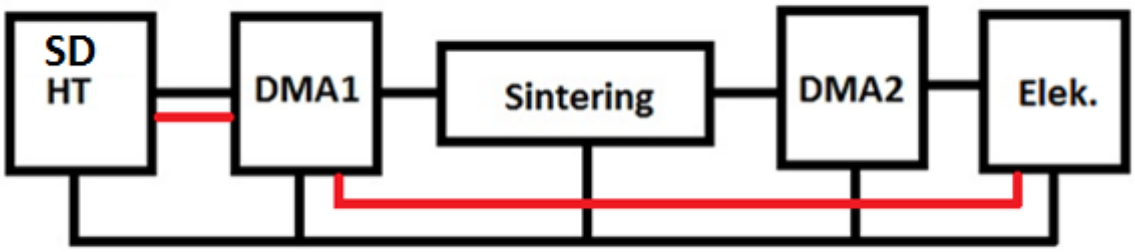

Figur 30 Setup of experimental system at the department of Solid State physics at Lunds University, at this point in May the APM had not yet been introduced to the system. The last point in the system is not as would be expected a CPC but an electrometer. The electrometer measures the electric current the charged particles generates passing it and then this current is calculated into particle number concentration. The lines in the figure between the different devices represent the path that can be set for the aerosol, the red line represent the path the aerosol was set to for the experiment in May.

The DMA set was custom made at the department of Solid State Physics with a sheath flow of 10 l/min. The sintering unit, electrometer and ESP deposition unit was also custom made. The SD and HT systems was of design described in chapter 9.

10.1.2 Method

The SD system was started and let to warm up and was set to a fix spark frequency of 300 Hz and a carrier gas flow rate of 6,2 l/min. For the course of the warm up period several scans was taken by DMA1 to ensure the production of a stable gold aerosol. When the system was deemed stable the first SMPS scan was taken, using DMA1, for the SD setting of 6,2 l/min. After the scan the carrier gas flow rate was changed, after the carrier gas flow rate was changed an SMPS scan was taken for the produced aerosol using DMA1. The carrier gas flow rates were 6.9, 5.9, 5.4, 4.90, 4.67, 4.43, 4.18, 3.93, 3.70, 3.40, 3.14 and 2,85 l/min.

The SMPS data was then corrected using the Fuchs charge distribution and the aerosol as it would be just exiting the particle generator was established. This was an important step since the DMA measurement system at the Solid State Physics department only produced size distributions of charged particles.

In order to establish a mass size distribution for these distributions effective density from the experimentation in June was used. An average density function was derived from the June SD 2,85 and 3,7 l/min settings and it was assumed that this average effective density function would be representative for the distributions generated in May. Using the effective density the mass size distributions was derived.

After the characterization process, size, effective density and mass distributions modeling of dosages took place. The dose was calculated for the Savi et al (2008) deposition chamber and for the human lung, in total and for the alveolar region. Size dependent deposition data was gathered from Savi et al (2008) and from the ICRP lung deposition model for both the total deposition and alveolar deposition (Bailey et al., 1994). The deposition data was used upon the size and mass size distributions and the size dependent deposition for both particle number and mass was acquired. The size dependent deposition, for particle number and mass, was acquired for the Savi et al (2008 deposition chamber, the human lung in total and the alveolar region.

Three methods was used to calculate the particle surface area. The first method was to assume that the *dme* of the particles is the true diameter of the particles and that the particles are spherical, the method is referred to as the *dme* method. The second method was to use the IA theory, referred to as the IA method. The IA theory is described in greater detail in chapter 6. The third method was to use DMA-APM data of the effective density to calculate the aggregate volume, hereby referred to as the APM method. The methodology of the APM method is to extrapolate the particle mass for every *dme* size and using the bulk density of gold to calculate the volume of the agglomerate. The method gives a very exact agglomerate volume under the assumption that the agglomerates consists of pure gold and no other elements. Both the IA and APM method generate particle volume data and in order to calculate particle surface area the size of the primary particles has to be known. The primary particle size was determined by TEM analysis in June and an average value was used. The number of primary particles per aggregate was then calculated for the IA and APM method and their area was summarized to generate the aggregate area. The mass and particle surface

area dosage was then calculated for the Savi et al (2008) deposition chamber, human lung in total and the alveolar region of the human lung.

The area for both the human lung in total and the alveolar area was set to 75m^2 and the breath rate used was 6 l/min. The deposition chamber calculations refer to one filter inset and the parameters modeled upon area a filter area of 4,52 cm^2 and a flow rate of 50 cm^3/min.

10.2 June – SD and HT

The experimentation in June was carried out using the SD system and the HT system of the Solid State physics department of Lunds Univerisity. The objective of the experimentation was to establish particle size distribution, mass size distribution, mass dose, particle surface area dose, effective density, fractal dimension and TEM imagery of a few selected particle sizes.

10.2.1 System setup

The experimental system was set up at the Solid State Physics department at the Lunds University.

The system was set up in the same manner as described in section 10.1.1, with the exception of the APM and CPC. The APM was introduced as described in figure 31, the electrometer was replaced with a TSI 3310 CPC. The other components are the same as in section 10.1.1. The components was integrated into a very dynamic system of tubing and any path between the different components could be set, see figure 31 for the system principle.

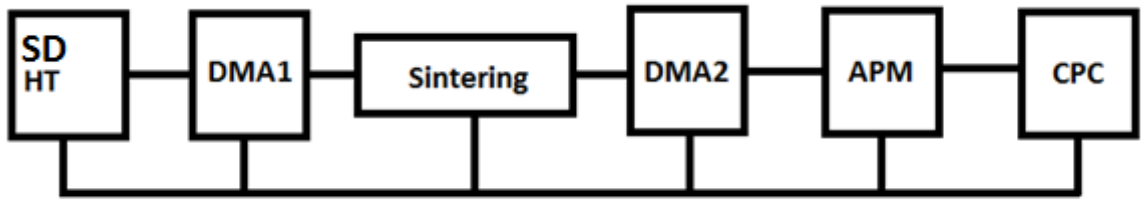

Figure 31 The setup of the experimental system at the Solid State physics department at Lunds University. Both SD and HT are aerosol generation methods, spark discharge and condensation respectively. Valves where placed at every section of the tubing and in every T junction allowing to create any path desired for the aerosol in the system.

The aerosol flow rate through the system was constant at 1,7 l / min and the flow was divided before the APM into one 0,8 l/min and one 0,9 l/min flow. One of these flows was passed into the APM and the other was released into the atmosphere through a particle filter. The flow was branched because the CPC draws aerosols at this rate. If the flow was not branched an overpressure would set in as the output of 1,7 is greater than the output of 0,8, an opening to the atmosphere eliminates this problem.

10.2.2 TEM

The primary particle size was determined for the two generation methods by analyzing TEM images. TEM sample grids was collected after DMA 1. Five aggregates for each deposited *dme* size and setting was analyzed. An average primary particle size was then calculated for each setting. The primary particle size derived during the analysis is the primary particle size

used in all calculations where necessary. The particles was deposited using an electrostatic deposition chamber.

10.2.3 Method

Experimentation in June took place over several days, the measurements of the SD system 2,85 and 3,7 l/min took place on to separate occasions and both the HT settings on the same day as the SD 3,7 l/min setting. Various measurements was taken for the course of the experimentation the method will however only describe the measurements relevant for this thesis.

The SD system was started and let to stabilize for a carrier gas flow rate of 2,85 l/min and spark frequency of 300 Hz. Several SMPS scans was taken to assure a stable aerosol generation. When the system was stable an SMPS scan for the setting was taken using DMA1. Mono disperse aerosol flows was selected using DMA1 and measured upon by the APM. Mono disperse fractions selected was 10, 15, 20, 40, 60 and 80nm *dme*. After the initial SMPS and APM measurements the aerosol was deposited onto a semiconductor silicon plate in a electrostatic deposition unit for TEM analysis. The deposition fraction was selected by DMA1 and bypassed every other unit to the deposition unit. The deposition was carried out for both 10 and 60nm *dme* agglomerates. These measurements concluded the first occasion.

On the second day the SD system was first measured upon. The methodology was the exact same as for the previously described i.e. for 2,85 l/min.

The second series of measurements on the second occasion was for the HT system and 1575 °C setting. The HT system was started and let to stabilize for a carrier gas flow rate of 1,7 l/min and a condensation evaporation temperature of 1575 °C. The methodology was the exact same as for the previously described i.e. for 2,85 l/min and 3,7 l/min for the SD system.

The second HT setting of 1625 °C was performed during the same occasion. The HT system was let to stabilize for a carrier gas flow rate of 1,7 l/min and a condensation evaporation temperature of 1625 °C. The methodology was the exact same as for the previously described i.e. for 2,85 l/min and 3,7 l/min for the SD system and HT system with the exception that only 60nm *dme* agglomerates was deposited for TEM analysis.

The SMPS data was then corrected using the Fuchs charge distribution and the aerosol as it would be just exiting the particle generator was established. Also particles of various *dme* was deposited and TEM analysis was performed by the department of Solid State Physics. Using the TEM imagery primary particle size analysis was performed.

In order to establish a mass size distribution for these distributions effective density was established for each generation method and setting. Mono disperse aerosol flows selected by DMA 1 was measured by the APM for 10, 15, 20, 40, 60 and 80 nm *dme* and effective density was established for each size distribution, see figure 32 for a typical APM measurement.

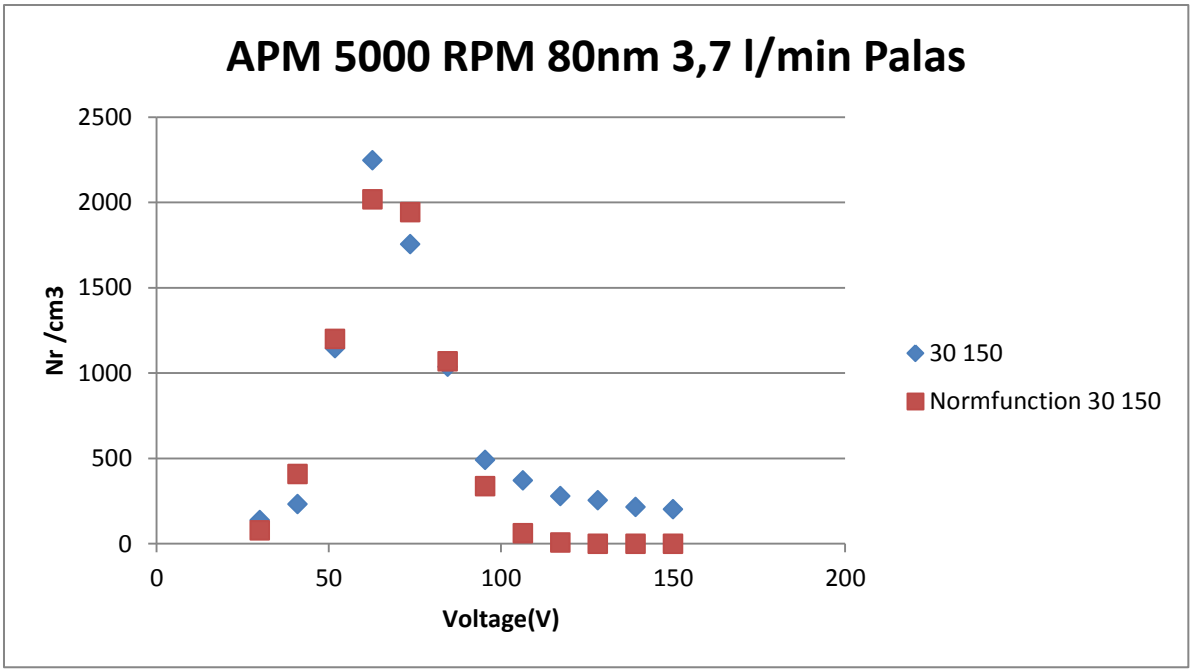

Figure 32 A typical APM result from the experimentation in June. Voltage is plotted against particle number concentration along with a normfunction fit to determine the mean voltage and mass for the particles. The graph is for 80 nm particles generated for SD with carrier gas flow rate of 3,7 l/min. The mass of the particles was calculated to 3,86 *10^-19 Kg.

After establishing the effective density the mass distributions was calculated. It was done by interpolating the size dependent mass of the particles and summarizing the total mass for each size fraction using the size distributions. In addition to the effective density the fractal dimension was calculated for each generation method and setting. The fractal dimension was calculated by fitting a power function to the size dependent effective density data, as described in chapter 6.7.

After the characterization process dose modeling and calculation of particle surface area dosage was performed using the exact same methodology as described in section 10.1.2. The same parameters for the ALI system and respiratory system was used as well.

11 Results

This section will present the collected results generated both through theoretical modeling and experimental results, the results will be presented in concordance with the thesis objectives.

11.1 May – SD

11.1.1 Particle size distributions

Particle size distributions was established for the SD system with a single spark generation frequency of 300 Hz and with carrier gas flow rates from 2,85 to 6,2 l / min, see figure 33.

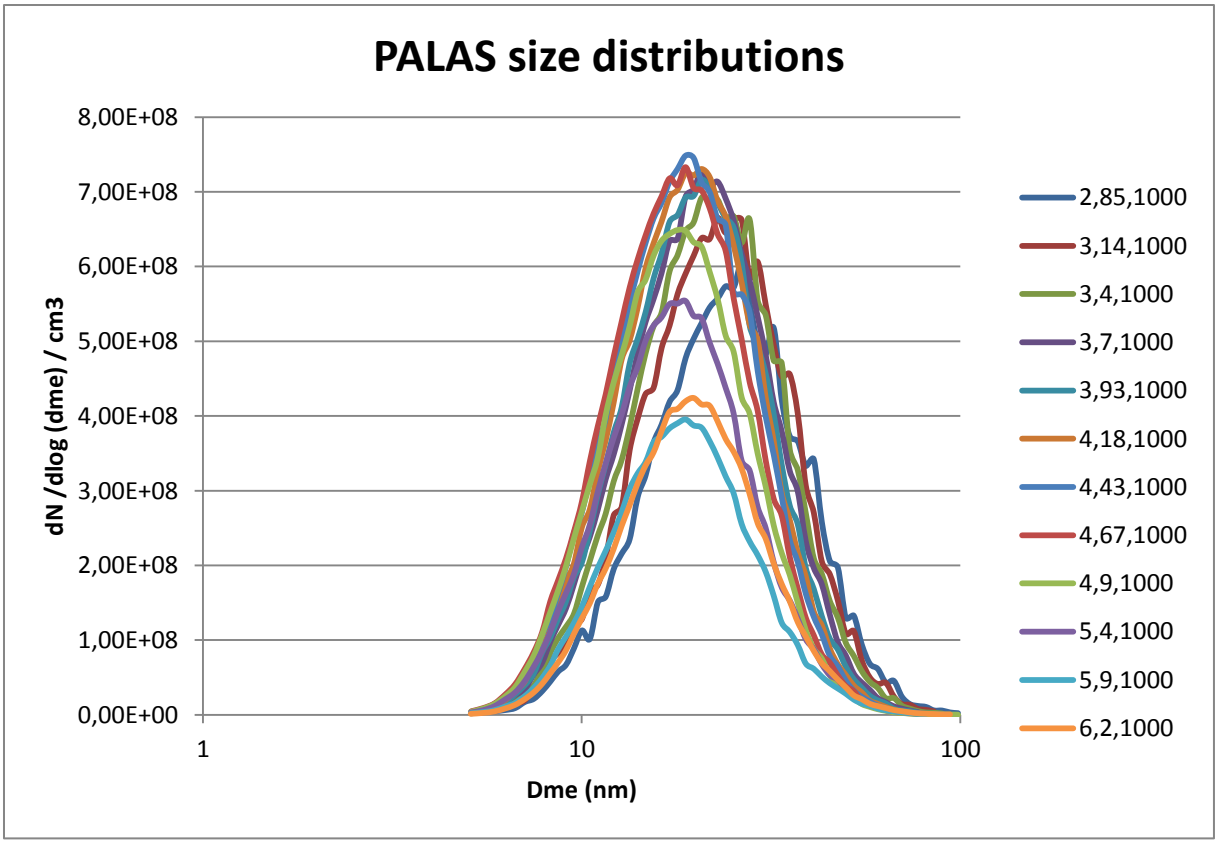

Figur 33 Particle size distributions generated by the SD sparkdischarge generator. The distributions are generated for 1000 scale, representing 300 Hz of spark frequenzy and for different carrier gas flow rates. The carrier gas flow rate is indicated to the right in the figure and is given as l / min. The Distribution is corrected according to the Fuchs charge distribution of negative single charged particles and are as displayed representative of the distribution before entering the SMPS system.

The mean median diameter of the size distributions are approximately 20 nm for the higher carrier gas flow rates, the mean median diameter seems to shift towards 30 nm as the carrier gas flow rate decrease towards 2,85 l/min.

The particle number concentration varies from $4{,}00 \cdot 10^8$ particles/cm^3 to $7{,}00 \cdot 10^8$ particles/cm^3 from 6,2 l/min to 3,93 l/min of carrier gas flow and drops to about $6{,}00 \cdot 10^8$ particles/cm^3 as the carrier gas flow decrease to 2,85 l/min. The maximum particle yield then is for a carrier gas flow of 3,93 l/min.

For the low carrier gas flow rates there seems to be a tradeoff between a high particle yield and a higher mean median diameter. Messing et al (2009) found that the mean median diameter for a carrier gas flow rate of 5,9 l/min and spark frequency of 300 Hz was about 20-30 nm *dme*, this compares well with the result of this thesis which also shows between 20 and 30 nm *dme*.

11.1.2 Mass size distributions

Mass size distributions were calculated using effective density data from the SD experimentation in June for each of the particle size distributions i.e. one particle size distribution combined with effective density generates on mass size distribution. The mass size distributions can be seen in figure 34.

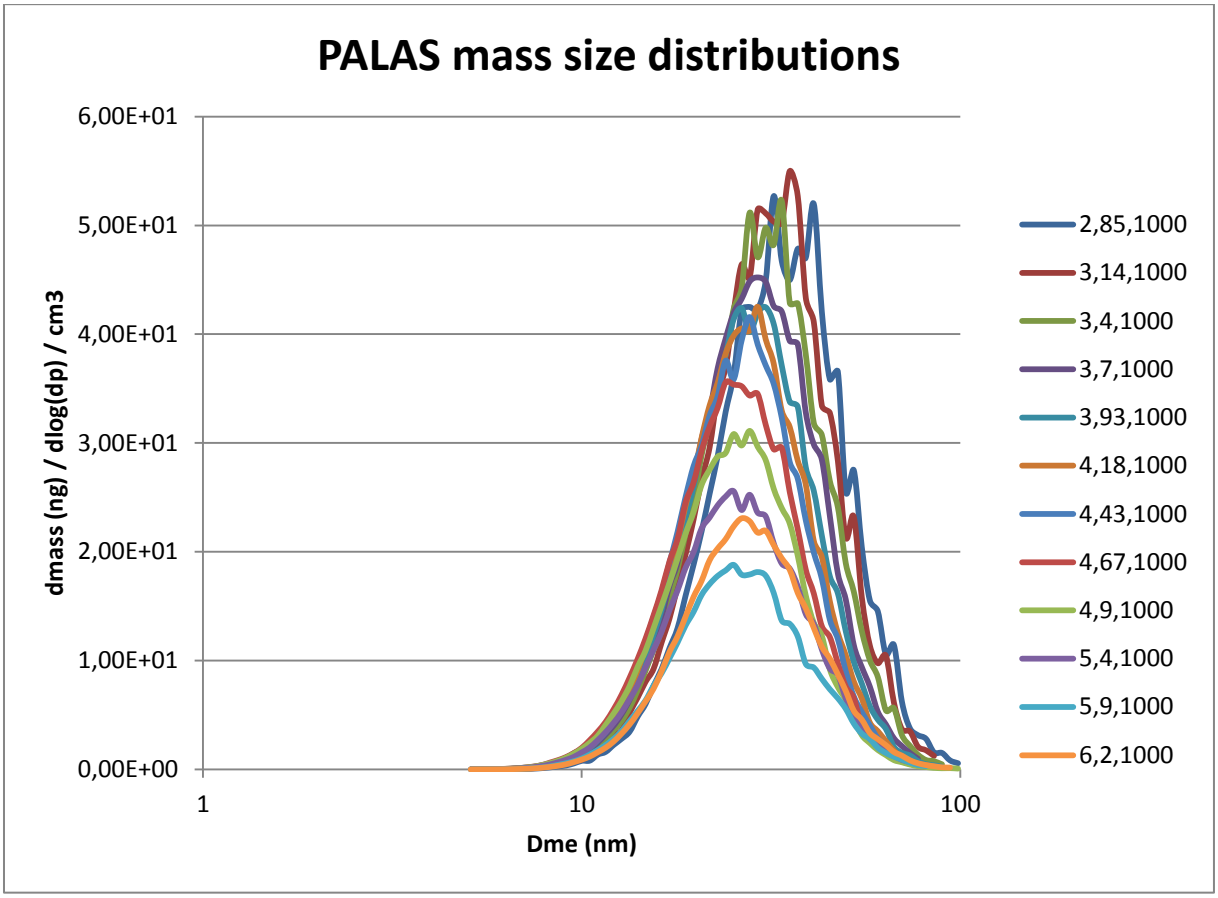

Figure 34 Mass size distributions calculated from the particle size distributions and the effective density generated during experimentation in June. The legend gives the actual carrier gas flow rate as the first number from the left followed by two decimals, followed by spark frequency given as 1000 scale resembling 300 Hz of spark frequency.

A carrier gas flow of 5,9 l/min result in the lowest mass output and 6,2 l/min the second lowest. The mass output thereafter increase as the carrier gas flow decrease, a carrier gas flow of 2,85 l/min seems to yield a comparable mass distribution and mass output to that of 3,14 l/min. Figure 33 of the particle size distributions show that the particle number decrease for the lowest carrier gas flows, the mass output does not decrease as carrier gas flow decrease. This means that the particles generally become fewer for the low carrier gas flows and also have more mass. The mean median diameter for the mass size distributions varies from 25-30 nm *dme* for 5,9 and 6,2 l/min to approximately 40 nm *dme* for 2,85 and 3,14 l/min.

11.1.3 Particle mass dose

The mass dose was calculated for each of the particle size distributions and for the deposition chamber, the human lung in total deposition and in alveolar deposition. The mass doses can be seen in figure 35.

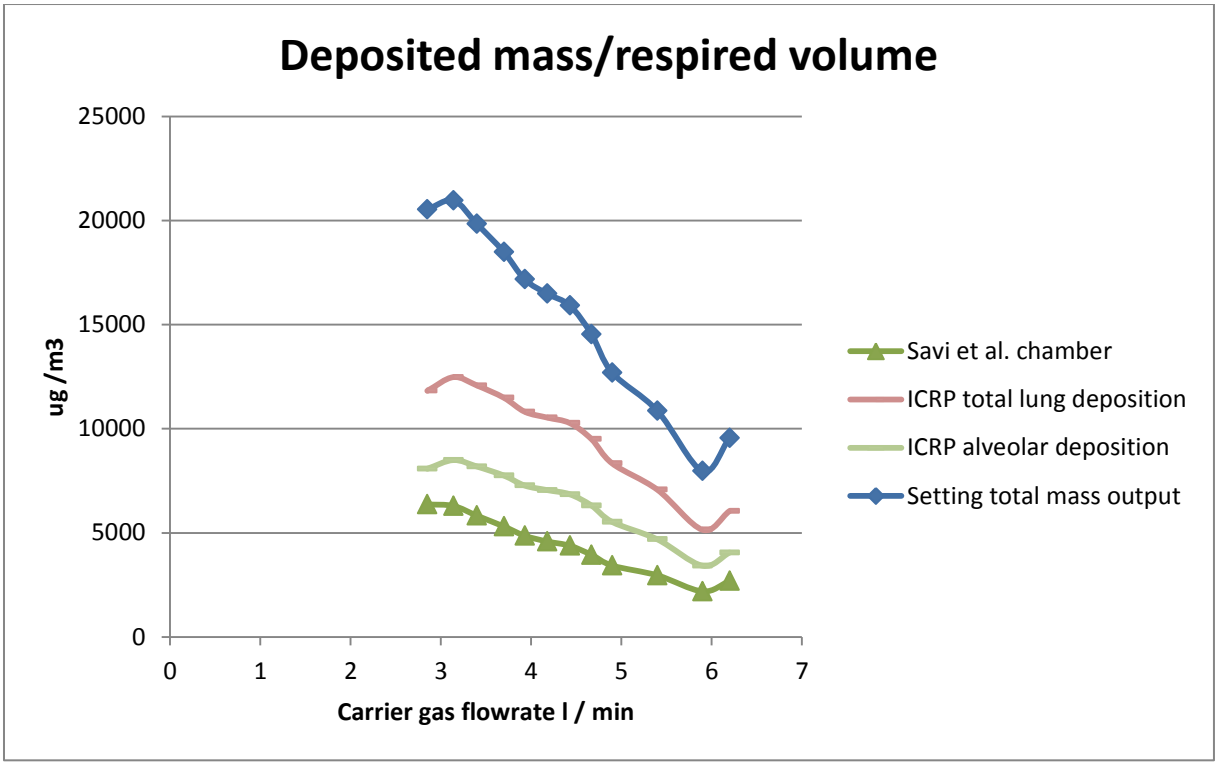

Figure 35 Mass doses for the Savi et al. deposition chamber and for total lung and alveolar deposition. Dose is given as mass per cubic meter of exposure air volume as a function of carrier gas flow rate. The dose is calculated so that the dosage value is what actually is deposited per unit volume.

The mass dose refers to the total particle mas per SD setting that actually deposit in either the Savi et al (2008) deposition chamber or the human lung. The mass dose is in figure 35 calculated as the total deposited mass per total respired aerosol volume i.e. if one where to respire one cubic meter of aerosol from a SD setting of 2,85 l/min and 300Hz approximately 6000 µg of gold would deposit in the deposition chamber. The deposition patterns are similar for the three deposition places. A higher deposition can be seen for a carrier gas flow of 6,2 l/min than 5,9 l/min which is consistent with a higher mass output for 6,2 l/min. Also a slight decrease of deposited can be seen for a carrier gas flow of 2,85 l/min compared to 3,14 l/min.

The mass dose per unit time and surface area can be seen in figure 36.

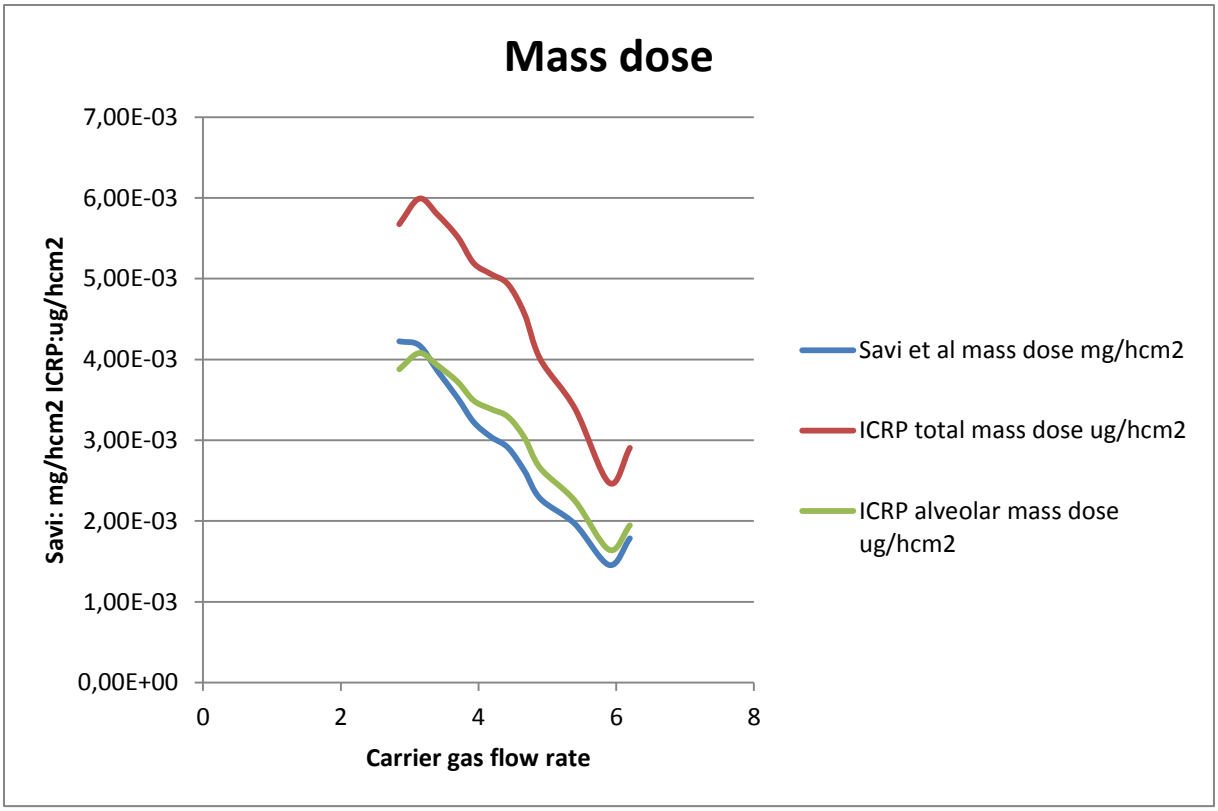

Figur 36 Mass dose calculated for the ICRP and ALI system. The mass dose is calculated as mass per unit time and deposition surface area and plotted against the carrier gas flow rate.

The mass doses in figure 36 has the same deposition pattern as in figure 35. The deposition for the deposition chamber is a factor 1000 greater than that for the ICRP lung deposition, this is due to the great surface area of the human lung.

11.1.4 Particle surface area dose

The particle surface area dose was calculated for the established particle size distributions from the SD system. The particle surface area was also calculated using three methods. The first method is assuming that the Dme of the particles is the real diameter and from that calculate the particle surface area, the second is to use the idealized aggregate theory by Lall et al 2008 to calculate the total particle surface area. The third method was to calculate the agglomerate volume using effective density data, referred to as the APM method. The effective density data used for the modeling was the effective density data from the experimentation in June. These will be referred to in this section as Dme based particle surface area, L & F based surface area and APM based respectively. The doses for the deposition chamber can be seen in figure 37 and the calculated doses for the human lung can be seen in figure 38.

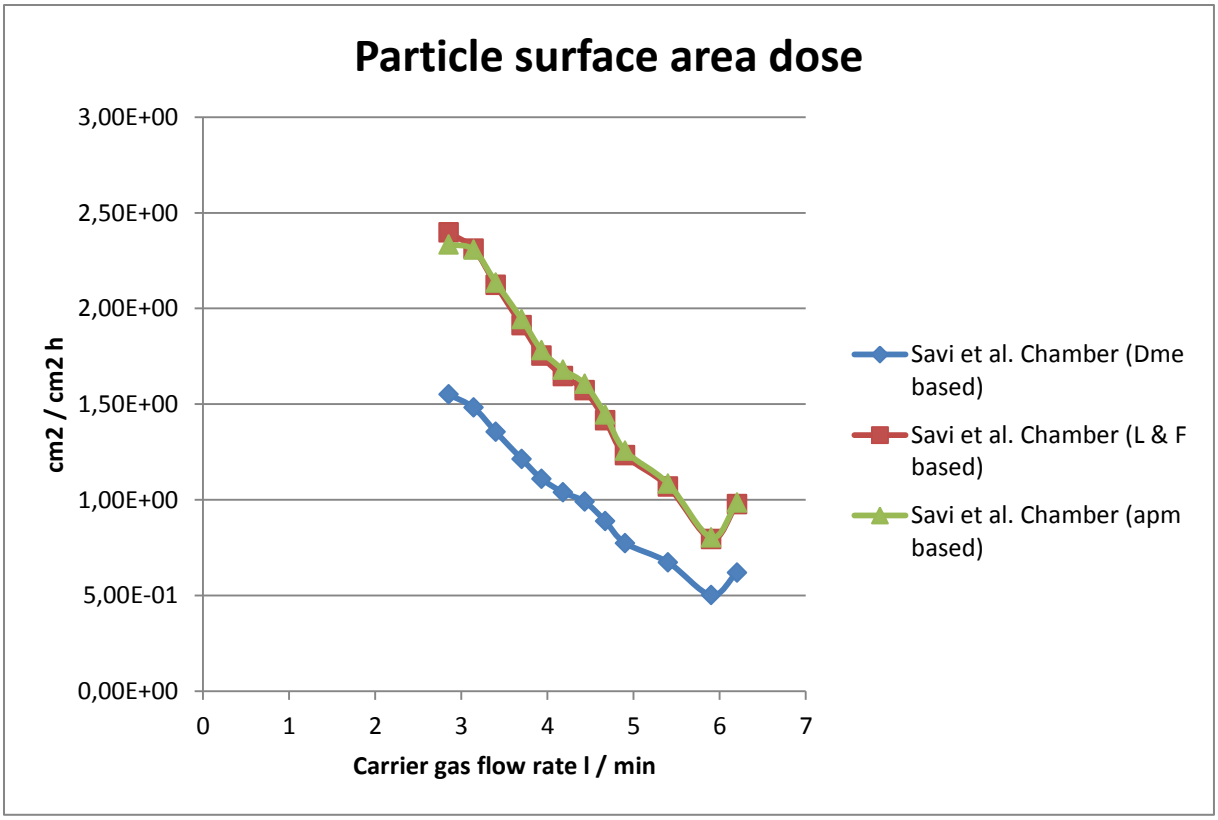

Figur 37 The modeled particle surface area dose for the measured particle size distributions. The particle surface area dose is in the figure given as particle surface area per deposition surface area. The dosage in the figure is for the deposition chamber and for both Dme based and L & F based particle surface area.

The dosage for the particle surface area has the unit cm^2/cm^2h i.e. total deposited particle surface per deposition surface area and hour. Figure 37 shows the modeled particle surface area dose for the deposition chamber, for all three methods of calculating the particle surface area. The dosage is highest for the lower carrier gas flows and decrease for the higher carrier gas flows. An increase in deposition can be seen for 6,2 l/min and is consistent with the increase of both mass and particle number compared to 5,9 l/min of carrier gas flow.

The dosage is comparable for all three methods of calculating the particle surface area. The IA method and APM method yields almost identical results, consistent with Lall et al (2008) that the IA volume and apm volume of agglomerates are almost identical. The *dme* metihd results in a slightly lower dose for all carrier gas flows.

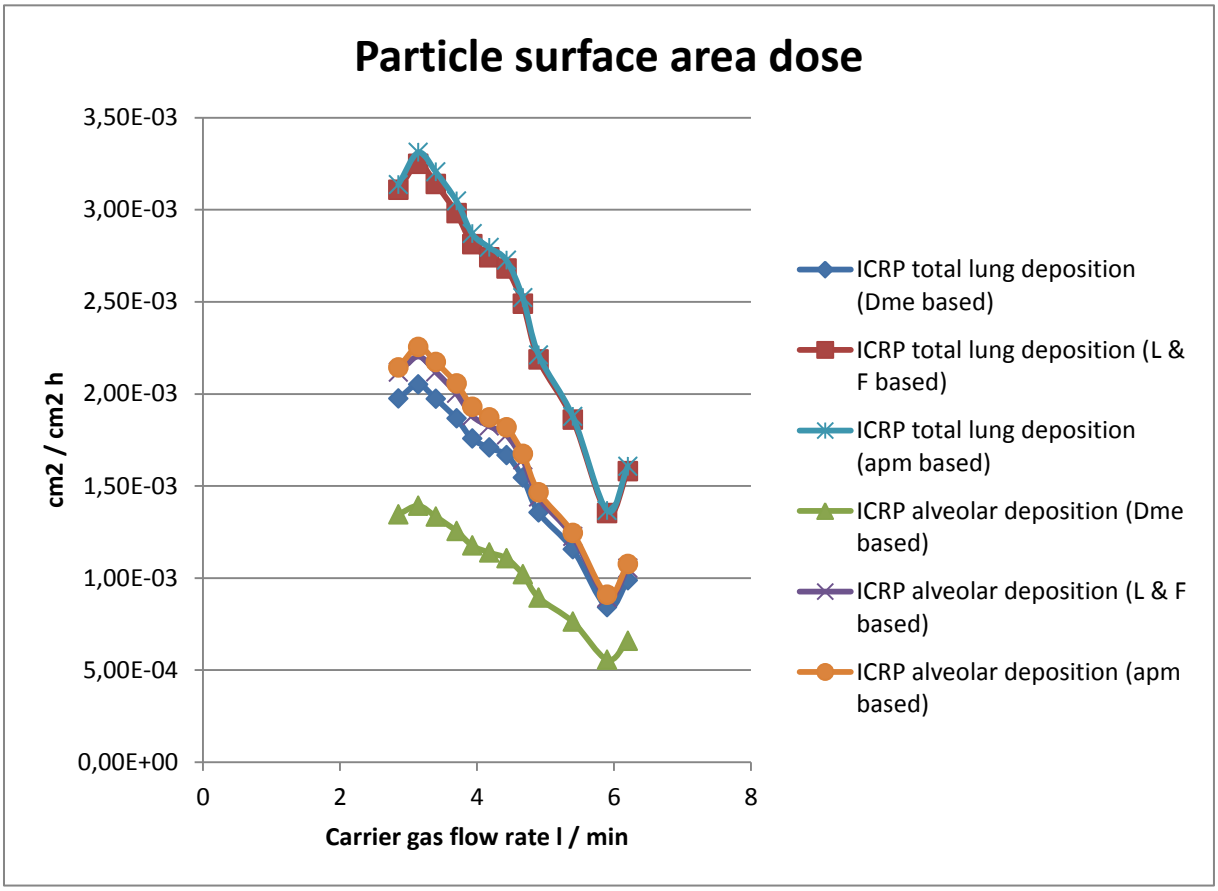

Figur 38 Particle surface area doses corresponding to those in figure 36, the doses in this figure is calculated using the ICRP deposition model. The doses is in plotted as a function of the carrier gas flow rate and for both Dme based and L & F based particle surface area dosage.

The particle surface area dosage for the human lung using the ICRP model is the same as for the deposition chamber. The dosage shoes the same pattern in the human lung and alveolar region as in the deposition chamber and is about a factor 1000 lower than in the deposition chamber, analogous to the mass dosage calculations this is due to the very high surface area of the human lung and alveolar region.

11.2 June – SD and HT system

11.2.1 Particle size distributions

The particle size distributions was established for the SD system and the HT system with the predetermined settings. The particle size distributions can be seen in figure 39.

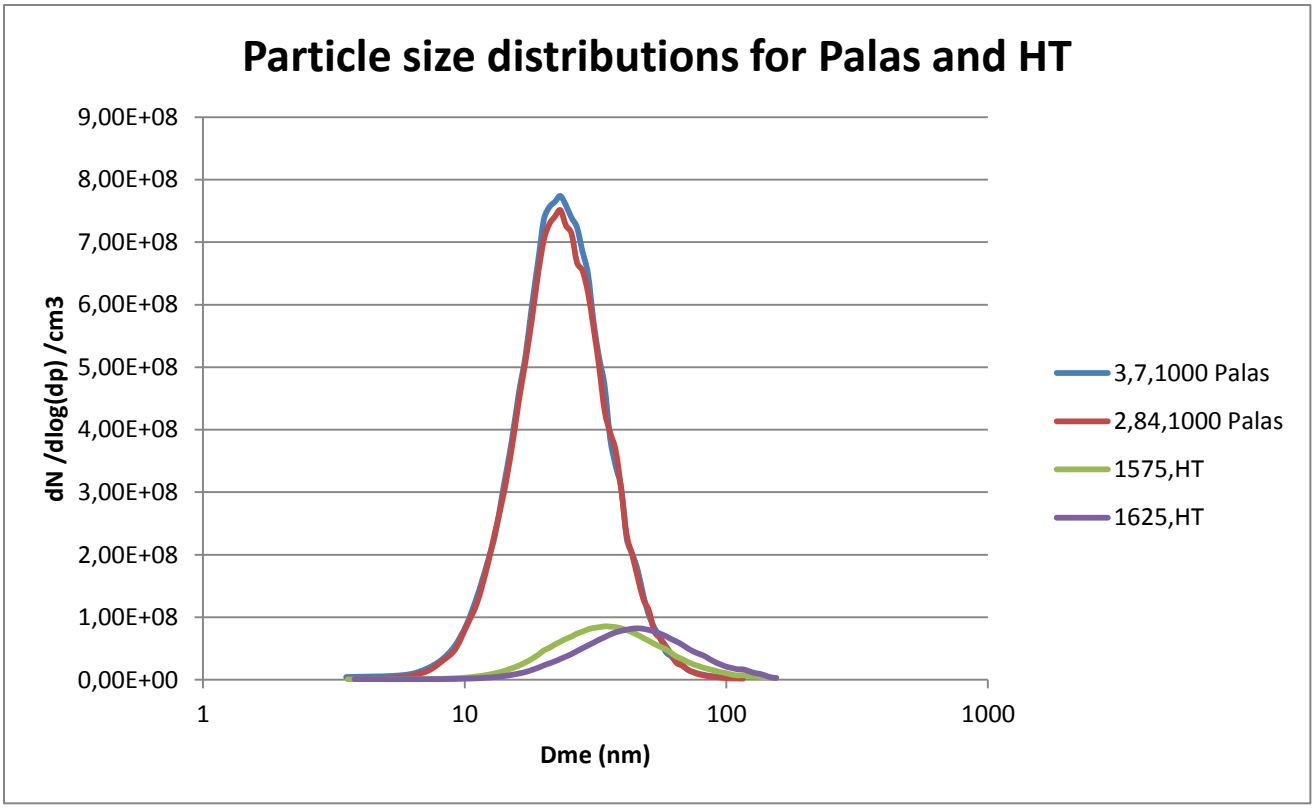

Figur 39 Particle size distributions generated for the SD and HT system in June. The SD was scanned for one spark generation frequency of 300 Hz and for two carrier gas flow rates 2,84 and 3,7 l/min. The HT system was scanned for two generation temperatures 1575 and 1625 °C. The Distribution is corrected according to the Fuchs charge distribution of positive single charged particles and is as displayed representative of the distribution before entering the SMPS system.

The two settings for the SD system, 2,85 and 3,7 l/min, results in similar particle size distributions as the same settings during experimentation in May. The particle yield for the HT system is significantly lower than for the SD system, almost a factor 10. The mean median diameter is larger for the HT system, about 50nm *dme* compared to the SD systems 30nm *dme*. The second HT setting, of 1625 °C, also has slightly higher mean median diameter than 1575 °C.

11.2.2 Particle mass size distributions

The particle mass size distributions was established for the SD and HT system. The mass size distributions was generated from the particle size distributions using the effective density function for each particle size distribution respectively i.e. each particle size distribution combined with that distributions effective density function generates a mass size distribution. The distributions can be seen in figure 40.

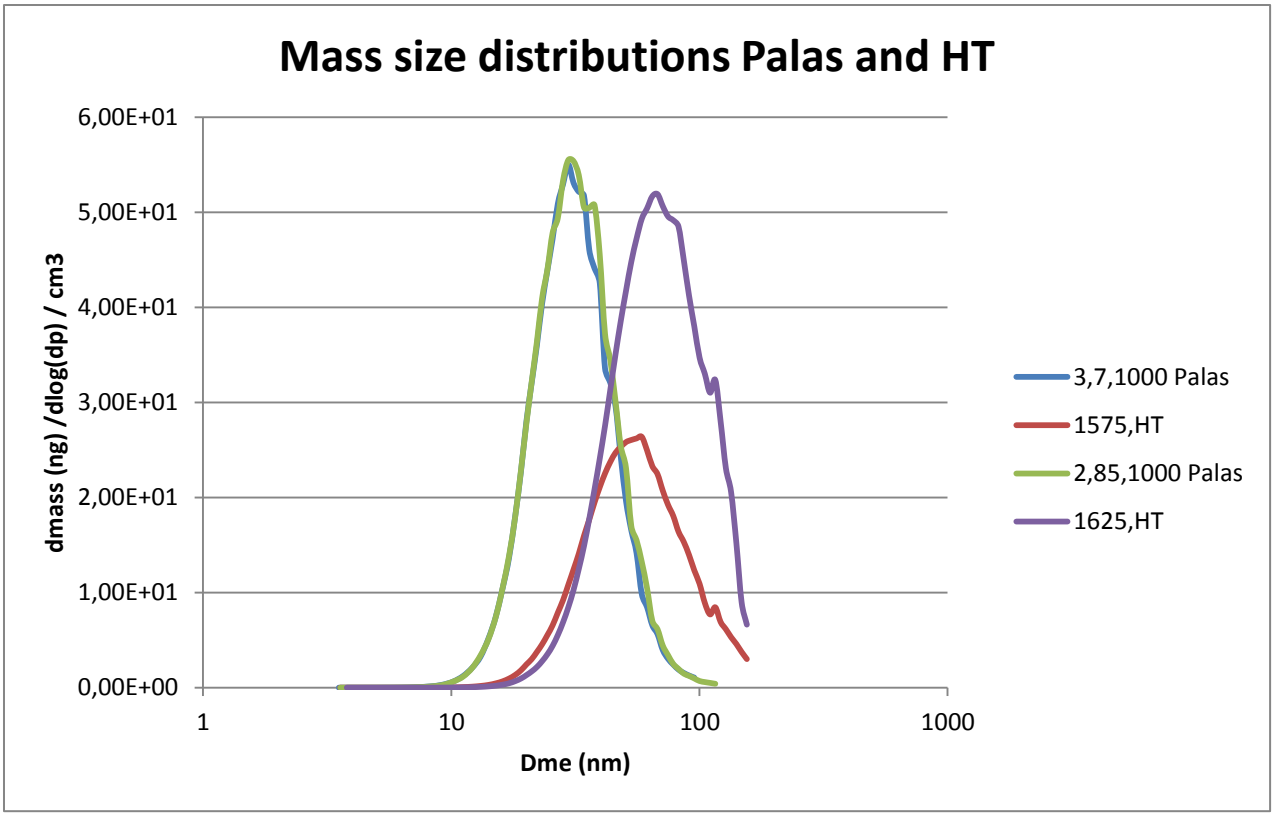

Figur 40 Mass size distributions generated from the particle size distributions using effective density functions established for each corresponding particle size distribution. The SD system was scanned for two carrier gas flow rates and for one spark discharge frequency 2,85 3,7 l/min and 300 Hz respectively. The HT system was scanned for two temperatures 1575 and 1625 °C of generation temperature.

The mass size distributions generated by the two SD settings, 2,85 and 3,7 l/min carrier gas flow, are just as the size distributions very similar and comparable to the ones generated during the experiment in May. The HT system produces comparable mass distributions to the SD system although the mass distributions for the HT system is significantly shifted to larger particles than the SD. The second setting of 1625 °C produces a very similar dose distribution to that of the SD systems settings, the first HT setting differs approximately a factor 2 from the SD system.

The mean median diameter for the mass distributions are significantly higher than for the SD system. Setting 1575 °C has approximately a mean median diameter of 60nm and 1625 °C approximately 70nm, the SD system has a mean median diameter of about 30nm *dme*. The SD systems mean median diameter for particle number and mass coincide, the most particle mass is also where the most particles can be found. However the HT system has a mean median diameter for size about 40nm and for mass about 60-70nm *dme*. The most mass can be found for fewer particles but with significantly more mass.

11.2.3 Particle mass dose

The mass dose was calculated for each of the particle size distributions and for the deposition chamber, the human lung in total deposition and in alveolar deposition. The mass doses can be seen in figure 41.

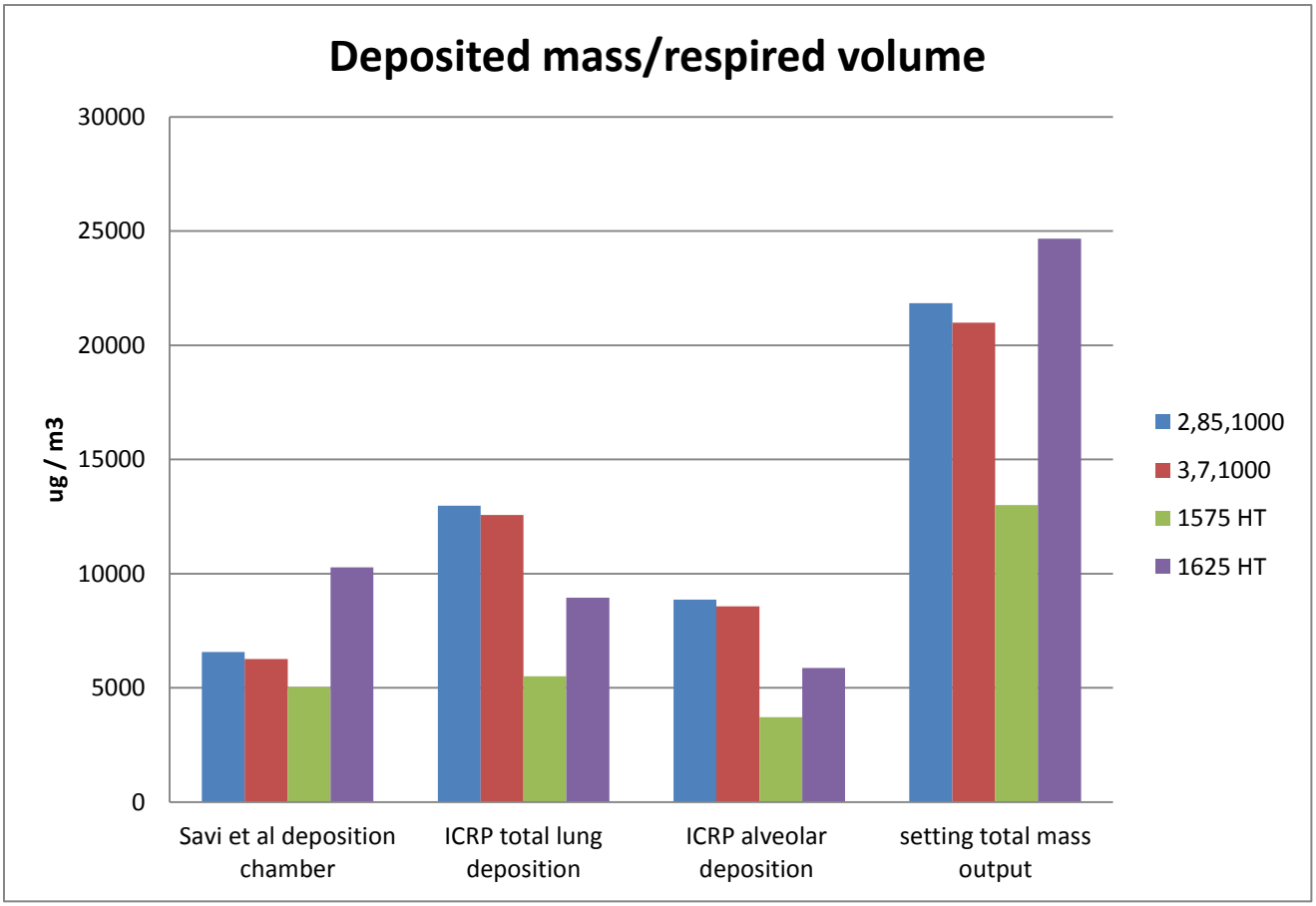

Figur 41 Mass doses for the Savi et al. deposition chamber and for total lung and alveolar deposition. Dose is given as mass per cubic meter of exposure air volume as a function of carrier gas flow rate. The dose is calculated so that the dosage value is what actually is deposited per unit volume. SD system is calculated for single spark frequency of 300 Hz and carrier gas flow rates of 2,85 and 3,7 l/min, HT system for generation temperatures of 1575 and 1625 °C.

The mass dose for the SD systems settings are highly similar to the corresponding setting for the experiment in May, the dose are approximately 6000 $\mu g/m^3$ for the SD settings both in May and June for the ALI.

The deposition in the human lung is similar to that of the deposition chamber with smaller differences. The SD settings seem to have a higher deposition in the alveolar tract and the human lung in total than the deposition chamber whereas the deposition chamber has a high deposition from the HT system settings similar to the deposition in human lung in total. The high deposition in the deposition chamber for the HT settings compared to the alveolar region can be explained by a difference in the deposition pattern between them see figure 9 and figure 29. The deposition in the deposition chamber is higher for the mean median diameter of the mass distribution for the HT settings than the alveolar deposition patterns by ICRP i.e. more particles with more mass deposit in the deposition chamber than the alveolar tract.

The SD settings has the highest deposition in the human lung in total and this is consistent with the fact that the human lung in total has a very high deposition efficiency, see figure 9, for the mean median diameter of the SD settings.

The mass dose per unit time and surface area can be seen in figure 42.

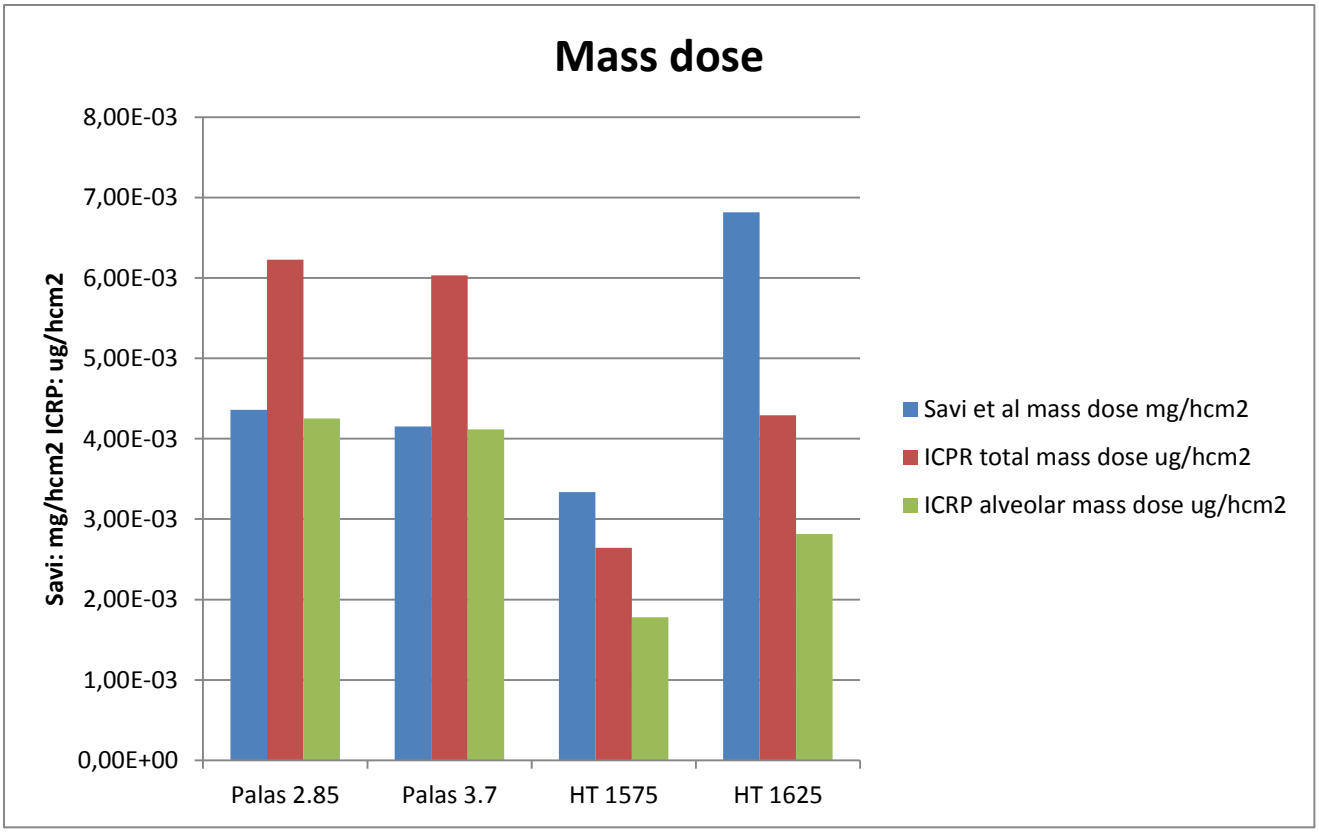

Figure 42 Mass dose for the HT and SD systems derived from experimentation in June 2010 at the department of Solid State physics at Lunds university. The mass dose is calculated for the ALI system and for the ICRP lung deposition model, the dose is given as mass per unit time and surface area. The calculated dose for the ALI chamber is a factor 1000 larger than the respiratory system, mainly due to larger deposition area in the human lung.

The mass dose calculated in figure 42 has the unit $\mu g/cm^2h$ i.e. micrograms per deposition surface area and hour of exposure, just as the mass dose calculated for the experiment in May. The deposition for the deposition chamber is approximately 1000 times higher than the deposition in the alveolar region and the lung in total. This is due to the high deposition surface area of the human lung compared to the deposition chamber. The deposition pattern in figure 42 is very similar to the pattern in figure 36 for the SD settings.

11.2.4 Particle surface area dose

The particle surface area dose was calculated for the established particle size distributions from the SD and the HT system. The particle surface area was also calculated using three methods. The first method is assuming that the Dme of the particles is the real diameter and from that calculate the particle surface area, the second is to use the idealized aggregate theory by Lall et al 2008 to calculate the total particle surface area. The third method is to use DMA-APM data for the effective density to calculate agglomerate volume and agglomerate surface area. These will be referred to in this section as Dme based particle surface area Lall et al 2008 based surface area and APM based surface area respectively. The doses for the deposition chamber can be seen in figure 43 and the calculated doses for the human lung can be seen in figure 44.

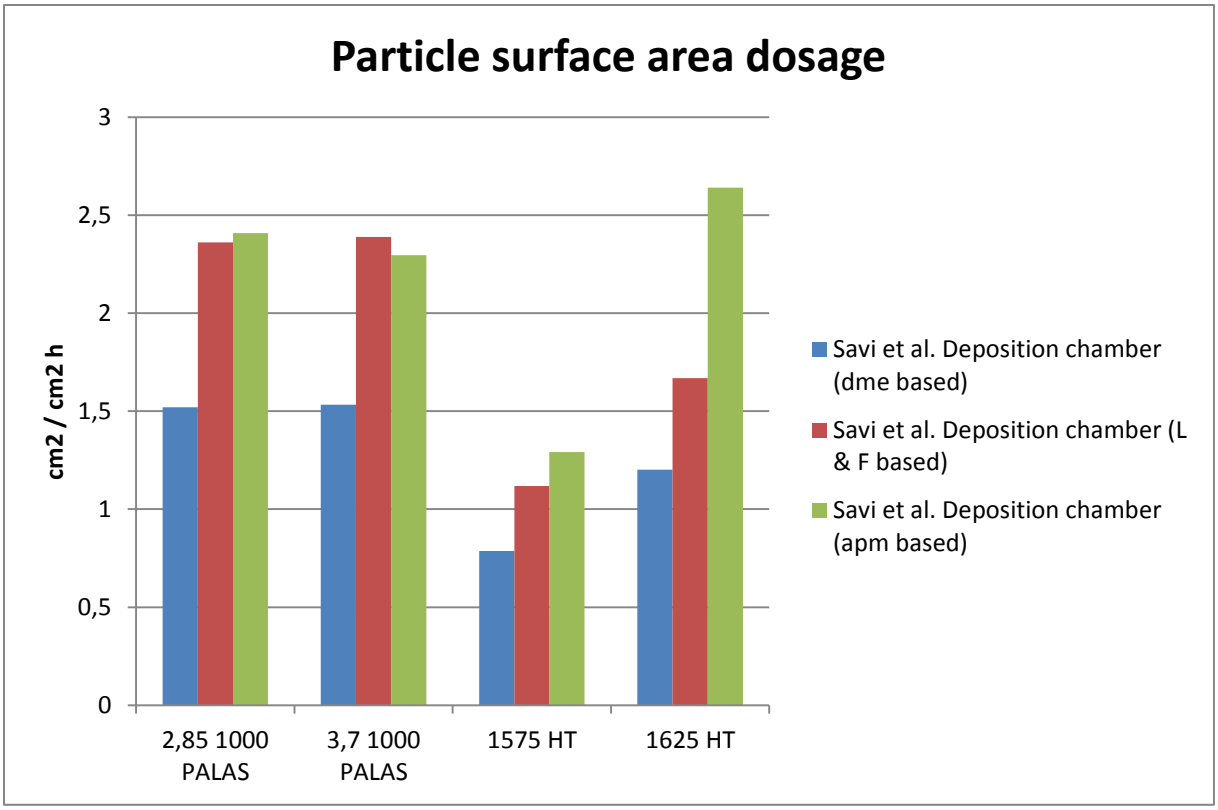

Figur 43 The modeled particle surface area dose for the measured particle size distributions. The particle surface area dose is in the figure given as particle surface area per deposition surface area. The dosage in the figure is for the deposition chamber and for both Dme based and L & F based particle surface area. . SD system is calculated for single spark frequency of 300 Hz and carrier gas flow rates of 2,85 and 3,7 l/min, HT system for generation temperatures of 1575 and 1625 °C.

The particle surface area dose calculated has the same unit as the experimentation in May, cm^2/cm^2h i.e. total particle surface area per deposition surface area and hour of exposure. The results in figure 43 compare well with the results in figure 37 for the SD system. The HT system settings yield slightly lower particle surface area doses except the APM based particle surface area dose for the HT 1625 °C setting which is the highest for all methods and other settings.

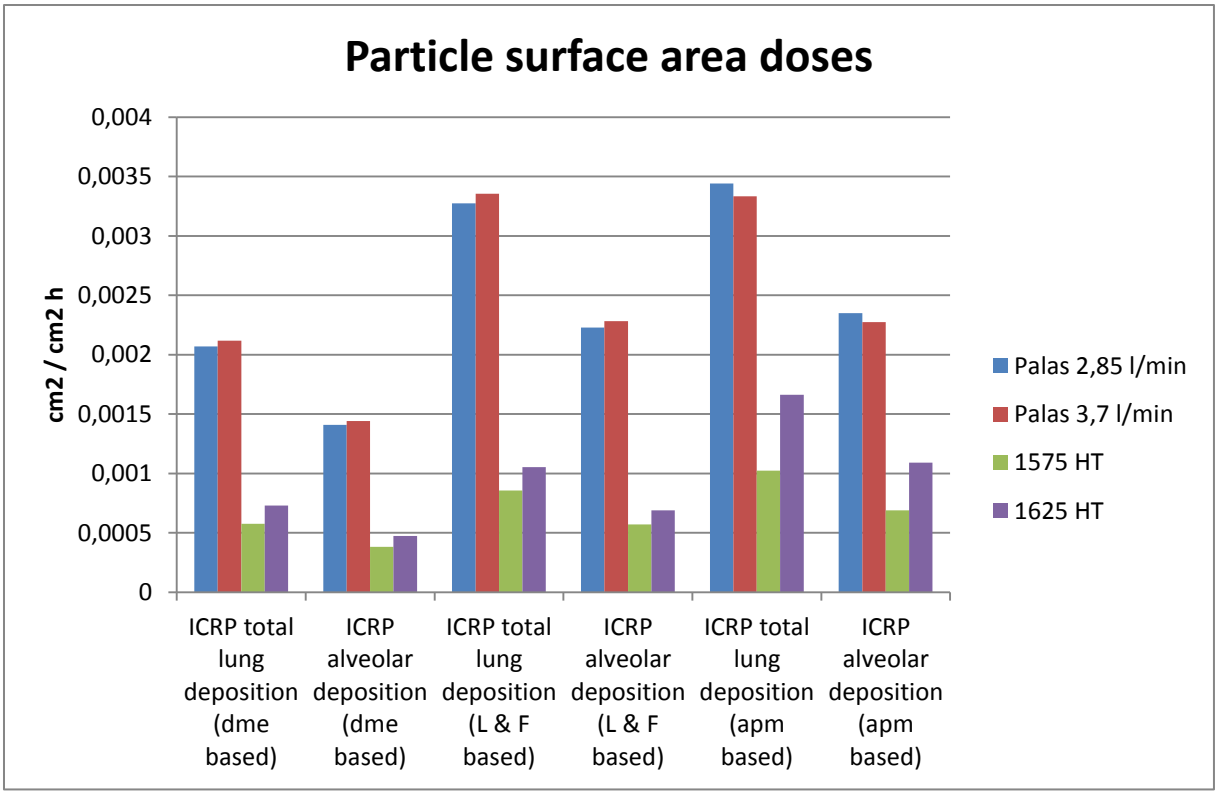

Figur 44 The modeled particle surface area dose for the measured particle size distributions. The particle surface area dose is in the figure given as particle surface area per deposition surface area. The dosage in the figure is for the ICRP model lung and alveolar deposition and for both Dme based and L & F based particle surface area. SD system is calculated for single spark frequency of 300 Hz and carrier gas flow rates of 2,85 and 3,7 l/min, HT system for generation temperatures of 1575 and 1625 °C.

The lung deposition calculated using the ICRP model in figure 44 compares well with the corresponding deposition from the experiment in May, see figure 38. The lung deposition both in the alveolar region and in the lung in total is significantly higher when the IA and APM method is used. The deposition pattern overall indicate a factor of approximately 1000 times lower deposition in the human lung than in the deposition chamber, due to the much larger deposition area in the human lung.

11.2.5 TEM imagery

In order to gain knowledge about primary particle size and the true state of agglomeration among the generated gold particles TEM imagery was carried out on various particle sizes. A comparison between 60nm gold agglomerates from the SD system and the HT system can be seen in figure 45.

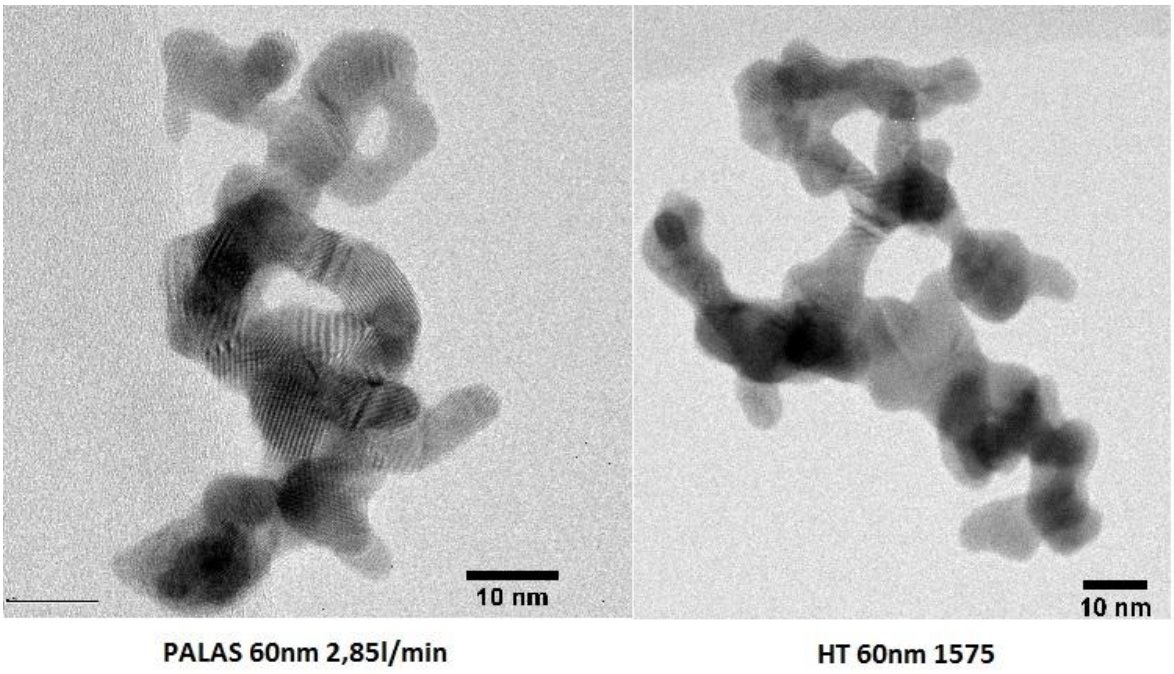

Figur 45 Two TEM images of 60nm gold agglomerates from both the SD and HT system. The SD system was sampled for TEM for the 300 Hz 2,85 l/min carrier gas flow setting and the HT system sampled for generation temperature of 1575 °C.

11.2.5.1 Determination of primary particle size

The primary particle size determined in figure 46 is used in all calculations for each method and setting respectively when necessary. For the Ht 1625 °C setting the primary particle size of the 60 nm particles was also used for the 10nm particles during calculations, this because 10nm particles was not deposited for TEM analysis for that setting.

Five agglomerates was analyzed using ImageJ for each generation method and setting, 10 primary particles was measured for each particle and when there was fewer than 10 as many as possible was measured upon.

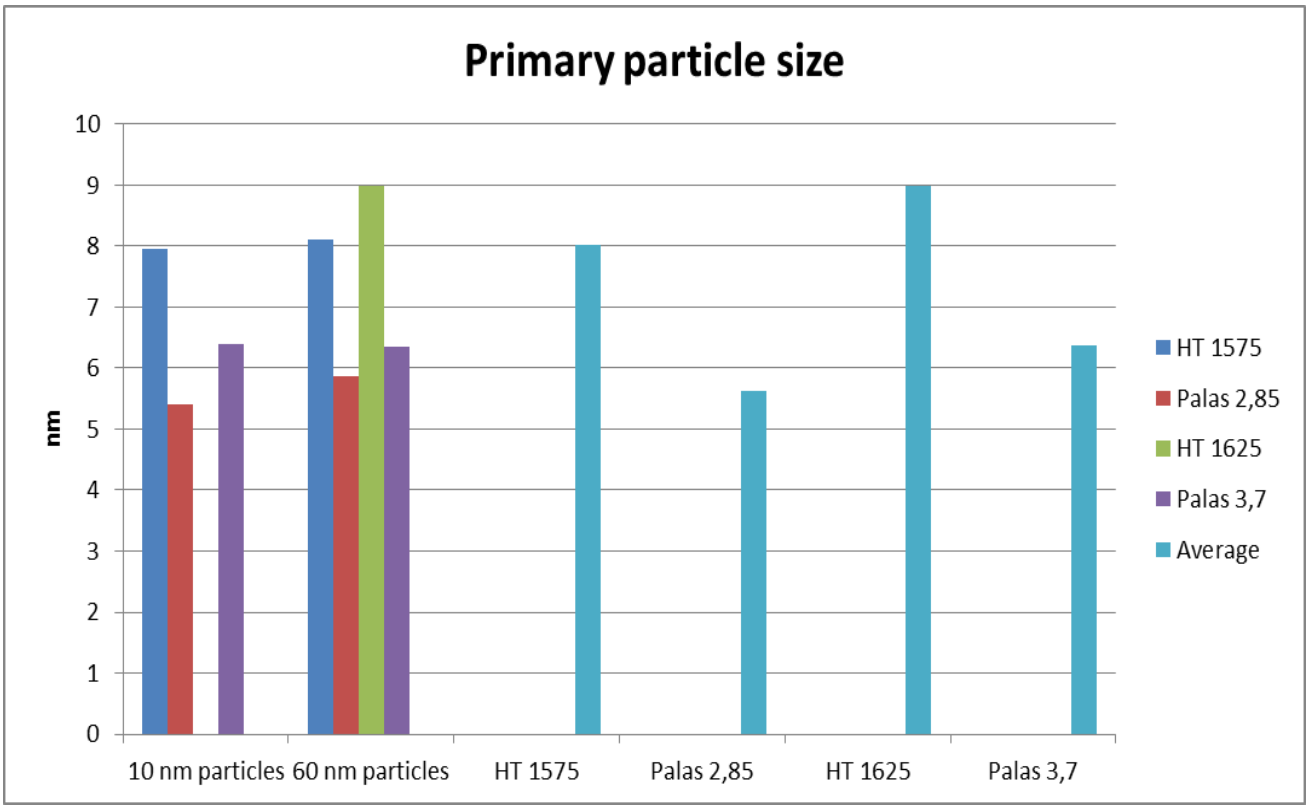

Figure 46 Analysis of TEM images in order to determine primary particle size. Primary particle size was determined for one setting per generation method. An average primary particle size was determined for each generation method.

There is a significant difference between the primary particle size between the two generation methods, within the same method the primary particle size only differs slightly between the settings. The average primary particle size for the HT system is 9nm and 8 for 1625 °C and 1575 °C settings respectively. For the SD system the average primary particle size for 2,85 l/min and 3,7 l/min are 5,5nm and approximately 6,3 respectively.

The reason behind the larger primary particle size produced by the HT system could be that more material is evaporated than in the SD system and larger primary particles can form.

11.2.6 Mass fractal dimension and effective density

The effective density was established for each of the particle size distributions respectively, the effective density was then used to calculate the mass size distributions.

Using the established effective density for the particle size distributions the mass fractal dimension *dfm* was calculated for each distribution respectively. Curves was fitted according to the method of establishing fractal dimension and can be seen in figure 47. From the curve fit was then also using the *dfm* methodology the fractal dimension number derived, see table 4.

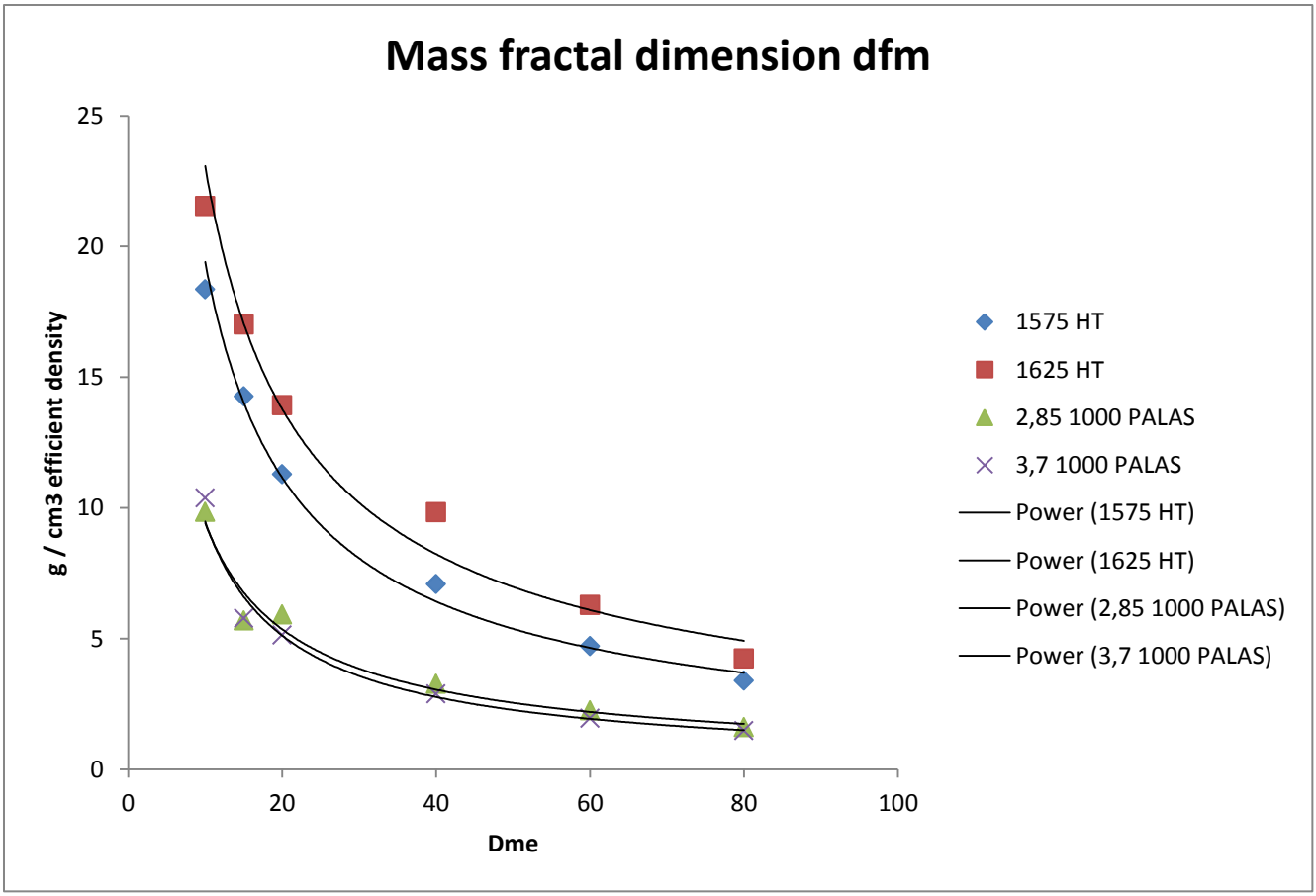

Figur 47 Fractal dimension curve fittings for the SD and HT system dervied from the effective density curves. The fractal dimension is based upon the effective density and the fit is based upon a power function where 3 minus the exponent resembles the fractal dimension. SD system is calculated for single spark frequency of 300 Hz and carrier gas flow rates of 2,85 and 3,7 l/min, HT system for generation temperatures of 1575 and 1625 °C.

The methods show a very similar *dfm* for the methods and settings, they lie within 2,111-2,256 *dfm*. The same *dfm* and different effective density indicate that the particles across methods and settings are agglomerated in a similar way but with different mass. This can be explained by the results from the primary particle analysis, see figure 45. For the HT system the average primary particle size is 2-3nm larger in diameter than the primary particles generated by the SD system. In addition there might be increased necking for the HT system, necking is the material that fuse the primary particles into agglomerates. The difference between the generation methods in primary particle size combined with the data on fractal dimension indicates particles similar in agglomeration across generation methods but agglomerates with more mass for the HT method.

Table 4 The mass fractal dimension number, dfm, calculated for each of the systems and settings for the experimentation in June.

System	Fit	dfm
1575 HT	$y = 121{,}97x^{-0{,}798}$	2,20
1625 HT	$y = 127{,}86x^{-0{,}744}$	2,26
2,85 1000 SD	$y = 61{,}359x^{-0{,}814}$	2,19
3,7 1000 SD	$y = 73{,}369x^{-0{,}889}$	2,11

12 Discussion and conclusions

12.1 IA, *dme* and APM particle surface area

The three methods used in this thesis to calculate particle surface area dosage are by assuming spherical particles with a diameter equal to the *dme* of the particles, the IA method and the APM methods described earlier.

The *dme* particle surface area is lower than the surface area calculated using the IA and APM theory. This is due to the fact that the volume calculated by the IA and APM method is divided into several primary particle volumes which then have their area summarized. The collected surface area of the many particles is greater than the one *dme* spheres surface area, this is also consistent with Lall et al (2008).

12.2 Generation methods and the FAS project

It is the conclusion of this thesis that both of the generation methods are suitable for use in the FAS project. Both methods, SD and HT, has the potential to generate a gold aerosol of such concentration that deposition can take place within an acceptable timeframe.

To reach a concentration of 2 cm2/cm2, which is consistent with literature for onset of inflammatory response, depending on setting and generation method approximately 1-2 hours of deposition would be required.

Both of the systems where during experimentation run for far longer than 2 hours and they both where stable during experimentation, so there should be no problems running them for the deposition time.

12.3 Deposition efficiency – the chamber and the lung

Looking at the results it is clear that the deposited particle surface area in the deposition chamber is significantly higher than what is modeled and calculated for the corresponding deposition in the lung. The deposition is roughly in the magnitude 1000 greater in the deposition chamber than in the lung in total and in the alveolar region. However the deposition takes the same principal “shape” when comparing the deposition chamber and the human lung, see for example figure 35 – 36. The deposition decrease as the carrier gas flow rate increase in both the deposition chamber and the ICRP modeling. The same trend can be

seen in figures 43 – 44 where the deposition takes on the same principal appearance but with a factor of about 1000 in difference.

The difference is logical since a high deposition efficiency allows for vast numbers of particles to be deposited in a small amount of time i.e. reach a relevant concentration fast.

In order to calculate the deposition in the deposition chamber data from Savi et al (2008) was used. The deposition used for the calculations was the one also modeled in Savi et al (2008). Savi et al (2008) also produced an experimental deposition efficiency which is lower than the one modeled. This should be taken into consideration when later using the deposition chamber, that the actual deposition could be somewhat lower than the one expected.

12.4 Workshop exposure and generation systems – a comparison

Waters et al (2009) states that 2 cm^2/cm^2 of particle surface area of exposure seems to be the exposure level after which inflammatory onset can be observed, study conducted for murine cells in vitro and in vivo. The particles used in the study were just as gold of low toxicity.

The particle yields in both particle number and mass very high both for the workshops and as generated by HT and SD. Compare for example figure 3 and any of the particle size distributions in figure 33. The particle number is as greatest almost 10^6 particles $/cm^3$ in figure 3, the maximum particle number in figure 33 is in the order of 10^8 particles $/cm^3$. The difference is significant and should be considered when looking at the particle deposition for the ICRP modeling.

Even with such high yields of particles the deposition modeling for the lung does not reach even near the limit dose of 2 cm^2/cm^2 for inflammatory onset due to low toxic particle exposure in any reasonable timeframe. If all gold deposited in the lung stayed, all clearance mechanisms failed, you would have to breathe many hundreds of hours at the particle size distributions produced in figure 33 to experience inflammation due to particle exposure, at least that is what theory would imply.

Also in this context the high concentration generated greatly decrease deposition time to reach a desired exposure level.

12.5 The particle toxicity – literature and generated doses

Doses generated by the SD and HT system reach a particle surface area dose of about 2 cm^2/cm^2 within 1 hour of generation and deposition. The dose is then comparable with that of other studies when inflammatory onset and adverse effects was observed.

According to the modeling of deposition in the respiratory system an equivalent exposure time will yield a particle surface area dose in the alveolar region about a thousand times lower than in the deposition chamber. This is due to the exposure area in the alveolar region, about 750000 cm^2 which drastically lowers exposure per unit area. As discussed in other sections a very high exposure in the deposition chamber is advantageous as it reduces deposition time greatly.

However it cannot be excluded that there still may be highly local areas of increased exposure in the lung where particle surface area doses might be high. These can be areas in the terminal bronchioles or higher where particles impact due to their inertia.

12.6 Particle structure

The experimentation in the particles show that they are agglomerates, *dfm* of about 2,3 and TEM imagery for confirmation of particle structure. Effective density increase as *dme* decrease for bot generation methods, as expected. The effective density is significantly higher for the HT system than for the SD, as are the primary particle size. At very low *dme* for the HT system the effective density becomes higher than bulk density for gold, unlikely this is the case cause gold has a high bulk density and the fact that the variance in the APM mass measurements increased for very small masses.

In the case for the HT system where effective density was very high the particles was most likely single primary particles that still had not agglomerated into larger particles. The primary particles was determined with TEM to be on average 8 nm for the HT system and the effective density where bulk density is achieved is for a *dme* of 10 nm. This supports that single primary particles constitutes the lower *dme* sizes.

12.7 Apparatus and measurements

The measurement apparatus worked well during experimentation. Occasionally when measuring with the APM the CPC was overloaded with particles and the so called APM transfer function was affected by this making the measurement somewhat less exact than if fewer particles had passed the CPC.

When measuring on particles with very small mass, very near the APM mass detecting limit of 0,01 femtograms. The variance in the APM mass determination increases. The variance can be partially explained by not optimal settings on the APM when measuring and the CPC overload of particles. It is this variance that for the HT system determines an effective density higher than gold bulk density for 10 nm particles.

This is one of the first times the APM measures particle mass so near to its detection limit, it remains to be fully determined what artifacts are introduced into the measurements due to diffusion and other parameters.

The data used for the course of this thesis remains to be corrected for offsets in the DMAs and the APM. The data will for the continued use in an article be corrected by using T-DMA measurements and APM and TEM analysis of sintered spherical particles.

12.8 For the future…

In order for the toxicological studies performed by the FAS project to be of high comparative value with other studies the methodology of the experiments must be described very clearly. During the course of this thesis I read many toxicological studies, some I understand are held in quit high esteem. A recurring flaw in many of them was that the exposure time was sometimes left out and sometimes only briefly mentioned. The time for exposure to a toxicant

is every bit as important as the dose of the toxicant and is the third dimension of a dose response relationship.

In the future when measuring on the aerosols generated by SD and HT system it could be a good idea to either use an electrometer where particle overload cannot occur or to use a dilution system to reduce the particle number concentration.

Model particles will be generated for protein interaction studies in the fall of 2010. It will be the first experiment where the gold nanoparticles will be used as model particles in toxicological studies. The aim is to determine how the low soluble low toxic gold nanoparticles interact with proteins in a relevant physiological solution, and from the results discuss the particle toxicity. For the experiment various doses of both mass and particle surface area will be used.

13 References

Agarwal, J. K. Gilmore, J. S. (1979). Continuous flow single particle counting condensation nucleus counter. J. aerosol Sci. 11:343-357.

Bailey, M. R. (1994). The new ICRP model for the respiratory tract. Radiation protection dosimetry. 53:107-114.

Colbeck, I. Ahmad, N. Ali, Z. (2009). The state of ambient air quality in Pakistan – a review. Environ Sci. Pollut Res. 17:49 – 63.

Connor, E. E. Mwamuka, J. Gole, A. Murphy, C. J. Wyatt, M. D (2005). Gold nanoparticles are taken up by human cells but do not cause acute cytotoxicity. Small journal. 3:325:327.

Daniel, M-C. Didier, A. (2004). Gold nanoparticles: Assembly, supramolecular chemistry, quantum size related properties, and applications towards biology, catalysis and nanotechnology. Chem. Rev. 104:293 – 346.

Donaldson, K. Borm, P. J. A. Oberdorster, G. Pinkerton, K. E. Stone, V. Tran, C. L. (2008). Concordance between in vitro and in vivo dosimetry in the proinflammatory effects of low toxicity low soluble particles: the key role of the proximal alveolar region. Inhalation toxicology. 20:53 – 62.

Ehara, K. Hagwood, C. Coakley, K. J. (1995). Novel method to classify aerosol particles according to their mass to charge ratio – aerosol particle mass analyzer. J. aerosol Sci. 27:217-234.

Gaschen, A. Lang, D. Kalberer, M. Savi, M. Geiser, T. Gazdhar, A. Lehr, C – M. Bur, M. Dommen, J. Baltensperger, U. Geiser, M. (2010). Cellular responses after exposure of lung cell cultures to secondary aerosol particles. Environmental science and technology. 44:1424 – 1430.

Håkansta, Carin. (2009). Projektansökan FAS dnr 2009-1291. Lunds universitet EAT.

Hinds, W. C. (1999). Aerosol technology. John Wiley & sons inc.

Isaxson, C. Pagels, J. (2009). Characteristics of welding fume aerosol investigated in three Swedish workshops. Journal of physics: Conference series 151(2009).

Kanomax. APM operation manual.

Knutson, E. O. Whitby, K. T. (1975). Accurate measurement of aerosol electric mobility moments. J. aerosol Sci. 6:453-460.

Knutson, E. O. Whitby, K. T. (1975). Aerosol classification by electric mobility: apparatus, theory and applications. J. aerosol Sci. 6:443-451.

Lall, A. A. Lutz Mädler, W. R. Friedlander, S. K. (2008). Nanoparticle aggregate volume determination by electrical mobility analysis: Test of idealized aggregate theory using particle mass analyzer measurements. Journal of aerosol science. 39(2008)403 – 417.

Lewinski, N. Colvin, V. (2008). Cytotoxicity of nanoparticles. Small – journal. 1:26 – 49.

Liu, B. Y. H. Pui, D. Y. H. (1974). Electric neutralization of aerosols. Aerosol Science 5:465-472.

Lovern, S. Klaper, R. (2006). Daphnia magna mortality when exposed to titanium dioxide and fullerene C60 nanoparticles. Environmental toxicology and chemistry.4(25)1132-1137.

McMurry, P. H. Wang, X. Park, K. (2002). The relationship between mass and mobility for atmospheric particles: a new technique for measuring particle density. Aerosol Sci technol. 36:227-238.

Messing, M. E. Dick, K. A. Wallenberg, L. R. Deppert, K. (2009). Generation of size selected gold nanoparticles by spark discharge – for growth of epitaxal nanowires. Gold bulletin. 42:1.

Monteiller, C. Tran, L. MacNee, W. Faux, S. Jones, A. Miller, B. Donaldson, K. (2007). The pro – inflammatory effects of low toxicity low solubility particles, nanoparticles and fine particles, on epithelial cells in vitro: the role of surface area. Occupational and environmental medicine. 64:609 – 615.

Nationalencyklopedien (2010). Pharynx, svalg.

Nationalencyklopedien (2010). Aerosol.

Nationalencyklopedien (2010). Andning.

Nationalencyklopedien (2010). Erytrocyt.

Nationalencyklopedien (2010). Fibroblast.

Nationalencyklopedien (2010). Fulleren.

Nationalencyklopedien (2010). Inflammation.

Nationalencyklopedien (2010). Interleukin.

Nationalencyklopedien (2010). Larynx, struphuvud.

Nationalencyklopedien (2010). Lunga.

Ott, W. Switzer, P. Robinson, J. (1996). Particle concentrations inside a tavern before and after prohibition of smoking: evaluating the performance of an indoor air quality model. Air & waste manage. Assoc. 46:1120 – 1134.

Pernodet, N. Fang, X. Sun, Y. Bakhtina, A (2006). Adverse effects of citrate / gold nanoparticles on human dermal fibroblasts. Small journal. 6:766 – 773.

Scheckman, J. H. McMurry, P. H. (2009). Rapid characterization of agglomerate aerosols by in situ mass mobility measurements. Langmuir 25(14), 8248 – 8254.

Socialstyrelsen. (2006). Partiklar i inomhusmiljön – en litteraturgenomgång.

Stephenson, D. Seshadri, G. Veranth, J. M. (2003). Workplace exposure to submicron particle mass and number concentrations from manual arc welding of carbon steel. AIHA Journal. 64:516 – 521.

Thostenson, E. T. Ren, Z. Chou, T. W. (2001). Advances in the science and technology of carbon nanotubes and their composites: a review. Composites science and technology. 61(2001)1899-1912.

Tran, C. L. Buchanan, D. Cullen, R. T. Searl, A. Jones, A. D. (2000). Inhalation of poorly soluble particles. II. Influence of particles surface area on inflammation and clearance. Inhalation toxicology. 12:1113 – 1126.

Virtanen, A. Ristimäki, J. Keskinen, J. (2004). Method for measuring effective density and fractal dimension of aerosol agglomerates. Aerosol science and technology. 38:437 – 446.

Walker, C. H. Hopkin, S. P. Sibly, R. M. (2002). Principles of ecotoxicology. CRC PRESS.

Wang, S. C. Flagan, R. C. (1990). Scanning electrical mobility spectrometer. Aerosol Sci technol. 13:230-240.

Waters, K. M. Masiello, L. M. Zangar, R. C. Tarasevich, B. J. Karin, N. J. Quesenberry, R. D. Bandyopadhyay, S. Teeguarden, J. G. Pounds, J. G. Thrall, B. D. (2009). Macrophage responses to silica nanoparticles are highly conserved across particle sizes. Toxicological sciences. 107(2):553 – 569.

www.metalund.lu.se (2010)

www.nano.lth.se (2010)

www.virtualmedicalcentre.com (2010) Respiratory system

Zimmer, T. A. Biswas, P. (2001). Characterization of the aerosols resulting from arc welding processes. J. aerosol Sci. 32:993-1008.